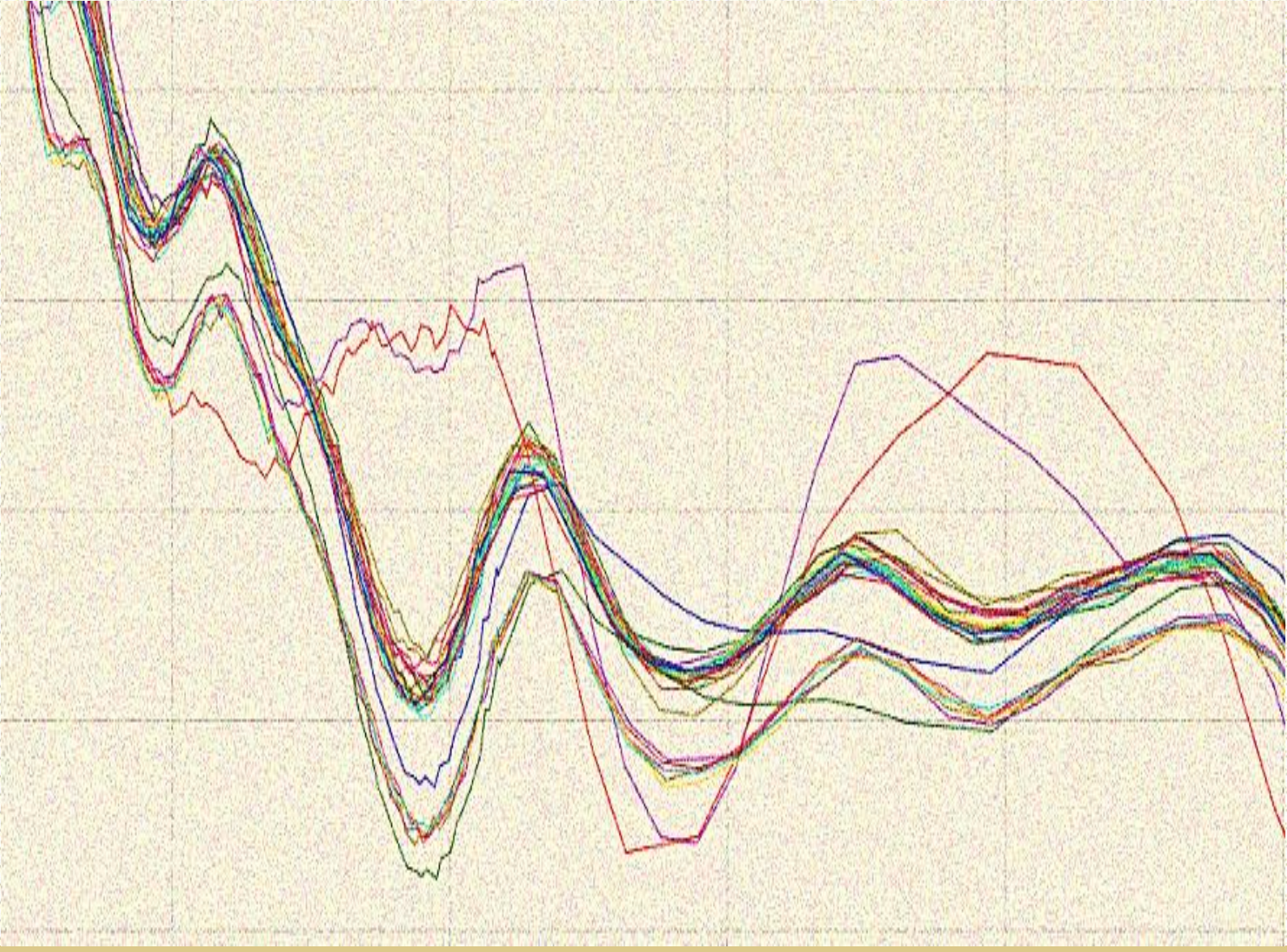

Rafael Veloso Ferreira

Investigation of the detection limits of ZnSe and Cu_2SnSe_3 secondary phases in $Cu_2ZnSnSe_4$ by XANES

Dissertation presented to the University of Coimbra in order to obtain the Master's degree in Engineering Physics

September 2017

· U C ·

Universidade de Coimbra

Rafael Veloso Ferreira

Investigation of the detection limits of ZnSe and Cu_2SnSe_3 secondary phases in $Cu_2ZnSnSe_4$ by XANES

Dissertation presented to the University of Coimbra
in order to complete the necessary requirements to
obtain the Master's degree in Engineering Physics.

Supervisor:

Prof. Dr. Susan Schorr (Helmholtz-Zentrum Berlin)

Co-supervisor:

Prof. Dr. Manuela Silva (University of Coimbra)

Coimbra, September 2017

Acknowledgements

First, I would like to acknowledge the Erasmus programme and Universidade de Coimbra for funding and providing a way of doing my Master's project in Berlin.

I want to express my most sincere gratitude to Prof. Dr. Susan Schorr, who provided me with the opportunity to work on this project and without whom these months living in Berlin wouldn't have been possible, during which I learned and experienced as much as I did. To Dr. Galina Gurieva, I am truly thankful for her indispensable guidance throughout all of this work, for always answering my many questions and for showing a great deal of patience through all of it. I honestly learned a lot from you and greatly enjoyed our many conversations and discussions.

I would like to thank the instrument scientists at the KMC-2 beamline at BESSY II, Dr. Daniel Többens and Dr. Götz Schuck, for their support in the XANES measurements, as well as the Helmholtz-Zentrum Berlin for providing the beamtime. For the microprobe beamtime, I thank the Freie Universität Berlin, as well as Fr. Christiane Behr for preparing the samples for measurements with this instrument.

I would also like to thank Prof. Dr. Claudia Schnohr and her group in the Institut für Festkörperphysik in Jena for their help in the sample preparation for XANES and for performing the measurements in the first beamtime. A special thanks to Konrad Ritter, who also personally instructed me in using the ATHENA program, provided essential calculations and made himself available for any questions I might have.

I'm grateful to everyone in the working group for making me feel like a part of it and for being great and fun people that I was happy to see every day. To my office colleagues and to the ones who I spent the most time with for many months - Julien, Frederike, René, Silvia, Albina and Meike (in order of appearance) - thank you for all the help, daily laughs and for being good friends both in and out of the office. I hope to see you again many more times. Special thanks to Meike because who knows where I would've lived during the last months if not for her, and for going along in those much needed balcony breaks.

I must also thank Afonso, who preceded me at HZB, for giving me advices picked up during his own time in Berlin as I was just starting mine. A big thank you to the ones who accompanied me during my time in university, those who became close friends and those who made even studying fun by making it a group activity.

An unmeasurable thanks to the ones most responsible for shaping these last 5 years, Fonitos (FONITOS!), my university family made up of friends that I think of as brothers, especially Oliveira, David, Diogo, Miguel, Basílio and Rafael. From this big group, I still have to single out Tondela, Jogui and Romão, with whom the greatest stories were made and the most fun was had. You always tried to push me into making the best decisions when I was unsure of myself and helped me in many other ways, sometimes by just being there. I hope to also have you with me in the future that lies ahead.

Finally, an indescribable thank you to my family, who raised and supported me from the real beginning. *Obrigado, Pai e Mãe.*

Abstract

The quaternary $Cu_2ZnSnSe_4$ (CZTSe) is a promising semiconductor material for absorber layers in thin film solar cells due to its direct band gap around 1 eV and high absorption coefficient larger than 10^4 cm^{-1} [6]. The highest conversion efficiency of CZTSe solar cells achieved so far is above 11.6% [7]. However, one troubling and common phenomenon in CZTSe-based photovoltaic devices is a low open-circuit voltage with respect to the band gap energy. A plausible reason for this could be a reduction in the effective band gap due to inhomogeneities in structure, phase, or composition in the absorber layer. To gain a detailed knowledge on the influence of phase inhomogeneities on the performance of solar cells, the understanding of detection limits of investigation methods is essential. The sensitivity limits of the conventionally used methods such as X-ray diffraction and Raman spectroscopy were studied recently [10]. This work aims to understand the real sensitivity levels of XANES to the presence of Cu_2SnSe_3 and ZnSe in $Cu_2ZnSnSe_4$, two very common secondary phases for this compound. Additionally, the effects of subjecting highly off-stoichiometric CZTSe samples containing many secondary phases to a second thermal annealing process were investigated, focusing on changes in their phase contents and the compositions of the CZTSe phases.

To achieve the main purpose of this work, two sets of polycrystalline powder samples were used. So as to simulate secondary phase-containing CZTSe absorbers, single-phase CZTSe powder was mixed with determined amounts of secondary phase powder – single-phase Cu_2SnSe_3 or ZnSe – in order to obtain a calibration series of CZTSe mixtures containing 1%, 2%, 3%, 5%, 10% and 20% of secondary phase. The two mixture sets were prepared into pellets and measured by transmission mode XANES at the Se and Cu K-edges. Data from these measurements were analysed with the ATHENA program [21] using a linear combination fitting (LCF) method.
The phase characterization of the re-annealed CZTSe samples was carried out by powder X-ray diffraction, while the compositional analysis was performed by wavelength-dispersive X-ray spectroscopy.

Results obtained have shown that XANES is capable of quantifying the ZnSe secondary phase at all concentrations within a small error bar. With this technique, it was also possible to detect the Cu_2SnSe_3 phase down to 5% concentration. Investigation on the influence of the CZTSe standard's stoichiometry and the addition of various secondary phase standards to the LCF

analysis had largely inconclusive results, particularly with the ZnSe mixtures, but revealed the necessity for further investigation on these topics.

Results from the techniques applied to the re-annealed samples showed that the secondary phase contents had remained identical in most samples and that the amount of distinct CZTSe phases did not decrease in any of them, although their composition had changed with respect to those previously present. In the end, it was determined that the annealing had no major benefits in increasing the homogeneity of the samples.

Resumo

O quaternário $Cu_2ZnSnSe_4$ quaternário (CZTSe) é um material semicondutor promissor para camadas de absorção em células solares de filme fino devido ao seu band gap direto com energia por volta de 1 eV e alto coeficiente de absorção maior que 10^4 cm^{-1} [6]. A maior eficiência de conversão das células solares CZTSe alcançada até agora é superior a 11,6% [7]. No entanto, um fenómeno preocupante e comum em dispositivos fotovoltaicos com base em CZTSe é uma baixa tensão de circuito aberto em relação à energia de band gap. Uma razão plausível para tal pode ser uma redução no band gap efetivo devido a heterogeneidades na estrutura, fase ou composição na camada de absorção. Para obter um conhecimento detalhado sobre a influência das heterogeneidades de fase no desempenho das células solares, a compreensão dos limites de detecção dos métodos de investigação é essencial. Os limites de sensibilidade dos métodos utilizados convencionalmente, como difração de raios-X e espectroscopia de Raman, foram estudados recentemente [10]. Este trabalho tem com objetivo compreender os reais níveis de sensibilidade de XANES à presença de Cu_2SnSe_3 e ZnSe em $Cu_2ZnSnSe_4$, duas fases secundárias muito comuns para este material. Adicionalmente, foram investigados os efeitos de submeter amostras de CZTSe altamente não-estequiométricas contendo muitas fases secundárias a um segundo processo de recozimento térmico, com foco em mudanças nos seus conteúdos de fases e as composições das fases CZTSe.

Para atingir o objetivo principal deste trabalho, foram utilizados dois conjuntos de amostras de pó policristalino. De modo a simular absorvedores CZTSe contendo uma fase secundária, o pó CZTSe monofásico foi misturado com quantidades determinadas de pó de fase secundária – Cu_2SnSe_3 ou ZnSe monofásicos – para obter uma série de calibração de misturas CZTSe contendo 1%, 2% 3%, 5%, 10% e 20% de fase secundária. Os dois conjuntos de misturas foram preparados em *pellets* e medidos por XANES em modo de transmissão nas *K-edges* de Se e Cu. Os dados das medições foram analisados com o programa ATHENA [21] usando um método de *fitting* por combinação linear (LCF).
A caracterização de fase das amostras CZTSe recozidas foi realizada por difração de raios-X, enquanto a análise composicional foi realizada por espectroscopia de raios-X dispersiva de comprimento de onda.

Os resultados obtidos mostraram que XANES é capaz de quantificar a fase secundária ZnSe a todas as concentrações dentro de uma pequena barra de erro. Com esta técnica, também foi possível detetar a fase Cu_2SnSe_3 até uma concentração de 5%. A investigação sobre a influência

da estequiometria do standard de CZTSe e a adição de vários standards de fase secundária à análise LCF apresentaram resultados bastante inconclusivos, particularmente com as misturas de ZnSe, mas revelou a necessidade de uma investigação mais aprofundada sobre esses tópicos. Os resultados das técnicas aplicadas às amostras recozidas mostraram que o conteúdo de fases secundárias permaneceu idêntico na maioria das amostras e que a quantidade de fases CZTSe distintas não diminuiu em nenhuma delas, embora a composição destas tenha mudado em relação àquelas anteriormente presentes. No final, determinou-se que o recozimento não teve grandes benefícios no aumento da homogeneidade das amostras.

Table of Contents

Abbreviations

BSE	backscattered electrons
CTSe	Cu_2SnSe_3
CZTSe	$Cu_2ZnSnSe_4$
LCF	linear combination fitting
PV	photovoltaics
WDX	wavelength-dispersive X-ray spectroscopy
XAFS	X-ray absorption fine structure
XANES	X-ray absorption near edge structure
XAS	X-ray absorption spectroscopy
XRD	X-ray diffraction

1. Introduction

1.1. Motivation

With the constant growth of the human population and its fast industrial development came a need for energy sources that is ever-increasing. So far, the world's energy demands have been fulfilled mainly by the use of fossil fuels. But the capacity of these energy sources is finite, so raising their consumption has always been a temporary solution to a problem that has grown consistently larger – eventually they will be depleted and cease to be an option. Additionally, their use is the greatest contribution to the current situation of global warming, which means that humanity´s main source of energy is also destroying the environment.

One of the alternatives for sustainable energy production is found in renewable energies, which allow the creation of cleaner energy by harnessing the power of the sun, wind and water. Specifically, a great deal of scientific and technological research has been carried out in the field of solar photovoltaics (PV) for the development of materials and technologies. As it stands, the solar energy market is dominated by crystalline silicon-based photovoltaic cells, accounting for around 93% of the total production in 2016, and whose record laboratory cell efficiency has reached 26.7% [1]. However, the existence of an indirect band gap decreases the probability of photon absorption in silicon and thus a thick absorber layer is required to make up for the low absorption coefficient. Due to this and to the costly purification process of Si, more market viable solar cell technology alternatives started being investigated.

The emergence of compound semiconductors has provided an opening into low-cost fabrication of thin-film solar cells, made possible by these materials' higher absorption coefficients which allow for a reduction in absorber layer thickness, and therefore lead to a decrease in production costs. The compound semiconductor used in thin-film technologies with the biggest market share is currently cadmium telluride (CdTe) [1]. But scalability of the CdTe PV industry is limited by the low availability of tellurium, which makes it an expensive element. Environmental concerns about the use of this compound are also raised by the fact that cadmium is a toxic heavy metal. $Cu(In,Ga)Se_2$ (CIGS) absorbers have also been the focus of a lot of research and have proven to be a reliable alternative to silicon in terms of efficiency, with record lab efficiencies exceeding the 21% mark [1]. However, the problem of abundance and cost remains, in particular due to the increased demand for indium in modern electronic device

industries which could result in future shortages of this element and increase costs above a viable limit. A number of strategies are being employed to surpass the downsides of these PV materials, but the existence of a compound without such aspects would improve the future outlook for the adoption of PV technologies.

The kesterite-type absorbers $Cu_2ZnSn(S,Se)_4$ (CZTSSe) are compounds which have also drawn much attention from the perspective of photovoltaic applications. These quaternary materials present characteristics that make them an ideal choice for this purpose, specifically a direct band gap with a tuneable energy in the range between 1.0 and 1.5 eV, and an absorption coefficient larger than 10^4 cm^{-1} [2]. Unlike CdTe or CIGS, elements contained in kesterite are earth-abundant and most are non-toxic, which make these compounds stand out as more environmentally friendly and economic alternatives. The efficiency limit for solar energy conversion in a single p-n junction as a function of the band gap from semiconductors used is known as the Shockley-Queisser limit [3], which considers that a maximum conversion efficiency of around 30% is achieved for band gaps in the range of 1.2 to 1.4 eV, meaning that kesterite semiconductor compounds present a near optimal band gap range. However, the current record conversion efficiency of kesterite-based thin film solar cells is still 12.6% [4]. The difficulty in reaching peak performance of these solar cells can be possibly attributed to a reduction in the effective band gap caused by inhomogeneities in the structural parameters and composition of the absorber layer, the occurrence of secondary phases and a non-ideal photovoltaic device structure [5]. Since it has been determined that an efficiency of 15% must be reached before kesterite solar cells can be considered a commercially viable solution, investigating the obstacles standing in the way of achieving higher cell efficiencies is essential for the future of these technologies. Therefore, a fundamental understanding of this material and possible performance-influencing factors is of great importance to the progress of solar cell applications research.

1.2. Objectives

Quaternary compounds such as kesterite carry an increased complexity associated with the number of components in the system, precipitating a higher variety and probability of occurrence of secondary phases. Such inhomogeneities are part of the group of factors that are considered harmful to the performance of solar cells, both due to their position within the layer and to the individual properties of each phase. Specifically, higher band gap secondary phases may behave as a barrier against the charge carriers when positioned near the junction, while phases with lower band gap can be responsible for a decrease in the open-circuit voltage by shunting the device. For this reason, the ability to detect and quantify the presence of secondary phases is extremely important for the purpose of acquiring detailed insight into their influence on device performances, and to subsequently discover ways of improving them.

This work is focused on selenide kesterite compounds $Cu_2ZnSnSe_4$ (CZTSe), which possess a direct band gap around 1 eV and for which the highest cell conversion efficiency attained is above 11.6% [6, 7]. The aim is to understand the sensitivity limits of one investigation method, XANES, when applied to the issue of secondary phase detection. The commonly occurring Cu_2SnSe_3 (CTSe) and ZnSe phases will be those for which the method will be studied, whose presence is hard to detect with conventional methods due to the strongly overlapping Bragg peaks of the structures. Among the most common secondary phases observed in kesterite, these are also expected to have a large damaging effect on the conductivity of the material because of their extreme-case band gap energies: Cu_2SnSe_3 has the lowest band gap at 0.8 eV, while ZnSe has the highest at 2.7 eV [8, 9].

The detection limits of the XRD and Raman spectroscopy methods for the Cu_2SnSe_3 and ZnSe phases in $Cu_2ZnSnSe_4$ have already been studied by A. Sousa [10], a work which this project follows by aiming to determine the sensitivity level of the XANES technique to the detection and quantification of both phases. Samples used to achieve this goal consist of two-compound mixtures of $Cu_2ZnSnSe_4$ with Cu_2SnSe_3 and ZnSe at various secondary phase percentages, and are the same as those used in the previous work. Reports from studies using this method already suggest that it is one of the few with the potential to quantitatively detect the ZnSe secondary phase in $Cu_2ZnSnSe_4$ [11], though testing of this capacity had yet to be performed. The theoretical basis behind XANES analysis also seems to indicate characteristics fitting for this problem, such as the ability to study the surrounding environments of specific atoms [12-14].

As a secondary objective, an investigation on the effects of re-annealing $Cu_2ZnSnSe_4$ samples is conducted. The samples in question are highly heterogeneous, being the product of attempts at synthesising very off-stoichiometric kesterite, and as such contain many secondary phases as well as multiple compositions of main phase in each. The intended purpose of this second annealing would be the reduction to a single kesterite phase composition and the minimization of the secondary phase contents in the individual samples. Determination of the actual effects of the process is made through the results of X-ray diffraction (XRD) and wavelength dispersive X-ray spectroscopy (WDX) measurements, following the same analysis performed on the samples after the first annealing. In this way, changes brought upon by the re-annealing can be promptly discovered by comparison between both sets of results.

2. Experimental

2.1. Sample Characterization and Preparation

The first set of samples used in this project consists of $Cu_2ZnSnSe_4$, Cu_2SnSe_3 and ZnSe powders and kesterite-secondary phase mixtures made from them. The full structural and chemical characterization of the samples and description of their synthesis can be found in the work of A. Sousa [10], which details the investigation where they were first used.

Two single-phase samples of slightly off-stoichiometric CZTSe were synthesized by solid state reaction, with chemical compositions being determined by performing WDX analysis. In this thesis, these samples will be referred to as Kest I and Kest II. The Kest I sample showed a slightly larger Cu deficit in comparison to Kest II while having a very similar Zn/Sn ratio, resulting in the $Cu_{1.98}Zn_{1.04}Sn_{0.98}Se_4$ composition, a mixture of B-G off-stoichiometry types. The composition of Kest II was determined as $Cu_{2.01}Zn_{1.03}Sn_{0.98}Se_4$, a mixture of G-F off-stoichiometry types, in this case. One grain of ZnSe was found in this sample – most probably resulting from cross-contamination during sample preparation for the microprobe measurements – so Kest II was mixed with the ternary compound in order to avoid any possibility of biasing the results, while Kest I was mixed with ZnSe. The atomic percentages determined by WDX analysis relative to this set of samples are presented in Table 1.1.

Sample	Cu (%)	Zn (%)	Sn (%)	Se (%)
ZnSe		51.1		48.84
Cu_2SnSe_3	34.2		16.96	48.78
Kest I	25.5	13.4	15.6	48.5
Kest II	25.7	13.2	12.5	48.6

Table 1.1 – Atomic percentages obtained by WDX analysis for the ZnSe, Cu_2SnSe_3 and kesterite samples.

With these powder samples, mixtures containing 20%, 10%, 5%, 3%, 2% and 1% of ZnSe or CTSe powder were prepared. As the actual amounts of secondary phase introduced in each mixture are somewhat different from the planned values, a table containing the actual percentages obtained for both phases is presented below.

Planned %	Obtained %	
	ZnSe	CTSe
20	20.10(2)	19.26(2)
10	10.50(1)	9.64(1)
5	5.01(1)	4.50(1)
3	3.10(1)	2.78(1)
2	2.01(1)	1.58(1)
1	1.01(1)	1.18(1)

Table 1.2 – Planned and obtained secondary phase percentages in the resulting mixtures.

To perform transmission mode XANES measurements, it is required to have concentrated samples so that the decrease in beam intensity is significantly below the possible variation due to counting statistics. Moreover, the samples must be in the form of highly homogenous pellets with constant thickness and free of pinholes [12]. The preparation of the mixture powders into samples fulfilling this criteria was performed at the Institut für Festkörperphysik in Jena, Germany, according to the procedure developed in the group of Prof. Dr. Claudia Schnohr. The amount of material necessary for an 8 mm diameter pellet and a transmitted intensity of around 20% was calculated using the knowledge of each material's absorption length and density, reaching the final result of 5.7 mg within an error bar of 1%. For each powder sample, an amount of 11.4 mg was carefully weighed, enough to produce two pellets, each 1 mm thick. Using weighing paper to ensure that no loss of material occurred, this amount was introduced into the zirconium oxide grinding ball of a FRITSCH Pulverisette 23 mini-mill, along with 200 mg of carbon to act as a binder. The introduced contents were milled for 30 minutes to ensure that a homogenous mixture was achieved.

Figure 1.1 – Pulverisette 23 mini-mill from the company FRITSCH [15].

Precisely 105.7 mg of the properly homogenised milling product were introduced into a pressing tool, like the one seen in Figure 1.2. The mixture was then pressed at up to 5 ton, increasing 1 ton every five minutes, at the end of which the compacted pellet is produced.

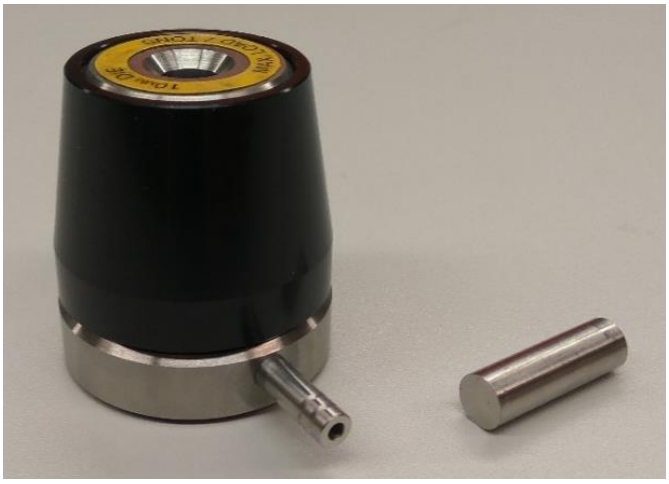

Figure 1.2 – Pressing tool.

Following this procedure for every sample, pellets of $Cu_2ZnSnSe_4$, Cu_2SnSe_3, ZnSe powders, and of $Cu_2ZnSnSe_4$-Cu_2SnSe_3 and $Cu_2ZnSnSe_4$-ZnSe mixtures were produced, adding up to sixteen pellets ready for the XANES measurements. Pellets of $Cu_2ZnSnSe_4$ stoichiometric reference, CuSe, Cu_2Se, SnSe and $SnSe_2$ were also prepared.

A second set of sample data comes from the investigation of L. E. Valle Rios on the structural trends in off-stoichiometric kesterite compounds [16]. During the referenced work, the intention was to synthesize $Cu_2ZnSnSe_4$ samples with several compositions within the A, B, C and D off-stoichiometry types, whose structure would then be studied. Some of these samples were measured by XANES, during the first synchrotron beamtime. The portion of the obtained data relative to the samples presented in Table 1.3 is used here as an example of this method's application to real-world measurement situations, taking into consideration the conclusions reached by studying the mixture samples.

No.	Sample	Cu/(Zn+Sn)	Error	Zn/Sn	Error	Secondary Phases
1	A0000-1	0.978	0.017	1.077	0.015	Single phase
2	A0050-1	0.911	0.016	1.127	0.016	Single phase
5	C0025-2	1.027	0.018	0.995	0.014	CuSe; Cu_2Se; ZnSe
7	A0025-3	0.967	0.017	1.045	0.015	Single phase
10	C0025-4	1.014	0.018	1.017	0.014	CuSe; Cu_2Se; ZnSe
12	B0050-4	0.998	0.017	1.042	0.015	CuSe; ZnSe
20	A0075-6	0.890	0.015	1.134	0.016	ZnSe
21	A0100-6	0.945	0.016	1.149	0.016	Single phase

Table 1.3 – Overview of the off-stoichiometric CZTSe samples synthesised by L. E. Valle Rios used in this work: Cation ratios and phase content information obtained from WDX analysis [16].

Finally, a set of samples consisting of eight highly off-stoichiometric and heterogeneous $Cu_2ZnSnSe_4$ powder samples, synthesized previously, were used to investigate the effects of the re-annealing process in their structural and chemical composition. Two samples for each of the A, B, C, and D kesterite off-stoichiometry types were available, all of which were pressed into pellets as a first step. For the pressing process, the pressing tool (Figure 1.2) is filled with sample powder until this fills most of its cavity, the sample is then compressed inside the holder by a hydraulic press, slowly increasing the pressure applied. After five minutes at the 2 ton pressure limit, the holder is released and the pellet is carefully removed from the inside, so it doesn't break from scraping against the walls of the cavity. The pressed samples were then put inside silica ampoules, which were evacuated to 10^{-5} mbar and sealed with a silica plug using a H_2/O_2 flame.

Figure 1.3 – Samples in pellet form after pressing process, stored inside silica tubes.

The sealed ampoules were taken to the furnace and heated at a rate of 50 K/h until the target of 750 °C was reached, around 50 °C lower than the melting point of the respective material. This temperature was kept for 300 h, after which the cooling process was initiated with a rate of 25 K/h, purposefully slow in an attempt to avoid the formation of additional secondary phases, to increase the order in the kesterite phase and to decrease the amount of kesterite phases with different compositions in each sample.

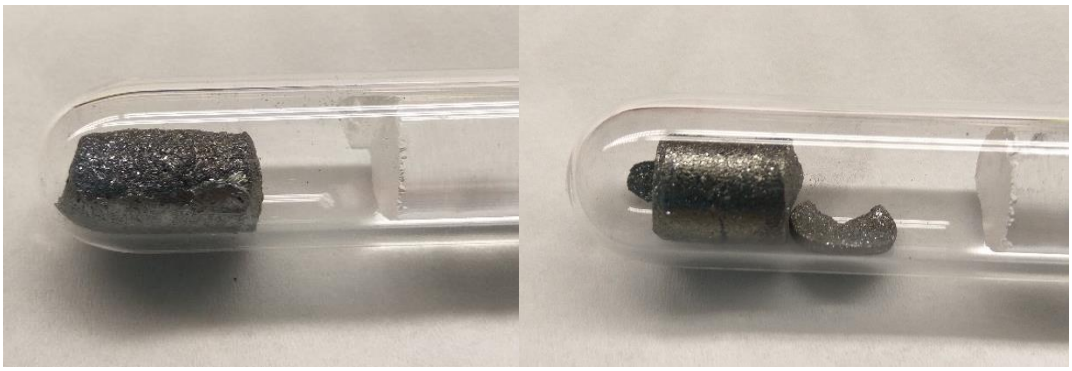

Figure 1.4 – Examples of samples after re-annealing.

The re-annealed samples were then ground in a Fritsch Pulverisette 0 Vibratory Micro Mill, where the mortar vibrates electromagnetically, grinding the sample though impact and friction between the grinding ball and the walls of the container.

Figure 1.5 – Pulverisette 0 Vibratory Micro Mill from the company Fritsch.

The structural and chemical contents of the re-annealed samples in powder form was evaluated by XRD and EPMA-WDX measurements, paying special attention to changes in the main and secondary phase contents.

2.2. XANES

X-ray absorption spectroscopy (XAS) is an analytical technique that studies the details of how X-rays are absorbed by an element's atoms at energies near and above its core level binding energy, known as the absorption edge. As XAS probes samples at an atomic level, it places few restrictions on the type of materials than can be analysed – all atoms have core electrons with well-defined binding energies, so absorption spectra can be measured for essentially every element by tuning the X-ray energy to the appropriate absorption edge.

When X-rays are incident on a sample, the highly energetic photons that make up the radiation can be absorbed by electrons located in the inner shells of the atoms in its composition. If the photon energy is greater than the binding energy of a particular electronic core level of a specific element, then electrons at that level can participate in this absorption process. Conversely, if the X-rays have energy below that of the binding energy, then the bound electrons will not be disturbed and will absorb no photons. In an X-ray absorption process, the relation between the transmitted intensity I_t and incident intensity I_0 is given by Beer's Law:

$$I_t(t) = I_0 e^{-\mu(E)t}$$

where t is the sample's thickness and $\mu(E)$ is the energy-dependent X-ray absorption coefficient. Over a large range of X-ray energies, the absorption coefficient is a smooth function of the photon energy E, varying with a dependence on the sample's density ρ, atomic number Z and atomic mass A approximately according to $\mu(E) \sim \rho Z^4/mE^3$. Therefore, $\mu(E)$ generally decreases with increasing photon energy. But when the energy is enough to fulfil the condition for absorption by a core electron, the photon is eliminated and a photoelectron-hole pair is created. This process leads to a sharp increase of the absorption coefficient, corresponding to the absorption edge. Above this energy, the difference between the photon and the binding energies is converted into kinetic energy of the photoelectron, as $\mu(E)$ now continues to decrease. The core-hole is filled by a higher energy electron after a short time (about 10^{-15} s), and the transition energy is released via X-ray fluorescence or Auger electron emission.

According to quantum mechanical perturbation theory, the transition rate between a core level and the final state is proportional to the product of the squared modulus of the matrix element M and the density of states $\rho(E_f)$:

$$\mu \propto |M|^2 \rho(E_f) \propto \left|\langle f | H_p | i \rangle\right|^2 \rho(E_f)$$

where $|i\rangle$ and $\langle f|$ denote the initial and final states, respectively, and H_p is the interaction Hamiltonian responsible for the transition, the electromagnetic field of the X-ray photon. These factors affect the absorption probability, causing a modulation of the absorption coefficient and thus creating the X-ray absorption fine structure (XAFS). Due to differences in the final states of the transitions, two regions are commonly distinguished in the XAFS spectrum. The first, known as extended X-ray absorption fine structure (EXAFS), is located at higher photon energies, around 30 eV above the edge. Photoelectrons in this region are promoted to a continuum state. The wave created in this process propagates outwards and is scattered by the neighbouring atoms. Interference between the outgoing and scattered waves occurs, in a manner that depends on the geometry of the absorber's surroundings and the photoelectron wavelength. Thus, the EXAFS final state is a superposition of outgoing and scattered waves. This region is independent of chemical bonding and relies on the atomic arrangement around the absorber atom, containing information about the coordination number, interatomic distances and structural disorder around a particular atomic species. Located at energies just above the absorption edge, is the region known as X-ray absorption near edge structure, or XANES. Here the photoelectron does not absorb enough energy to escape into the continuum, so instead excitation takes place to unoccupied bound states of the absorbing atom. This can lead to a strong increase of the absorption coefficient at X-ray energies corresponding to the energy difference between the core level and these bound states.

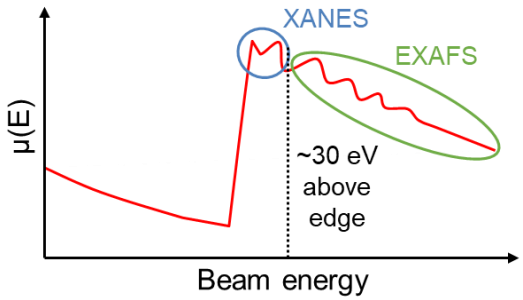

Figure 1.6 – Absorption coefficient μ(E) versus photon energy E. Fine structure above the edge is divided into XANES and EXAFS regions.

Since excitations occur to bound states, XANES is sensitive to the chemical bonding. Different oxidation states and the nearest neighbours of the absorbing atom therefore introduce characteristic features in this region, both in its position and shape (Figure 1.7). The shape of the XANES region is also influenced by multiple scattering effects dependent on the three-dimensional symmetry of the crystal structure. This provides a means of distinguishing between different crystal phases. In simpler terms, XANES functions like an atomic probe whose features grant a view into the crystal structure of materials, as if seen from the perspective of the absorber atoms.

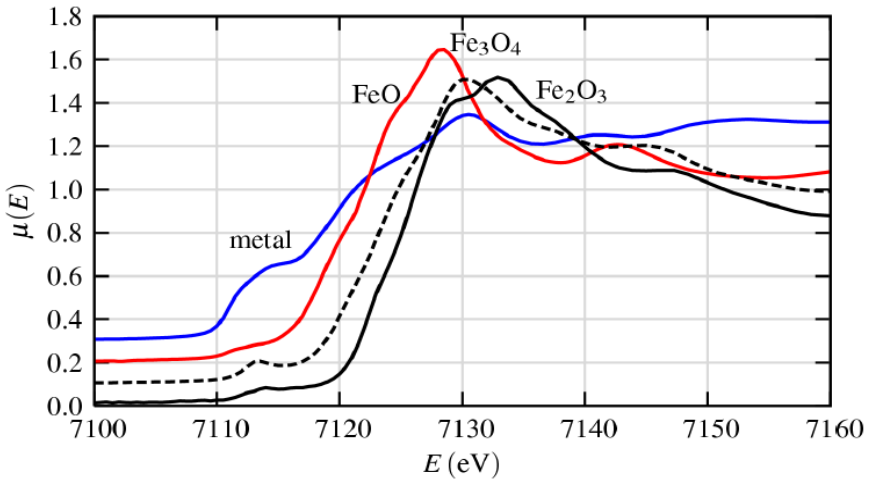

Figure 1.7 – XANES spectra of Fe metal and several of its oxides, measured at the Fe K-edge [13].

These aspects are the reason why XANES is thought to be an appropriate method for the detection of secondary phases in powder and thin film samples alike, with already several studies supporting this theory [11, 17]. In this work, measurements at the Cu and Se K-edges have been performed. To get an idea of how suitable these measurements might be for the purpose of detecting and quantifying the Cu_2SnSe_3 and ZnSe secondary phases in $Cu_2ZnSnSe_4$, it is useful to look at the structure around the edge elements in all the phases considered. In the case of CZTSe-ZnSe mixtures, the surrounding environment of the selenium atoms is very different depending on which phase they are bound to: in the first case, the nearest neighbours of Se consist only of Zn; in CZTSe, the surroundings are populated with Cu and Sn atoms, besides Zn (Figure 1.8). Therefore, it can be expected that XANES signals from these two structures would be different enough for ZnSe to have a notable impact on the overall spectrum from the mixtures and to be consequently easier to detect.

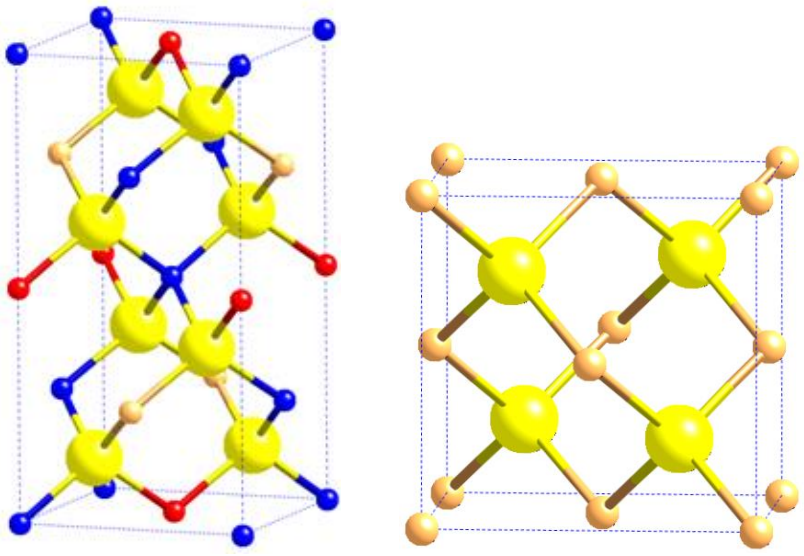

Figure 1.8 – $Cu_2ZnSnSe_4$ and ZnSe structures (Cu - blue, Zn - orange, Sn - red, Se - yellow).

In the case of CZTSe-CTSe mixtures, the selenium atoms are surrounded by almost the same elements in both configurations with the exception of zinc in CZTSe, which could translate into more difficulty in measuring a detectable signal difference. This similarity is even larger when measuring at the Cu K-edge, as copper atoms are only bound to selenium in both configurations.

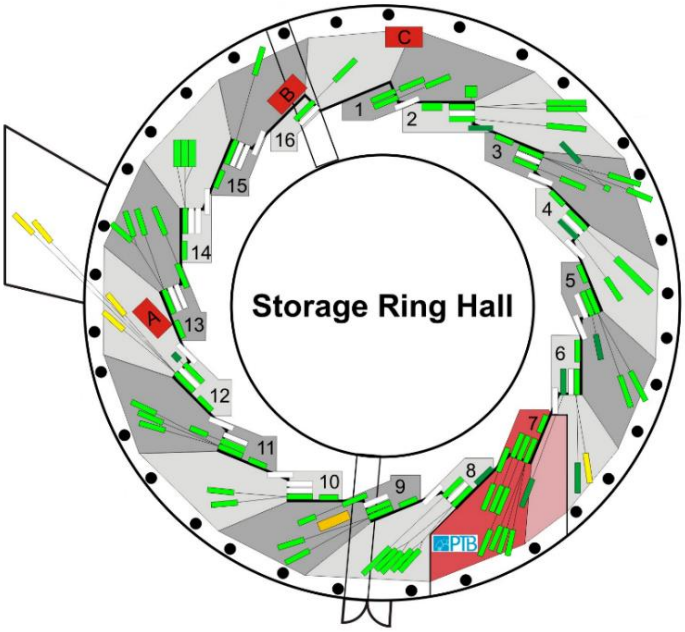

Figure 1.9 – Floorplan scheme of the BESSY II synchrotron facility [18].

Due to requiring a continuous energy spectrum and high X-ray flux, most XAS experiments are performed at synchrotron radiation sources. In these particle accelerators, electrons produced by an electron source are injected into a linear accelerator, prior having their energy increased in the booster ring. When the energy is sufficient, the electrons are transferred to the storage ring, where a series of bending magnets placed in curved sections forces the particles to keep to a constant circular path inside the ring. As a charged particle's direction of motion is changed by traversing a magnetic field, electromagnetic radiation is emitted, characterized by a continuous energy spectrum over a wide range of wavelengths (from infrared to hard X-rays), high intensity, strong polarization and a pulsed nature. Modern synchrotron facilities also have additional elements placed in the straight sections of the ring called insertion devices. These are constituted by a series of alternating magnetic fields that force the electron beam to perform either strong (wiggler) or gentle (undulator) oscillations. Wigglers emit a broad beam of incoherent radiation characterized by increased intensity and a continuous energy spectrum reaching much higher energies than those obtained from a bending magnet. Undulators emit a narrow beam of coherent radiation with amplified intensity at certain wavelengths. Electromagnetic radiation is delivered to experimental stations by beamlines, the

source of which (bending magnet, wiggler or undulator) can be chosen to suit the experimental requirements. Beamlines are also usually configured to meet these requirements, and contain various elements to do so. Mirrors are used to collimate and focus the beam while apertures and slits define its size. A double crystal monochromator is used to select X-rays of a very narrow energy band by using the criterion for Bragg diffraction.

Speaking generally, the absorption coefficient can be measured directly by way of the incoming and transmitted beam intensities (transmission mode) or indirectly by means of the intensity of the incoming beam and of the decay products such as X-ray fluorescence or Auger electrons (fluorescence or electron yield mode). In transmission mode, as used in this work, both the incoming and the transmitted beam, I_0 and I_t, are measured by ion chambers. Detecting the voltage or current generated in the ion chamber counting chain is inherently simpler than detecting single photons with a solid state detector, as is often used in fluorescence mode measurements. Having the same type of detector for both beams also has the advantage of a common energy dependence between them. However, transmission measurements require concentrated samples such that the difference between I_0 and I_t is significantly larger than the variation due to counting statistics. Furthermore, samples must be highly homogeneous, of constant thickness and free of pinholes. Absorption spectra were then obtained by plotting the natural logarithm of the ratio between I_t and I_0.

Room temperature measurements of XANES in transmission mode were performed on the XANES endstation of the KMC-2 beamline [19] at the BESSY II synchrotron radiation source, during two beamtimes. Mixture samples containing ZnSe were measured at the selenium K-edge, while those containing Cu_2SnSe_3 as well as most standards were measured at both the selenium and copper K-edges. The energy of the incident X-ray beam was selected using an Si(111) double crystal monochromator.

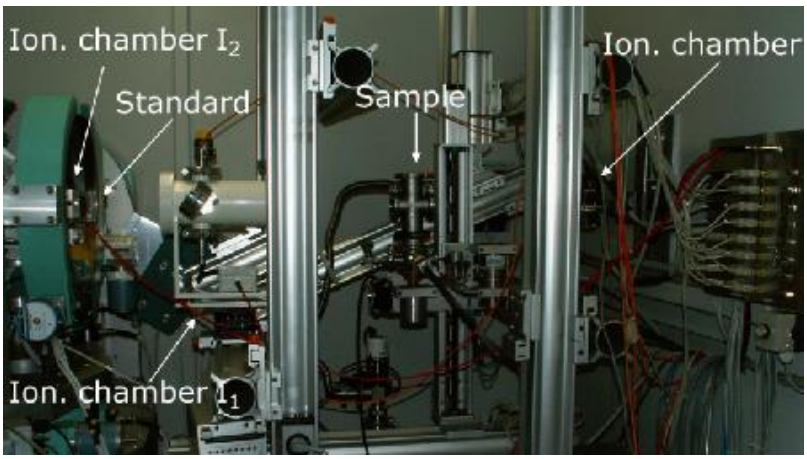

Figure 1.10 – KMC-2 beamline experimental setup for XANES [20].

Theoretical calculations of the fine structure in the XANES region are complex and their accuracy is still very limited. For this reason, analysis typically consists of comparing the measured spectra to those of measured standards and quantifying the ratios by which these are present in the sample using linear combination fitting. A fundamental requirement in this type of analysis is the calibration of the energy scale and the alignment of different spectra. To this end, the known reference used to calibrate the beamline monochromator is measured simultaneously with each sample, which in transmission mode is easily achieved by using the setup shown in Figure 1.11. The reference spectra can then be used to align the energy scales of the sample spectra.

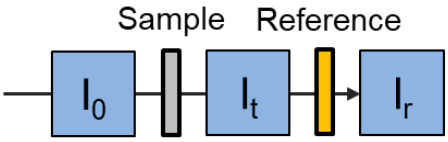

Figure 1.11 – Transmission mode setup. I_0 is the incident beam, I_t and I_r are the sample and reference transmitted beams, respectively.

Data analysis in this work was performed by using the FEFF/IFEFFIT software package, specifically the ATHENA program [21]. In general, analysis is divided into two parts, with the first consisting of the spectra normalization. In the energy region below the absorption edge, each spectrum is fitted by a linear pre-edge line. Above the absorption edge, the spectrum is usually approximated by a linear or quadratic post-edge line. The edge step is defined as the difference between the two lines at the absorption threshold E_0. Normalized spectra are obtained by subtracting the pre-edge line over the whole energy range, dividing by the step height and flattening the spectra above E_0 to account for different slopes of the pre-edge and post-edge lines. The resulting normalized spectrum equals zero below the edge, exhibits a step height of one and oscillates around this value for energies above E_0.

The second part of the analysis is the linear combination fitting (LCF), where sample spectra are compared to those of known standards. The spectrum of an analysed sample is modelled by weighing the spectrum of each considered standard i with a factor x_i and adding them as

$$\mu_{calc} = \sum_i x_i \mu_i$$

This method works well if the number of potential chemical environments for the absorbing atom in the sample, and thus the number of standards, is small and if the spectra from the standards have enough distinguishable features to differentiate between them.

The weight of each LCF standard given by the factor x_i is a measure of the percentage of absorber element atoms bound to the phase of standard i with respect to the total amount found in the analysed sample. The mass percentages of the standards in the sample are therefore not directly determined from the results of the linear combination fitting. To calculate the mass percentage m_i, a relation to the LCF or XANES factor x_i is first established, given by

$$m_i . M = \frac{x_i . Z}{n_i} M_{Pi}$$

where M is the total mass of the sample, Z is the number of absorber element atoms in the sample, n_i is the number of absorber atoms in the elementary cell of phase i and M_{Pi} is the mass of the elementary cell of phase i. From the mass percentage of absorber element in the elementary cell

$$a_i = \frac{n_i . M_A}{M_{Pi}} \Leftrightarrow \frac{M_{Pi}}{n_i} = \frac{M_A}{a_i}$$

where M_A is the atomic mass of the absorber element, a new relation can be found

$$m_i . M = Z . M_A \frac{x_i}{a_i}$$

Adding for all the standards used in the linear combination fitting

$$M = Z . M_A \sum_j \left(\frac{x_j}{a_j}\right) \Leftrightarrow \frac{Z . M_A}{M} = \frac{1}{\sum_j \left(\frac{x_j}{a_j}\right)}$$

and noting from the previous relation that

$$\frac{Z . M_A}{M} = m_i \frac{a_i}{x_i}$$

the mass percentage of phase i is finally found to be determined by

$$m_i = \frac{\frac{x_i}{a_i}}{\sum_j \left(\frac{x_j}{a_j}\right)}.$$

2.3. XANES Data Analysis

The ATHENA program used in the analysis of the XANES data relies heavily on user-defined parameters, meaning that proper results can only be reached by knowing how to choose these correctly. In order to understand the steps taken to process the data in later chapters, a guide on how to use this software will now be presented. The process delineated applies to all manner of spectra measured in transmission mode; however, some edge-specific characteristics require the user's best judgement on how to follow certain steps. Situations of this type for the K-edges used in this work will be referred later on, in their own chapters.

The first step in the data analysis simply consists of importing the data itself. In their most basic form, each sample data file should consist of columns filled with numeric values, a format which Athena should be able to recognize. In the import window, each column must then be identified as I_0, I_t and I_r, in order to produce the reference and sample absorption spectra. This concludes the initial importing process, though additional sample data may always be added later.

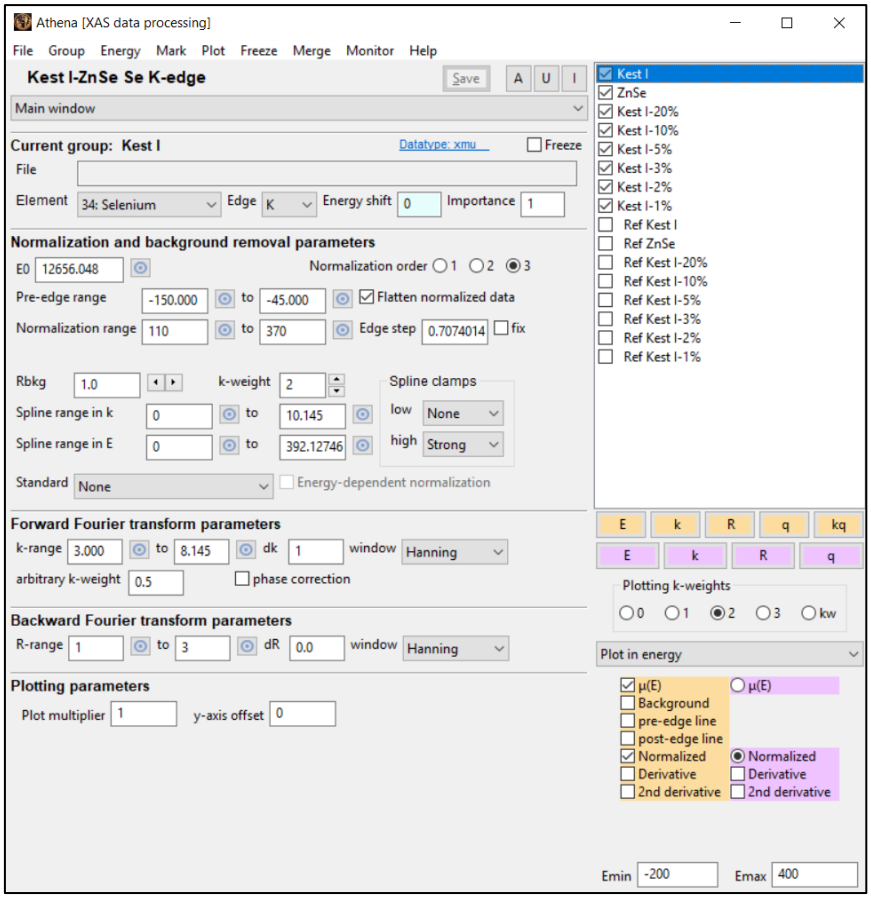

Figure 1.12 – Main window in Athena.

Following the data import is the normalization of the reference spectra in the Main Window (Figure 1.12). At this stage, it is useful to select a random reference spectra as the standard to which all the remaining ones will later be aligned. The objective at this point is to find the pre-edge and normalization range values that provide the best normalized spectra. A useful criteria for choosing the post-edge correctly is that the corresponding line should mostly intersect the middle of the XAFS fluctuations, such that the normalized data oscillates around unit height.

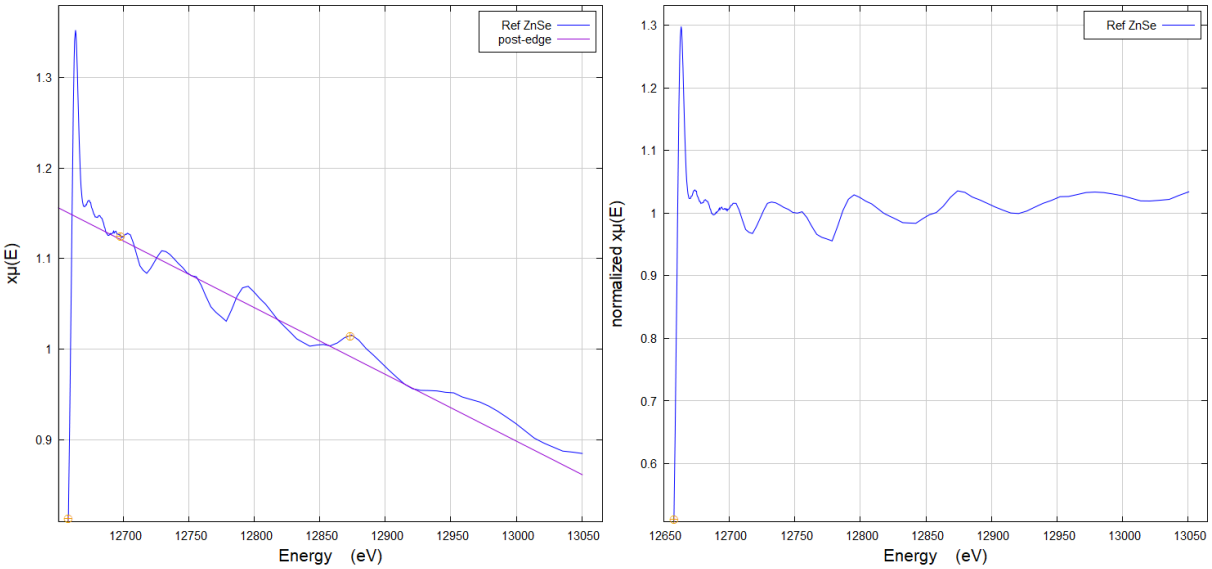

Figure 1.13 – Incorrect choice of post-edge line in the reference spectrum of ZnSe measured at the Se K-edge and resulting poorly normalized data.

The knowledge of the K-edge energy value works as a global reference point among the reference spectra, which is necessary to perform their alignment. Experimentally, the edge position is usually defined as the energy where the normalized data is roughly at half-height (around 0.5), corresponding approximately to the absolute maximum in the spectra's first derivative. However, one will likely find that the normalized standard's energy at this point is different from the theoretical K-edge energy, which means that the measured data from that set requires an energy shift. If the difference is larger than 1 eV, the energy shift should take into account the influence of the monochromator angle θ by using the formulae:

$$\Delta\theta = \theta(E_0') - \theta(E_0)$$

$$\theta_i = \sin^{-1}\left(\frac{hc}{2dE_i}\right)$$

$$E_i' = \frac{hc}{2\mathrm{d}\sin(\theta_i + \Delta\theta)}$$

where E_0' is the theoretical K-edge energy, E_0 is the energy found at half-height, E_i and E_i' are the measured and shifted energy values, respectively, and d is the distance between lattice planes of the crystal monochromator.

Afterwards, the reference spectra's value of E_0 can be changed to the theoretical edge energy in ATHENA's main window, which should now be within 1 eV of the half-height point. With the setting of this point on all the reference spectra, there is now a common marker among all of them with which to correctly perform the alignment that follows. Changing to the "Align data" window, one has to choose their standard and then align the remaining spectra to it. Again, if an alignment shift is bigger than 1 eV, then this should be done using the formulae above. Correctly aligning the reference spectra means that the sample spectra have become aligned as well and therefore ready to be normalized. The considerations at this step are the same as for the references; however, the E_0 value of each sample spectrum should now be chosen so as to match its energy at half-height.

By taking all the previous steps, the spectra are now ready for the linear combination fitting stage. In the proper window, the standards whose presence in the sample should be weighed are chosen, as well as the range for which the fitting should be performed. The resulting fit should be evaluated by the user – the statistical parameters χ^2 and R-factor can be misleading in many cases and are more meaningful in the context of comparing several fits of the same sample, therefore a close look comparing the fitted spectrum to the measured data should be the foremost single fit evaluation method. In cases where the linear combination fit provides unsatisfying results, one should look into the previously chosen normalization or fitting parameters and try different values, or perhaps consider that an additional standard's weight may be missing in the linear combination fitting. [21, 22]

The steps described can be found in the next page in an organized way, so as to streamline the process of using this program.

Import data → Select Numerator (I_0) and Denominator (I_t) → Check "Natural log" → "Data type" μ(E) → Select Reference Channel Numerator (I_t) and Denominator (I_r) → OK

Main Window

1. Choose random reference spectrum as the standard
2. Normalize standard: set pre-edge and post-edge lines
    a. Rule of thumb: post-edge line should intersect the middle of the fine structure fluctuations
    b. Check if ranges work with the other references
3. Set E_0 to theoretical K-edge energy
    a. If difference between K-edge energy and energy at half-height is bigger than 1 eV, shift energy by taking into account the influence of the monochromator angle

Align Data

4. Align each reference spectrum with the standard
    a. If shift is bigger than 1 eV, shift energy by taking into account the influence of the monochromator angle

Main Window

5. Normalize sample spectra
6. Set value of E_0 of each sample to the normalized data's energy at half-height

Linear Combination Fitting

7. Select standards to be weighed
    a. Always reset starting weights with each fit
8. "Fit this group" or "Fit all combinations"
9. Evaluate fit results
    a. Compare fitted spectrum against measured spectrum
10. If fit quality is low, check for possible error inducing parameters

2.4. X-ray Diffraction

X-ray diffraction (XRD) is an analytical technique used to study the crystal structure of materials, able to provide qualitative information on the phases that they contain. The instrument of measurement, the diffractometer, consists of three basic elements: a cathode ray tube, a sample holder and an X-ray detector. The radiation is generated in the evacuated tube, where heating of a tungsten filament results in the emission of electrons. These are then accelerated by application of a voltage towards a copper anode, bombarding it. When the incident particles have sufficient energy, electrons from the inner shells of the anode's atoms are dislodged and characteristic X-ray spectra are generated. Filtering of the spectrum is performed in order to obtain the monochromatic X-ray radiation required for X-ray diffraction, whereby the component with the desired wavelength is selected. The filtered X-rays are then collimated and directed towards the sample, a mass of finely ground polycrystalline powder.

When the incident X-rays penetrate the sample, a signal in terms of a diffraction pattern is detected in the case that the atoms are arranged in a periodic manner, such as what exists in a crystalline material. Diffraction at the atoms can be geometrically considered as the reflection of the X-ray beams at the lattice planes of the material. Constructive interference occurs at specific incident angles for which the path difference of the beam reflected at an array of lattice planes *hkl* of particular lattice spacing *d* is equal to an even multiple *n* of the wavelength λ, resulting in diffraction maxima along the 2θ space and finally creating the entire diffraction pattern. The relationship that translates this condition allows a convenient treatment of X-ray diffraction and is known as the Bragg equation

$$n\lambda = 2d_{hkl} \sin\theta.$$

The diffraction angles θ of all reflections depend on the structural properties, specifically the lattice, and are therefore indicative of the material being measured The Bragg-Brentano geometry of a diffractometer (Figure 1.14) is popular for it rapidness and is commonly used for powder diffraction. Both the X-ray source and detector move along the goniometer circle at the same angular velocity $\vec{\omega}$, sweeping through the full range of angles, with the sample constantly rotating in a fixed point.

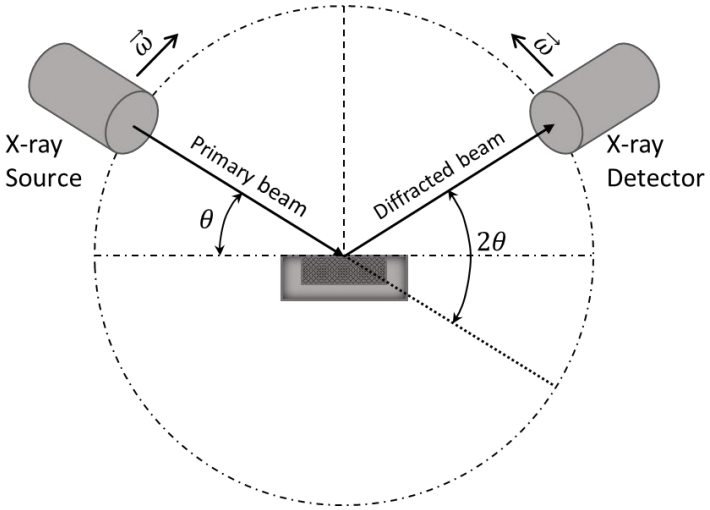

Figure 1.14 – Simplified scheme of the Bragg-Brentano geometry.

For this work, XRD measurements of the eight re-annealed samples were conducted at the Helmholtz-Zentrum Berlin using a PANalytical X'Pert PRO MPD diffractometer operating with copper Kα radiation ($\lambda = 1.54056$ Å). In preparing each sample, we made sure that a smooth flat surface was present at the top of the holder to prevent preferred orientations as much as possible. All the measurements were performed at room temperature with a sample spinner stage where the sample was placed, a range of 2θ from 10° to 140° with 0.0131° step size, with scans running for one and a half hours to produce high resolution patterns. The X-ray source was equipped with a 10 mm mask, a 0.04 rad soller slit and a $\frac{1}{4}^{\circ}$ divergence slit. A PIXcel X-ray detector was used with a P8 anti-scatter slit, a 0.04 rad soller slit and a nickel filter, with the diffractometer operating on a power supply of 40 kV and 40 mA.

Analysis of the diffraction patterns was carried out using the PowderCell software [24]. The procedure consists of adding simulated diffraction patterns, or standards, of compounds that may be present in the measured powders, starting with the main phase – which, for this case, is $Cu_2ZnSnSe_4$. Measurement parameters – the zero shift and background level – are quantified so that the standards match the measured pattern as closely as possible. The shift of the kesterite main phase's lattice parameters is also taken into account. In order to roughly adjust the *a* and *c* parameters, the positions of peaks *400* and *008* are used. Simulated patterns of all the possible secondary phases are added and tested to determine how well their characteristic peaks match those in the pattern. When the presence of a secondary seems possible, an optimization of the measurement and lattice parameters can be performed by the software.

2.5. Wavelength-dispersive X-ray Spectroscopy

With the application of the wavelength-dispersive X-ray spectroscopy (WDX) technique, the chemical characterization of samples under analysis can be performed, providing qualitative and quantitative information on the elements that are part of their compositions. This is achieved by using an electron microprobe analyser (EMPA) unit, which irradiates an electron beam onto the surface of the sample being analysed and measures the characteristic X-rays that are generated in the process. When a material is bombarded by an electron beam with energy that is high enough to interact with the innermost shells of its atoms, bound electrons can be scattered, consequently leaving a vacancy in their former shell. This state is unstable and therefore the vacancy is quickly filled by an electron from an outer shell. The transition to a lower energy level causes the emission of a photon whose energy equals the difference between the two energy levels, and for a transition to the K shell this energy is in the X-ray region of the electromagnetic spectrum. Since each element has a unique electronic structure, investigating the wavelength or energy of the radiation emitted in this process leads to the identification of the elements present in the sample's composition.

An EMPA unit is equipped so that signals from characteristic X-rays and backscattered electrons (BSE) can be measured by appropriate detectors. X-rays can be measured by either wavelength-dispersive or energy-dispersive X-ray spectroscopy (EDX) – WDX sorts the radiation according to wavelength by using Bragg diffraction from several diffraction elements to separate and select wavelengths of interest, which are then directed to proportional detectors; EDX makes use of a solid state semiconductor detector to convert the energy of X-rays produced by the sample into electrical voltages of proportional magnitudes, the originated pulses are therefore correlated to the characteristic X-rays. Though EDX can perform analysis on multiple elements simultaneously with a short counting time, WDX usually provides more precise measurements with lower detection limits because of its superior peak resolution and better peak-to-background ratio, meaning that the overlap between peaks of similar energies is much smaller. Besides this, an EDX system also has lower count rates and poor reproducibility, whereas an WDX system tends to have a count rate about ten times higher, making it a better a better choice for reliable quantitative analysis. [25]

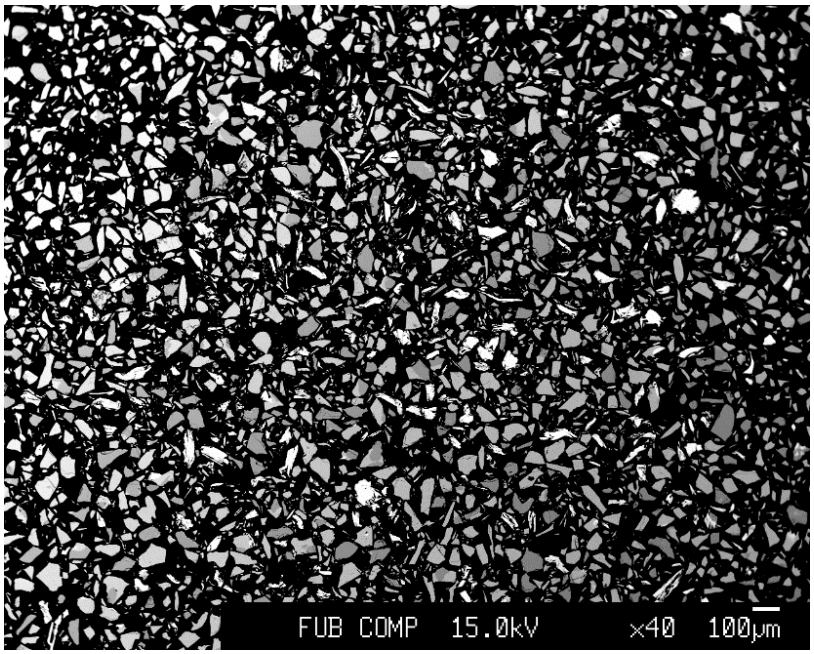

Figure 1.16 – Backscattered electron micrograph showing variety of shades in the grains.

With the backscattered electron detector of the EMPA unit, micrographs of the sample's surface can be quickly obtained with a range of possible magnifications. Heavy atoms – with higher atomic number *Z* – scatter electrons more strongly than lighter elements, thus a BSE image allows a preliminary identification of different phases when a distinguishable contrast between the grains is observable. Prior to the measurements, small areas of the sample's surface are first analysed through the BSE detector so that intact grains of different shades – and in principle, compositions – can be purposefully marked to be measured, ensuring that the data obtained will be as close as possible to a complete representation of the sample's structural and chemical contents. Each imaged area of the sample's surface is saved, serving as the sample map where every grain that will be measured is numbered. After an optical microscope is used to make sure that the surface of the sample is in focus, all the measurement lines are set in a way that the electron beam only hits the surface of the grains, to avoid values influenced by interstitial spaces.

To perform the compositional and phase analysis of the re-annealed samples, EPMA-WDX measurements were performed at the Institute of Geological Sciences of Freie Universität Berlin, using a JEOL JXA 8200 SuperProbe EPMA unit. Randomly collected portions of each powder sample were put into small vials, to be embedded in an epoxy matrix, flattened into a sample holder, and mechanically polished to achieve a clean surface. Prior to the measurements, a conductive carbon film was deposited on the surface of the sample holders, using a Leica EM SCD 500 carbon evaporation device, to prevent damage from the electron

beam to the samples. The calibration of the WDX measurements was done by choosing crystal standards of Cu, Zn, Sn and Se, splitting them among three available channels and then performing an element peak search to evaluate the configured setups.

To achieve high accuracy of the compositional parameters, lines consisting of ten to fifteen measurement points were set within each grain and around 55 to 60 grains were measured in every sample. Points with total mass and atomic percentages too far from 100% were filtered out and every grain's elemental ratios were compared against one another to eliminate those that were clearly deviations from the rest, averaging over the remaining points. Grains with similar percentages of elements were considered as belonging to the same phase, grouped and averaged over, so that information on each measured phase and their composition was obtained.

3. XANES analysis of Mixture samples

In this chapter, the XANES data measured from the mixture samples is analysed. The first sections deal with the investigation on the detection limits for the two secondary phases. Steps taken in processing each set of data are presented, leading up to the results of the analysis, from which conclusions are then drawn.

3.1. Analysis of Kest II-CTSe mixtures measured at the Cu K-edge

Analysis of the Kest II-Cu_2SnSe_3 mixtures started by performing a preliminary normalization of the data's reference spectra. The normalized standard's energy at half-height was found to be 8980.671 eV. It was thus required to shift the raw data's energy by -1.671 eV while taking into account the influence of the monochromator angle, according to the procedure described in Chapter 2.3, to match the energy at half-height to the theoretical Cu K-edge energy value of 8979 eV [21].

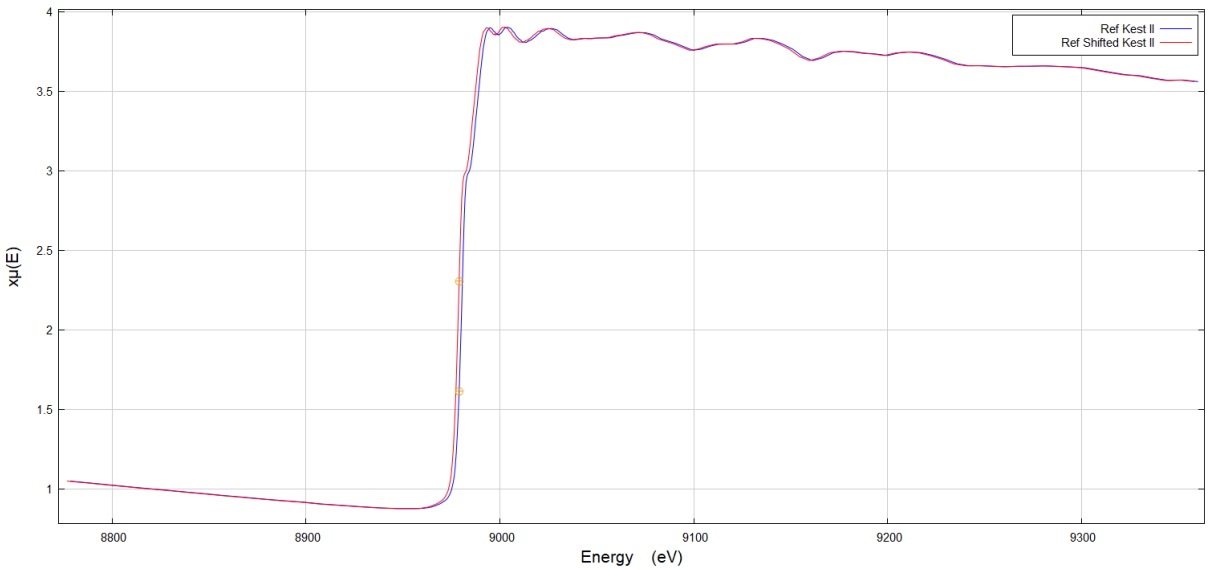

Figure 3.1 – Comparison between the raw and shifted data of the Kest II-CTSe mixtures set measured at the Cu K-edge, using the Kest II reference spectrum as an example.

With the shifted data, the reference spectra were normalized with a quadratic polynomial using a normalization range from 47 to 304 eV, so as to have the post-edge line intersect the XAFS fluctuations mostly through the middle. The intention was that the normalized reference spectra would have their fluctuations around unit height while also seemingly growing less intense as the energy increased. A pre-edge range from -190 to -45 eV was chosen.

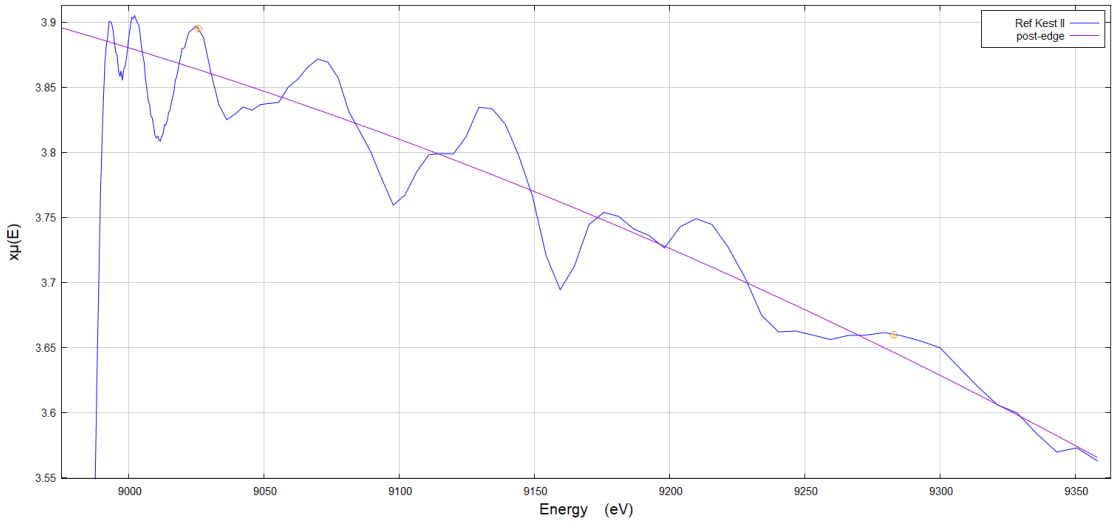

Figure 3.2 – Post-edge line on the Kest II reference spectrum measured at the Cu K-edge.

In order to study the effect of the normalization choice on the quality of the LCF results and choose the most appropriate one, three different normalization ranges were tested. The criteria for how to set the range values was based on the position of the post-edge line relative to the fine structure fluctuations. These can be described as follows:

1. The post-edge line intersects as many fluctuations through the middle as possible;
2. The post-edge line leaves out most of the fluctuations immediately succeeding the absorption edge;
3. The post-edge line is adjacent to the third fluctuation succeeding the edge, ignoring the preceding ones.

The parameters of each normalization and examples of the corresponding post-edge lines and normalized spectra are shown below.

	Normalization 1	Normalization 2	Normalization 3
Pre-edge range	-190 to -45 eV	-190 to -45 eV	-190 to -45 eV
Normalization range	110 to 37 eV	198 to 350 eV	94 to 360 eV
Polynomial order	2nd	2nd	2nd

Table 3.1 – Parameters of each normalization choice applied to sample spectra measured at the Cu K-edge.

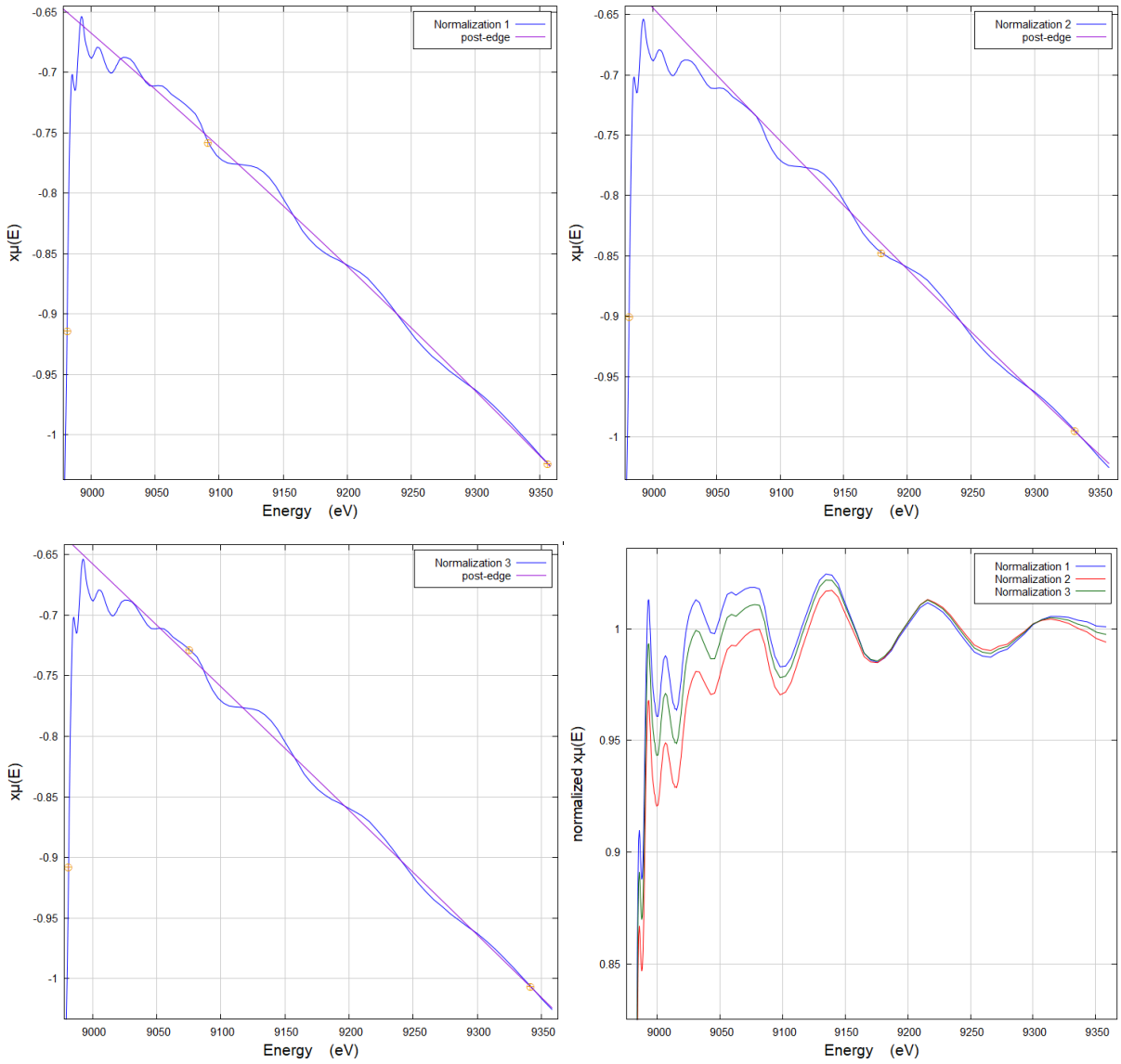

Figure 3.3 – Post-edge lines of each normalization and normalized spectra for sample spectra measured at the Cu K-edge, using the Kest II sample spectrum as an example.

The linear combination fitting was performed for each sample with all three normalizations applied and using the Kest II and the Cu_2SnSe_3 sample spectra as standards, over a range of -20 to 50 eV relative to the edge position. The evaluation of the results was primarily based on comparing the closeness of the fitted spectra to the measured data, with statistical parameters and phase weight percentages being consulted for additional information when adequate. To have a clear way of discerning between normalization alternatives, the weight percentages of Cu_2SnSe_3 obtained by LCF were plotted graphically, as seen in Figure 3.4.

Looking at the fits obtained from applying the second normalization to the spectra shows that these are usually the ones furthest from the experimental data – something also indicated from having the highest R-factors – and, indeed, weight percentages of the ternary phase are either overestimated or considered non-existent when using this normalization range. The first and third normalizations produce fitted spectra of very similar quality, as well as R-factors. In such cases, it is acceptable to consider the weight percentages of Cu_2SnSe_3 obtained as the criteria for choosing between the two normalizations. While results from the third normalization only detect the presence of secondary phase at 20%, results from the first normalization already detect the presence of Cu_2SnSe_3 starting from 5%, with the weight percentage determined at 20% concentration being actually closer to the real value. Taking everything into consideration, the first normalization, which intersects most of the fine structure fluctuations, was determined to be the best choice to analyse the CTSe mixtures measured at the Cu K-edge.

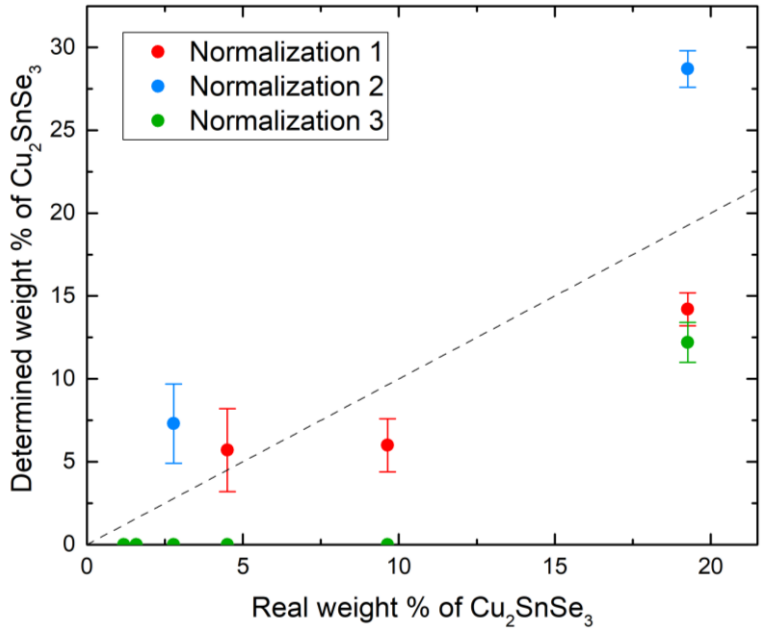

Figure 3.4 – Weight percentages of CTSe determined by LCF of the spectra measured at the Cu K-edge, for each normalization range applied.

Focusing on the results obtained with the chosen normalization range shows that the presence of the ternary only starts to be measurable at a concentration of about 5%, as stated before. Weight percentages determined after this point are somewhat far from the real values and get further away as the concentration increases, suggesting that quantification of the CTSe phase with this method is impossible. However, it can be concluded that the XANES detection limit for Cu_2SnSe_3 in CZTSe is found at 5% concentration when measuring at the Cu K-edge.

Sample	Real CTSe %	XANES CTSe %	Error %	Determined CTSe %	Error %	Absolute Error (%)
Kest II - 20%	19.26(2)	17.6	1.4	14.2	1.0	5.1
Kest II - 10%	9.64(1)	7.6	2.2	6.0	1.6	3.7
Kest II - 5%	4.50(1)	7.2	3.3	5.7	2.5	1.2
Kest II - 3%	2.78(1)	0.0	0.0	0.0	0.0	2.8
Kest II - 2%	1.58(1)	0.0	0.0	0.0	0.0	1.6
Kest II - 1%	1.18(1)	0.0	0.0	0.0	0.0	1.2

Table 3.2 – Results from LCF analysis of the Kest II-CTSe mixtures' spectra measured at the Cu K-edge.

It is interesting to look now at the normalized spectra of the standards used in this section and compare them with the considerations made about the environment surrounding the copper atoms in each structure. In Figure 3.5, it can be observed that the XANES region of the Cu_2SnSe_3 spectrum shows almost the same energy dependence as that of Kest II. Although there are some differences, these seem to be mostly restricted to the maxima and are not of a very high degree. Such localized differences could probably be expected from the highly homogeneous surroundings of both samples, as previously stated. Nevertheless, in spite of the low contrast between the spectra, a 5% concentration of CTSe in CZTSe can already be detected.

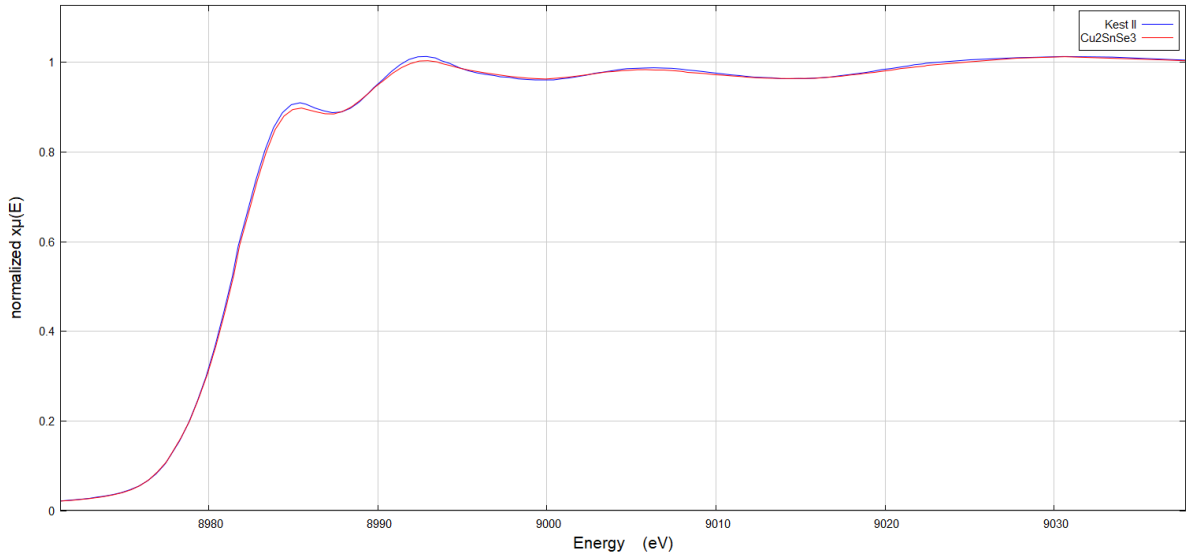

Figure 3.5 – Comparison between the XANES regions of the Kest II and CTSe normalized spectra measured at the Cu K-edge.

3.2. Analysis of Kest I-ZnSe mixtures measured at the Se K-edge

Through the preliminary normalization of the reference spectra it was determined that the normalized standard's energy at half-height was located at 12646.23 eV. The raw data therefore required a shift of 11.77 eV that took into account the influence of the monochromator angle, according to the procedure described in Chapter 2.3, to place the energy at half-height at the theoretical Se K-edge energy value of 12658 eV [21].

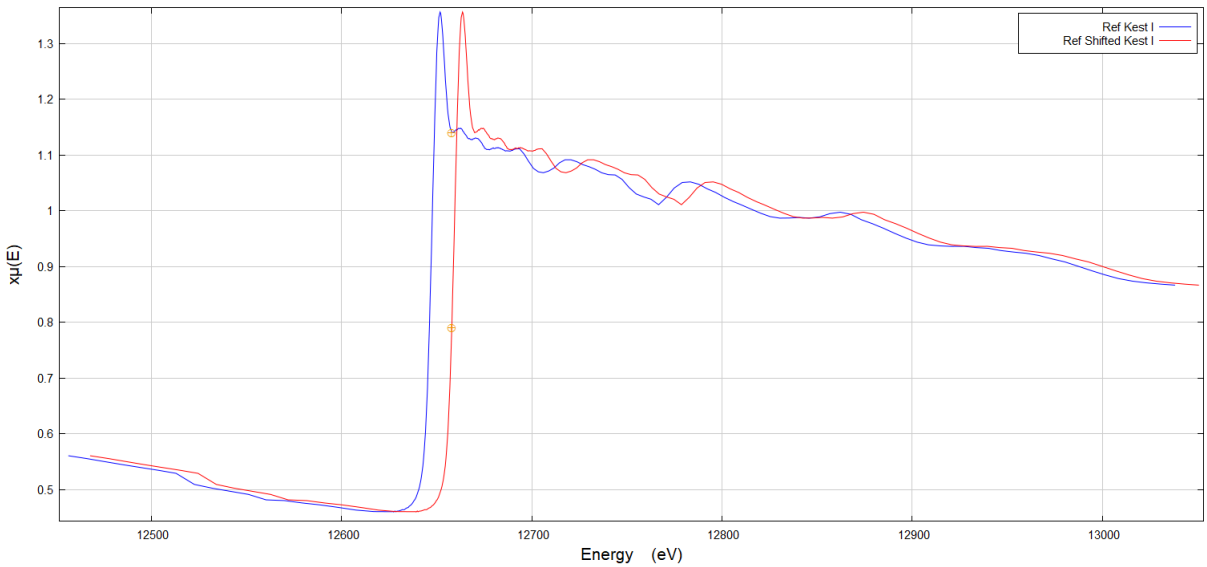

Figure 3.6 – Comparison between the raw and shifted data of the Kest I-ZnSe mixtures measured at the Se K-edge, using the Kest I reference spectrum as an example.

Using the shifted data, the normalization of the reference spectra was performed once more. Because the absorption close to the edge in selenium rises much higher than in copper, a quadratic polynomial in a normalization range from 145 to 366 eV was chosen. The objective in defining this post-edge range was that the corresponding line would be below the higher fluctuations just after the edge, while still following the rising trend of the last one and intersecting those in between through the middle. For the pre-edge, a range from -150 to -35 eV was used.

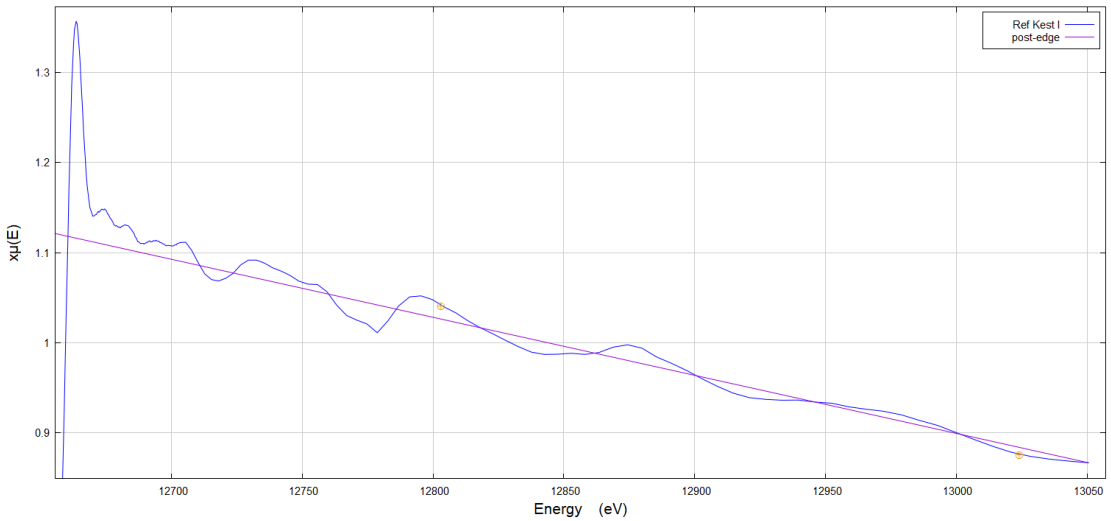

Figure 3.7 – Post-edge line on the Kest I reference spectrum measured at the Se K-edge.

The reference spectrum of Kest I showed some deviations from the rest of the data group in the pre-edge region (Figure 3.8), however, there was no way to match it to the other reference spectra without causing more serious misalignments. In the end, the objective at this stage is only to have aligned reference spectra, which was still accomplished by ignoring these deviations.

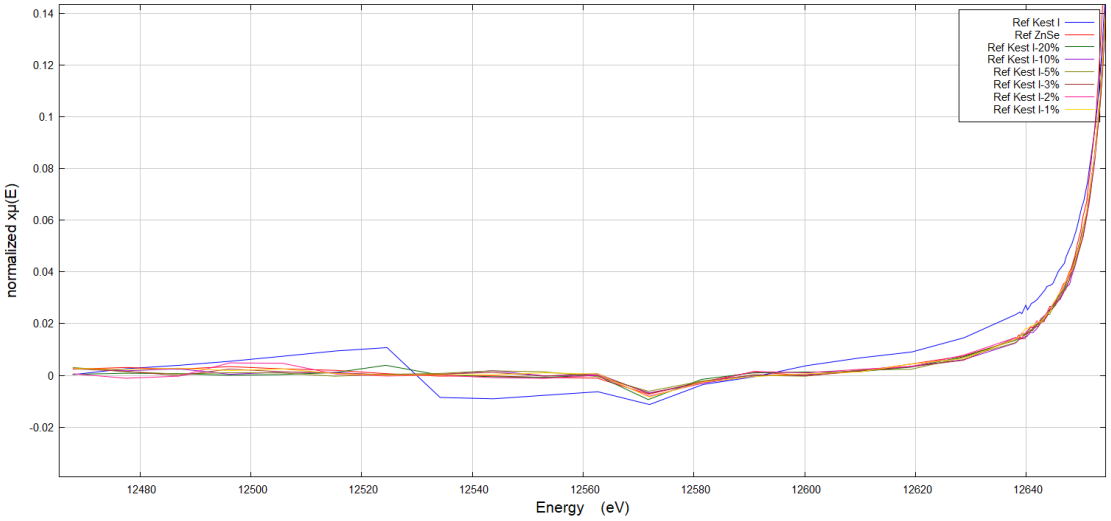

Figure 3.8 – Deviations of the Kest I reference spectrum in the pre-edge region.

Proceeding to the normalization of the sample spectra, three normalization ranges were tested as was done for the previous Cu K-edge measurements. The criteria for how to set each normalization range continue to be the same as before. In spectra measured at this edge, however, it really is impossible to intersect every single fluctuation due to the much higher absorption observed close to the edge, which means that the post-edge line will always be positioned in a way that it goes under first fluctuations after the edge. The parameters of each normalization and examples of the corresponding post-edge lines and normalized spectra are shown below.

	Normalization 1	Normalization 2	Normalization 3
Pre-edge range	-150 to -45 eV	-150 to -45 eV	-150 to -45 eV
Normalization range	120 to 315 eV	110 to 370 eV	165 to 385 eV
Polynomial order	1st	2nd	1st

Table 3.3 – Parameters of each normalization choice applied to sample spectra measured at the Se K-edge.

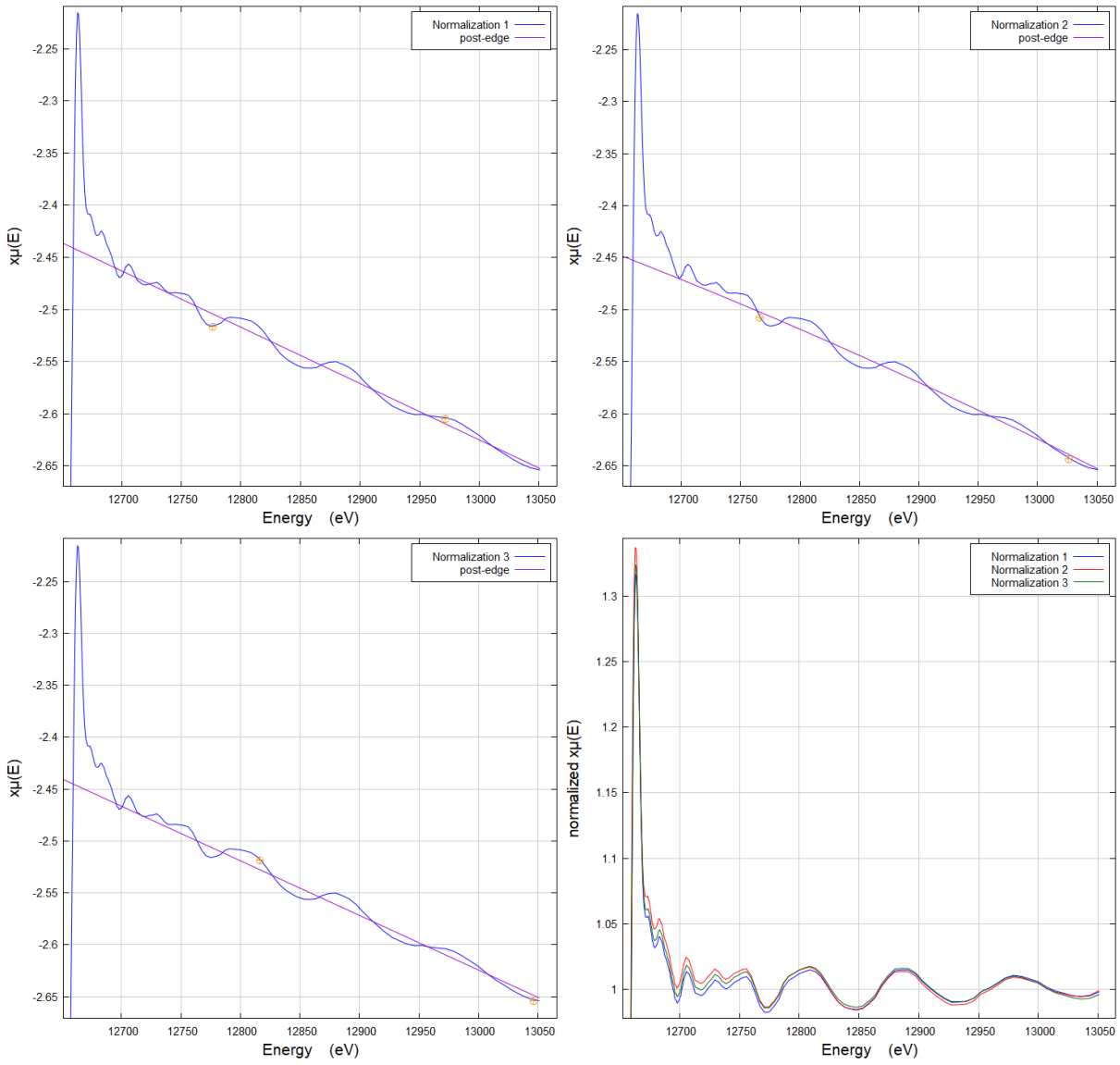

Figure 3.9 – Post-edge lines of each normalization and normalized sample spectra plotter together, using the Kest I spectrum as an example.

The linear combination fitting was performed for each sample with all three normalizations applied and using the Kest I and the ZnSe spectra as standards, over a range of -20 to 50 eV relative to the edge position. Evaluation of the results was carried out in the same way as before.

In general, there is not a lot of distinction across fitted spectra obtained by applying the different normalizations. Additionally, all fits match the measured data to a satisfying degree, even to the point where it is hard to identify common areas of poor fitting among normalization alternatives for each sample. It could be hypothesised that this, together with the proximity of the determined ZnSe weight percentages to the real values that is also observed for every concentration (Figure 3.10), is an indication that XANES is a good method to detect the ZnSe phase in CZTSe. A high contrast between the spectra of both phases that should make the presence of ZnSe distinguishable is then also likely to make the method more impervious to a less ideal normalization, since the presence of ZnSe is still identified in the same way regardless of this choice. Ultimately, the second normalization was chosen to analyse the ZnSe mixtures measured at the Se K-edge, on the basis that its application produces the weight percentages closest to the real values.

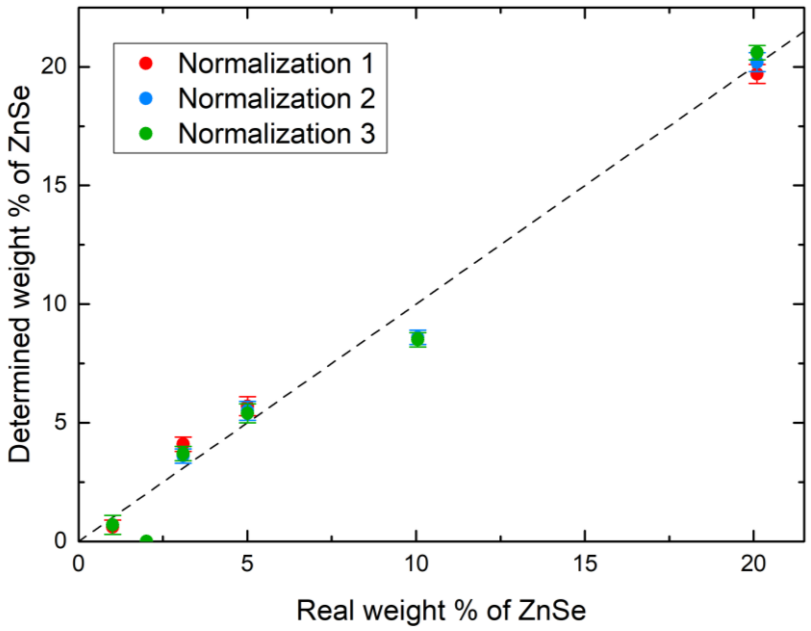

Figure 3.10 – Weight percentages of ZnSe determined by LCF of the spectra measured at the Se K-edge, for each normalization range applied.

Concentrating on the chosen normalization's results alone, it is clear that detection of the ZnSe phase appears to be possible at all concentrations. The lack of detection at 2% could potentially be justified due to statistical effects, wherein the pellet or even the small area of which is hit by the X-ray beam simply had a low concentration of ZnSe from the time of its preparation; this possibility seems plausible when considering the strong detection still seen at 1%. Indeed, the actual weight percentages obtained are close enough to the real values to conclude that even quantification of the ZnSe phase in CZTSe with small relative error is possible across all concentrations, when measuring at the Se K-edge.

Sample	Real ZnSe %	XANES ZnSe %	Error %	Determined ZnSe %	Error %	Absolute Error (%)
Kest I - 20%	20.10(2)	21.5	0.5	20.2	0.4	0.1
Kest I - 10%	10.05(1)	9.3	0.3	8.6	0.3	1.4
Kest I - 5%	5.01(1)	5.9	0.4	5.5	0.4	0.5
Kest I - 3%	3.10(1)	3.9	0.3	3.6	0.3	0.5
Kest I - 2%	2.01(1)	0.0	0.0	0.0	0.0	2.0
Kest I - 1%	1.01(1)	0.8	0.4	0.7	0.4	0.3

Table 3.4 – Results from LCF analysis of the Kest I-ZnSe mixtures' spectra measured at the Se K-edge.

At this point, the characteristics that distinguish the normalized spectrum of the kesterite standard from that of the secondary phase investigated are again looked into. As expected, given the very different surroundings of the selenium atoms in the two structures, observing Figure 3.11 shows that the ZnSe spectrum is very distinct from that of Kest I throughout most of the XANES region. Such a difference could be looked at as an indication that it would be easy to weight the influence of this phase on the mixture spectra and, as mentioned above, as a feature that would make the choice of normalization less impactful.

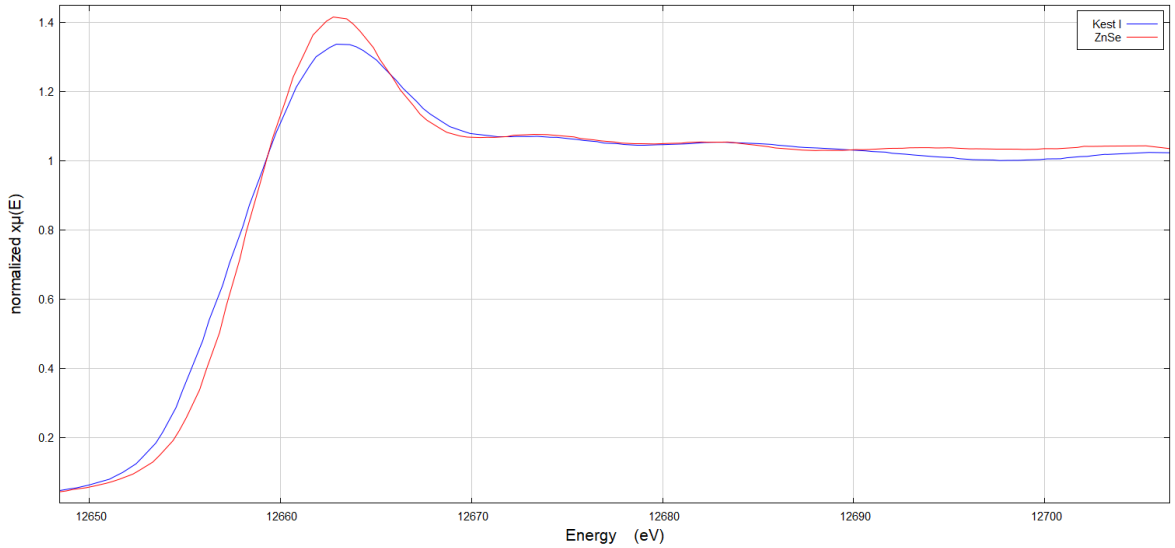

Figure 3.11 – Comparison between the XANES regions of the Kest I and ZnSe normalized spectra measured at the Se K-edge.

3.3. Analysis of Kest II-CTSe mixtures measured at the Se K-edge

The usual preliminary normalization of the reference spectra revealed that the standard's energy at half-height was located at 12645.967 eV, a slightly lower value than the one found for the data group of the ZnSe mixtures also measured at this edge. This meant that a shift of 12.033 eV taking into account the influence of the monochromator angle was necessary for this data group, according to the procedure described in Chapter 2.3, to place the energy at half-height at the theoretical Se K-edge energy value of 12658 eV [21].

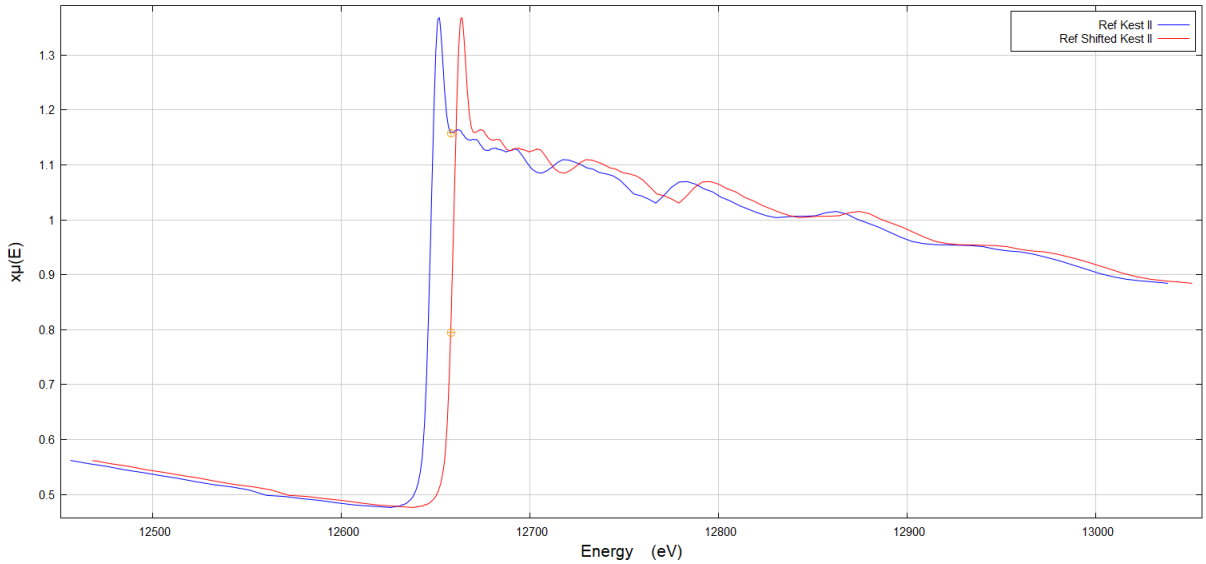

Figure 3.12 – Comparison between the raw and shifted data of the Kest II-CTSe mixtures measured at the Se K-edge, using the Kest II reference spectrum as an example.

Being measured at the same edge, the normalization applied to the reference spectra of the shifted data was identical to that applied to the ZnSe mixtures data. For the same reason, the normalization test on the sample spectra was also performed with the same normalization ranges, taking notice that application of the same ranges was still able to provide well normalized sample spectra. The LCF was performed for each sample using the Kest II and the CTSe spectra as standards, over a range of -20 to 50 eV relative to the edge position.

Evaluation of the results obtained from the LCF analysis reveals a situation different from what was observed in the previous section. Fitted spectra across normalization options are still without much distinction and match the measured data to a high degree. Similarly, Figure 3.14 shows that the determined weight percentages of CTSe are close to each other at concentrations for which the phase is detected, but these weight percentages are now also much further from the real values. Regardless, the spectra obtained from application of the third normalization can be identified as the slightly poorer fits to the measured data, which is also

indicated from having the highest R-factors. The fit quality from the first and second normalizations are near indistinguishable, so the first one was chosen by using the criterion of which one generally results in the weight percentages closest to the real values.

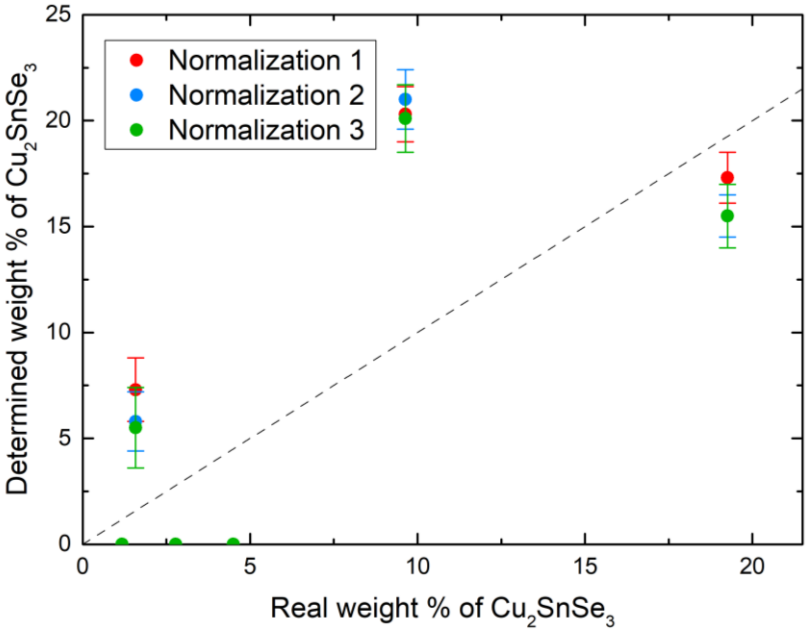

Figure 3.14 – Weight percentages of CTSe determined by LCF of the spectra measured at the Se K-edge, for each normalization range applied.

The weight percentages obtained with the chosen normalization show that the presence of CTSe is measurable at 2% and above 10%. The lack of detection at 3% or 5%, however, suggests detection below those concentrations is not very precise and therefore 10% would be the actual detection limit. Quantification at 10% is impossible due to the highly overestimated percentage determined. With the relative error of the percentage determined at 20%, quantification appears to be more plausible, but the lack of a logical trend in the results and spread of results from the normalizations suggests that it may lack precision. In the end, it can be concluded that the detection limit of XANES for Cu_2SnSe_3 in CZTSe is located at 10% when measuring at the Se K-edge, possibly with a limited quantification capacity at 20%.

Sample	Real CTSe %	XANES CTSe %	Error %	Determined CTSe %	Error %	Absolute Error (%)
Kest II - 20%	19.26(2)	16.9	1.4	17.3	1.2	2.0
Kest II - 10%	9.64(1)	19.9	1.5	20.3	1.3	10.7
Kest II - 5%	4.50(1)	0.0	0.0	0.0	0.0	4.5
Kest II - 3%	2.78(1)	0.0	0.0	0.0	0.0	2.8
Kest II - 2%	1.58(1)	7.1	1.6	7.3	1.5	5.7
Kest II - 1%	1.18(1)	0.0	0.0	0.0	0.0	1.2

Table 3.5 – Results from LCF analysis of the Kest II-CTSe mixtures' spectra measured at the Se K-edge.

A close look at the Kest II and CTSe spectra used as standards in this section shows that they have almost the same energy dependence, similarly to what was observed for the spectra of these samples measured at the Cu K-edge. There is, however, a higher degree of distinction particularly in the region of the rising edge and at the absorption maximum, which is expected given that the surroundings of the selenium atoms are slightly more different in the two structures compared to the copper atoms. Unlike the case of ZnSe, where many fine structure fluctuations that have no match in the Kest I spectra are observed and the degree of distinction is very large, what is observed for CTSe might explain why results do not reach the same level of precision and, more notably, why detection is not possible at secondary phase concentrations lower than 10%.

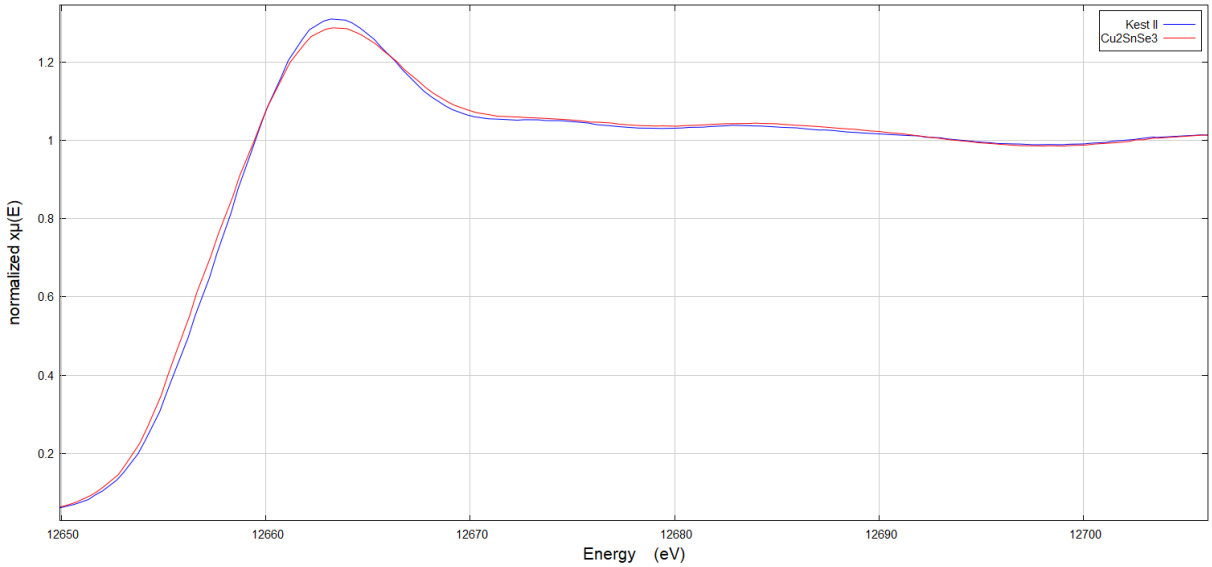

Figure 3.15 – Comparison between the XANES regions of the Kest II and CTSe normalized spectra measured at the Se K-edge.

3.4. Additional secondary phase standards

Investigation with the XANES method under real-world conditions implies taking into consideration the existence of multiple secondary phases in the samples measured. Therefore, it is important to test how robust the method's detection capacity is under such conditions, when there is some certainty regarding the contents of the samples being analysed. To this end, the LCF analysis performed in the previous section was repeated with additional secondary phase standards considered in the linear combination fitting of the spectra, with evaluation of the results comparing the quality of the fits and the determined Cu_2SnSe_3 or ZnSe weight percentages to the original ones.

Starting with the Kest II-CTSe mixtures measured at the Cu K-edge, the secondary phase standards added to the analysis of this set of samples were CuSe and Cu_2Se. To have an idea of how these specific phases may be relevant to the objective of this section, Figure 3.16 shows the XANES regions of the normalized sample spectra of all standards used in the analysis. As observed previously, the spectra of Kest II and CTSe are quite similar, especially in their energy dependence. The spectra of CuSe and Cu_2Se, on the other hand, are quite different from each other and from the original standards, showing several large differences in the lower energy regions but also some noticeable separation for higher energies. Results from LCF analyses weighing standards with distinctions as large as these should serve as good gauges of upper-end sensitivity.

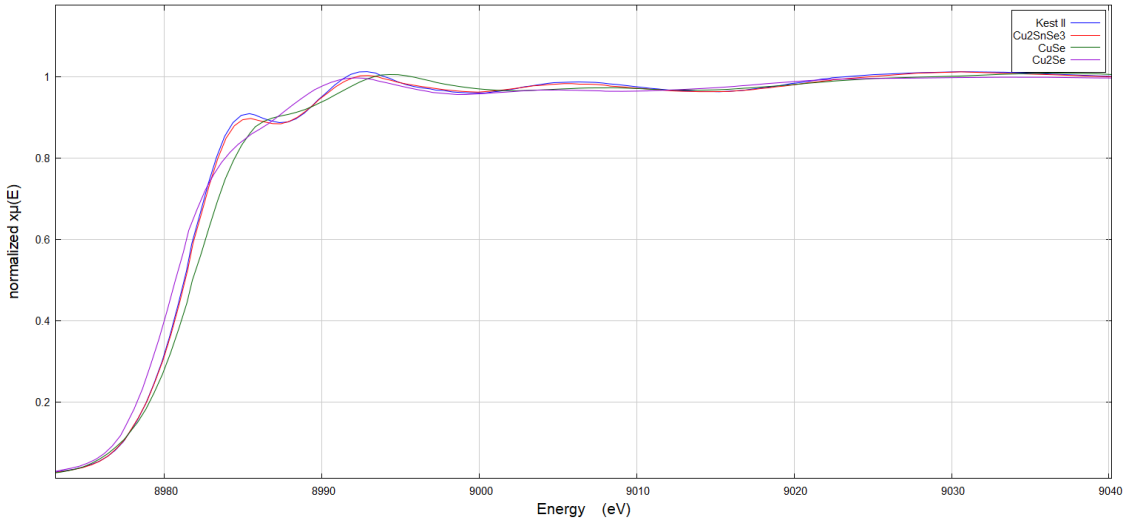

Figure 3.16 – Comparison between the XANES regions of the Kest II, CTSe, CuSe and Cu_2Se normalized spectra measured at the Cu K-edge.

Fit quality among sets of standards used is very comparable, making it almost impossible to indicate fits worse than the original ones. The CTSe weight percentages obtained for each LCF performed are presented in Figure 3.17. Detection of CTSe continues to only occur after 5%, and weight percentages obtained with the Cu_2Se standard added in the analysis are very close to the previously determined values, however, the additional secondary phase is also detected after the 5% sample though at concentrations no higher than 0.5%. Results with the CuSe phase added are dramatically different, with CTSe percentages increasing as much as 4%, although no CuSe is detected in any of the samples. This means that the percentages of CTSe determined were influenced by having the analysis consider the presence of the additional standard even if in the end it was never detected, which implies that one should be careful with such results when using this method.

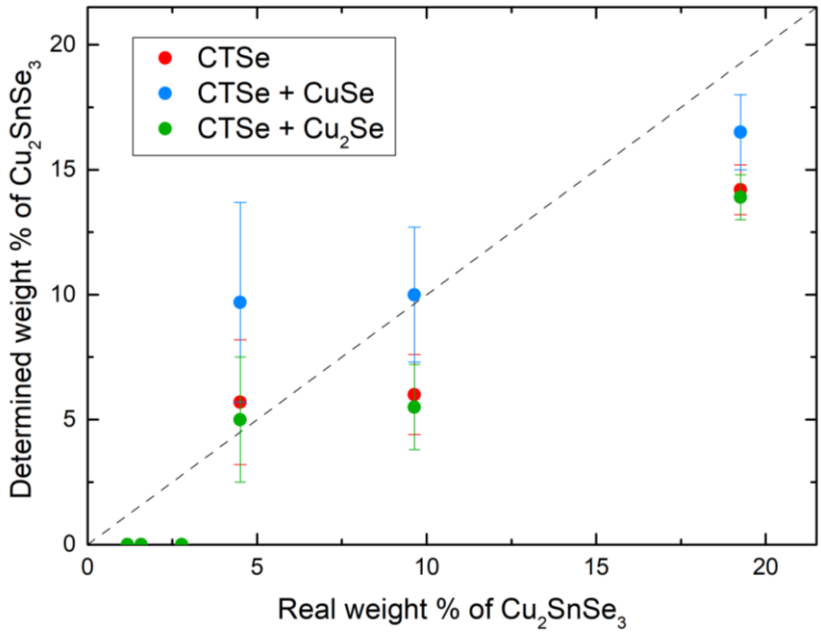

Figure 3.17 – Weight percentages of CTSe determined by LCF of the spectra measured at the Cu K-edge, for each secondary phase standard added.

The fact that only Cu_2Se was detected in this section could mean that the XANES region of its spectrum has enough similarities with the spectra of Kest II and CTSe to be mistakenly detected by LCF analysis, and looking at Figure 3.16 shows that it is closer to them than the spectrum of CuSe. However, there is also the possibility that the mixtures actually have some concentration of the Cu_2Se phase. The compositions of the Kest II and CTSe powder were analysed by WDX and found to be homogenous, but the accuracy of this method of analysis is very dependent on statistical factors since only select grains have their composition determined. Therefore, it is not impossible that existing secondary phases are missing from the group of selected grains or even from the amount of powder extracted for the measurements, particularly

if their concentrations are small. The low weight percentages determined for the Cu_2Se phase could support this possibility, but their detection in every sample would likewise go against a statistical explanation. Because of these factors, it is difficult to make hard conclusions about the detection of Cu_2Se. In the end, it can still be concluded that the detection capacity of CTSe in CZTSe at the Cu K-edge wasn't damaged from the introduction of multiple standards, since the detection limit is still observed at 5%.

The secondary phase standards added to the analysis of the Kest I-ZnSe mixtures measured at the Se K-edge were CTSe, Cu_2Se and SnSe. To again form an idea on how these specific phases may be useful to the objective of this section, Figure 3.18 shows the XANES regions of the normalized sample spectra of the standards used. Observations regarding the comparison between the ZnSe and Kest I spectra have already been exposed, and the CTSe spectrum shows the same lower degree of differences as when compared to Kest II. The spectrum of Cu_2Se is somewhat comparable to ZnSe in some small regions, but the spectrum of SnSe is completely apart from any of the others. So two of the additional secondary phases are close to either the Kest I or ZnSe spectrum and the other one is very different from any of them, which consist of good conditions for this study.

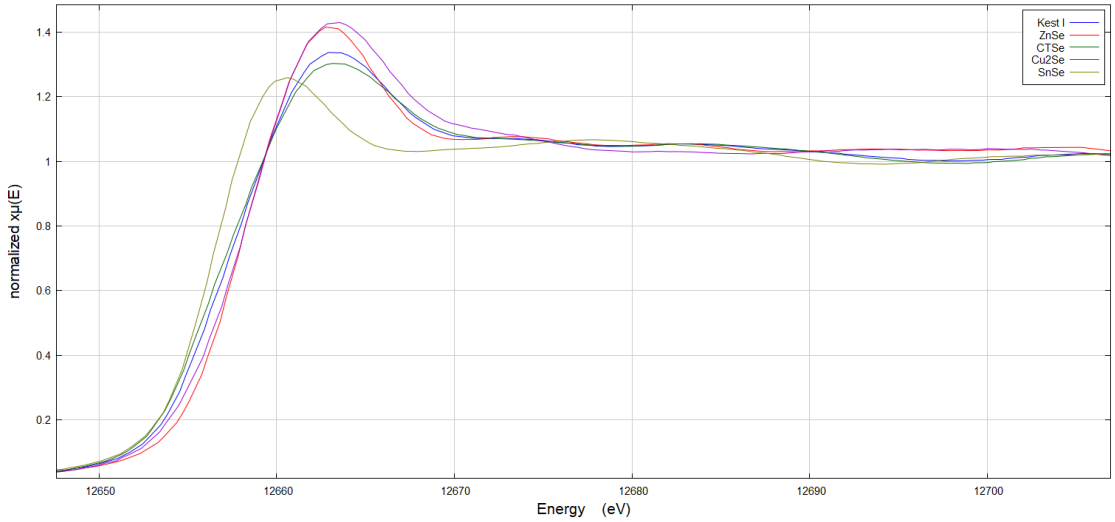

Figure 3.18 – Comparison between the XANES regions of the Kest I, ZnSe, CTSe, Cu_2Se and SnSe normalized spectra measured at the Se K-edge.

Fit quality among sets of standards used is also very comparable this time, which again makes it hard to indicate fits worse than the original ones. The ZnSe weight percentages obtained for each LCF performed are presented in Figure 3.18. Weight percentages of ZnSe obtained with the addition of the Cu_2Se and the SnSe standards are very close to the original values, and even though no Cu_2Se is detected in any of the samples, the ZnSe percentages only changed by negligible amount. Detection of the SnSe phase occurs between the 3% and 10%

sample and reaches 1%, which is surprising given that its spectrum is the most different among standards, but because the same statistical explanation used above could be applied here, conclusions cannot be drawn. Results with the CTSe phase added are the most distinct – ZnSe weight percentages above the 10% sample remain almost equal, where there is no CTSe detected; but below this point they increase by as much as 6%, which is accompanied by the detection of the CTSe phase at weight percentages ranging from 10.4% to 18.2%, at its highest. Results with this standard cannot be entirely explained by an incomplete data in the WDX analysis since the weight percentages determined for CTSe are higher than the already overestimated percentages of ZnSe. This means that a false detection of CTSe is occurring at a high degree for these, accompanied by an overestimation of the ZnSe phase concentration. The closeness between the CTSe and Kest I could be a better explanation for what is observed but whatever the reason may be, it is clear that XANES analysis of the ZnSe phase in CZTSe at the Se K-edge was not resistant to the introduction of the CTSe standard, at least at ZnSe concentrations below 10%. However, analysis has proven resistant to the introduction of the Cu_2Se standard and the capacity for detection is not affected, as the ZnSe phase is still detected in all samples.

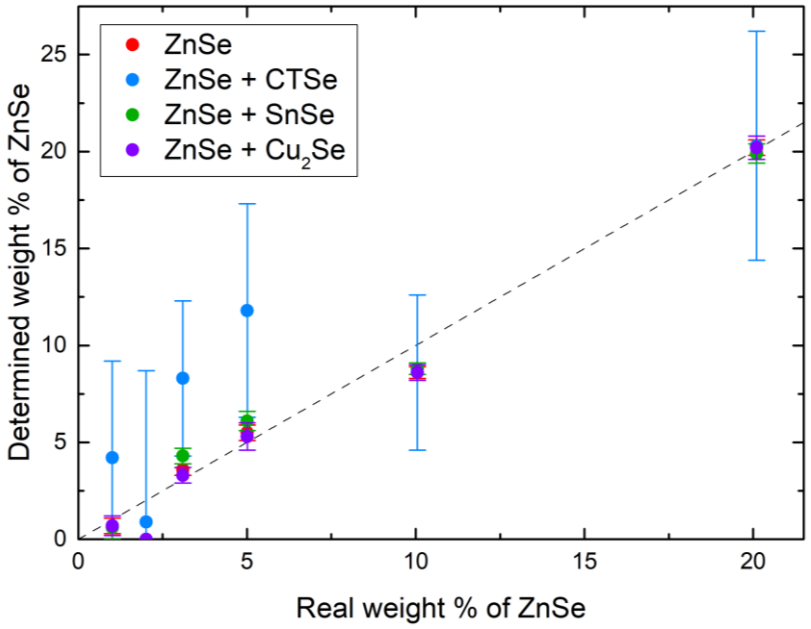

Figure 3.19 – Weight percentages of ZnSe determined by LCF of the spectra measured at the Se K-edge, for each secondary phase standard added.

For the Kest II-CTSe mixtures measured at the Se K-edge, the secondary phase standards added to the analysis were ZnSe, Cu_2Se and SnSe. Figure 3.18 shows the XANES regions of the normalized sample spectra of the standards used but observations are equivalent to the ones made above. In this case, however, CTSe is both the standard of study and the one most similar to Kest II.

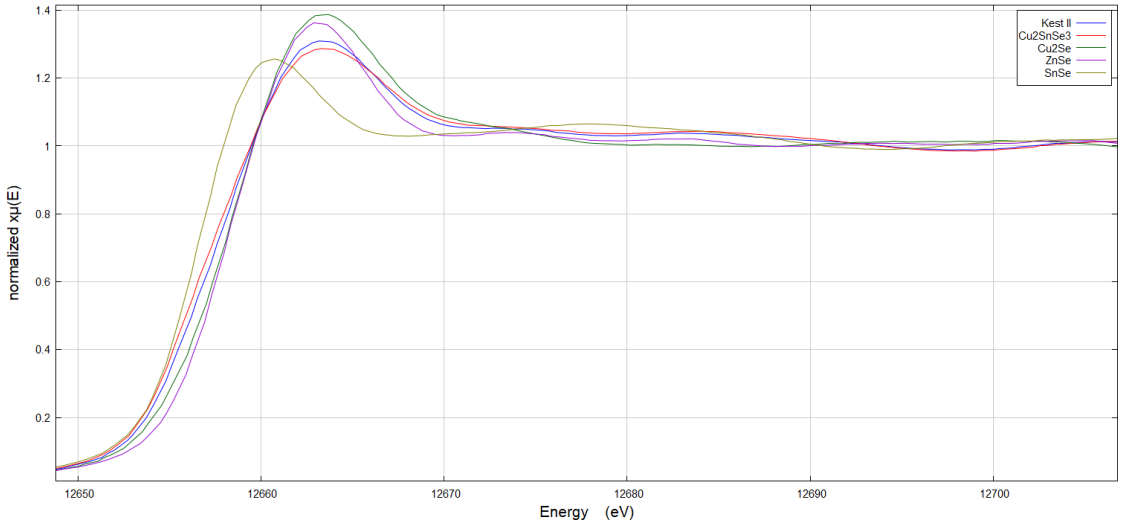

Figure 3.20 – Comparison between the XANES regions of the Kest II, CTSe, Cu_2Se, ZnSe and SnSe normalized spectra measured at the Se K-edge.

Once again, the fit quality observed among all sets of standards is very similar to the original fitted spectra, also meaning that they all fit well to the measured data. The weight percentages of the CTSe phase obtained from the LCF analysis for each standard added are presented in Figure 3.21. Weight percentages of CTSe obtained with the addition of the SnSe standard are generally the closest to the original values, with detection of the SnSe phase itself only occurring in the 10% sample at a percentage of 1%. With the ZnSe and the Cu_2Se standards introduced in the analysis, the CTSe weight percentages become very spread out from the original values – with differences reaching 15% for the case of adding the ZnSe standard – though detection is still observed in the same samples as before. Detection of the Cu_2Se occurs in all samples except the 1% and 10% ones, at weight percentages from 3.8% to 6%. ZnSe is detected in the 1%, 5% and 10% samples, with percentages ranging from 2.2% up to 5.7%. The weights of the ZnSe and Cu_2Se standards determined in the analysis are usually below those determined for the CTSe phase, however, those are also above the real values which means that false detection of the added standards is indeed observed. Thus, the likeliest conclusion is that XANES analysis of the CTSe phase in CZTSe at the Se K-edge was not resistant to the additions of the ZnSe phase – akin to what is seen in the inverse case – and of the Cu_2Se phase. The detection capacity alone, however, is not affected since CTSe is still detected above concentrations of 10%.

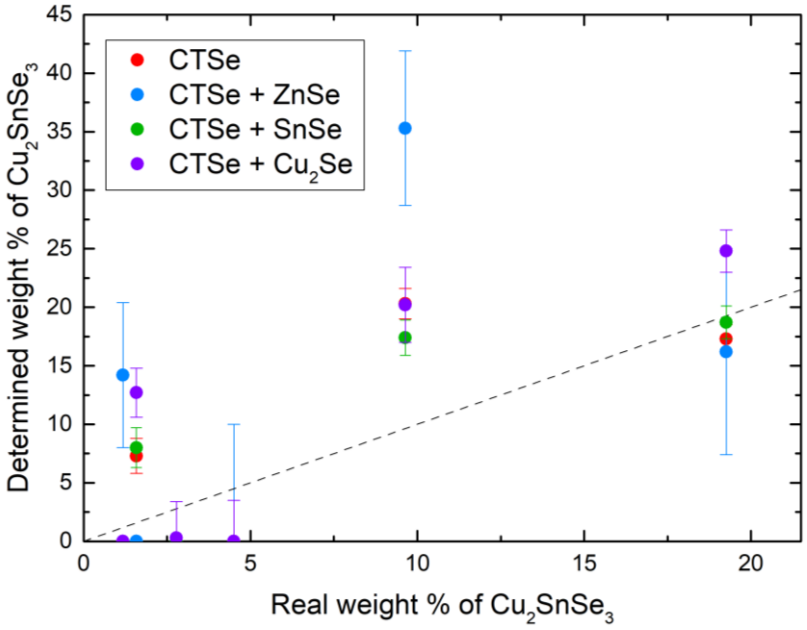

Figure 3.21 – Weight percentages of CTSe determined by LCF of the spectra measured at the Se K-edge, for each secondary phase standard added.

General conclusions of this study seem to be that, even if certain secondary phases can be falsely detected when adding their standards to the XANES analysis, the capacity for the detection of the CTSe and ZnSe phases is retained. Still, these observations are limited to the additional phases used and concrete conclusions are difficult to achieve just from this study, therefore further investigation should be performed.

3.5. Stoichiometry of the $Cu_2ZnSnSe_4$ standard

Since the XANES method of analysis is solely based on a linear combination of standards whose presence in the contents of the sample of study is possible, the importance of using correct standards is a topic that should be investigated. Specifically, $Cu_2ZnSnSe_4$ is a compound with a lot of flexibility in its structure and composition, allowing for a wide range of off-stoichiometric compositions, with all kinds of point defects [16, 26]. The probability of having a perfectly matching standard is, consequently, extremely small.

To study the degree of impact from the choice of CZTSe standard, the XANES analysis performed in the first sections of this chapter were repeated, using all the measured kesterite samples. Besides the off-stoichiometric Kest I and Kest II samples, a stoichiometric CZTSe reference (CZTSe_SR) measured during the second beamtime was also used, so results using two standards other than the one actually present in the mixtures were obtained for each group of data. The normalizations applied to the sample spectra in this section continue to be the ones determined as the best choices in the previous sections.

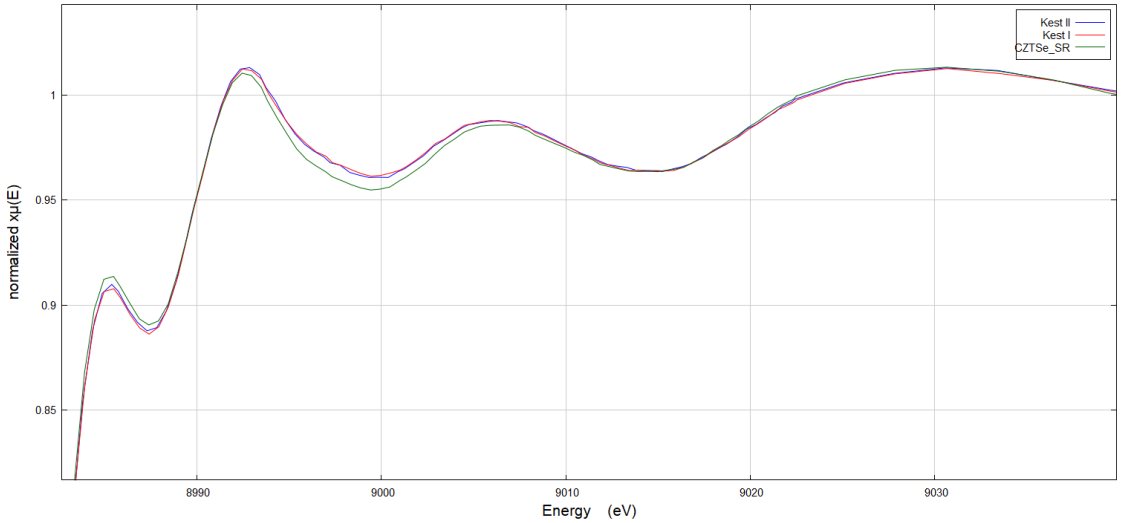

Figure 3.22 – Comparison between the XANES regions of the Kest II, Kest I and CZTSe_SR normalized spectra measured at the Cu K-edge.

Beginning with the Kest II-CTSe mixtures measured at the Cu K-edge, a preliminary comparison between the spectra of the three kesterite standards (Figure 3.22) shows that the off-stoichiometric samples appear to mostly coincide at all energies, which would be expected given the similar compositions of these standards. Conversely, the XANES region of the stoichiometric reference's spectrum has a couple of evident areas of separation from the other spectra in the lower energy regions. Taking all this into consideration, the most interesting case of study can be expected from the use of CZTSe_SR.

The Cu_2SnSe_3 weight percentages resulting from the LCF analysis with each kesterite standard can be observed in Figure 3.23. Upon looking at the data obtained, it is immediately understood that the choice in standard had a great effect in the analysis. Results show an ordering in amount of CTSe determined depending on which CZTSe standard was used – the use of Kest I produces slightly lower weight percentages of the ternary than those determined with the correct standard; on the other hand, use of CZTSe_SR displays percentages much higher than those obtained with Kest II. Additionally, the same trend appears to be followed by every set of results – except at below 5%, where the use of CZTSe_SR causes the detection of some seemingly random CTSe concentrations. These observations indicate that using a kesterite standard with incorrect stoichiometry for the detection of the CTSe phase when measuring at the Cu K-edge could have a large influence on the weight percentages determined, and the use of Kest I shows that the difference in stoichiometry does not have to be very big to introduce a noticeable effect. The almost constant trend seen in the Figure 3.23 also means that the percentages themselves would still present plausible results even if there was some indication about the relative concentrations of CTSe phase in a group of samples.

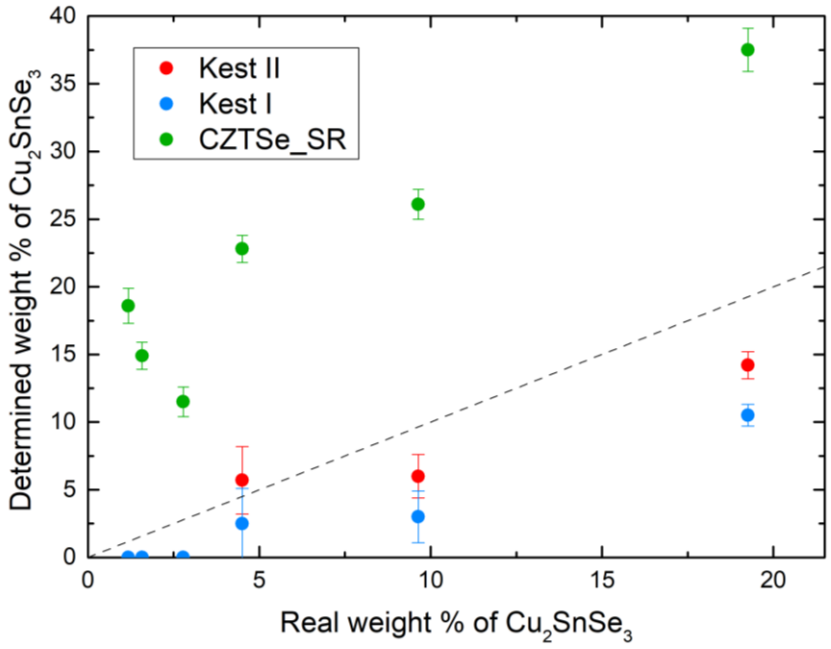

Figure 3.23 – Weight percentages of CTSe determined by LCF of the spectra measured at the Cu K-edge, for each kesterite standard used.

The results obtained with the standards can only be taken into consideration if the fitted spectra match the measured spectra within a certain degree of quality. By comparing all the fits, it can be concluded that none of them could be pointed out as being the product of a wrong choice of standards, as exemplified in the figures below. Thus, the conclusions made above still stand, as using any of these standards continues to result in acceptable fitted spectra.

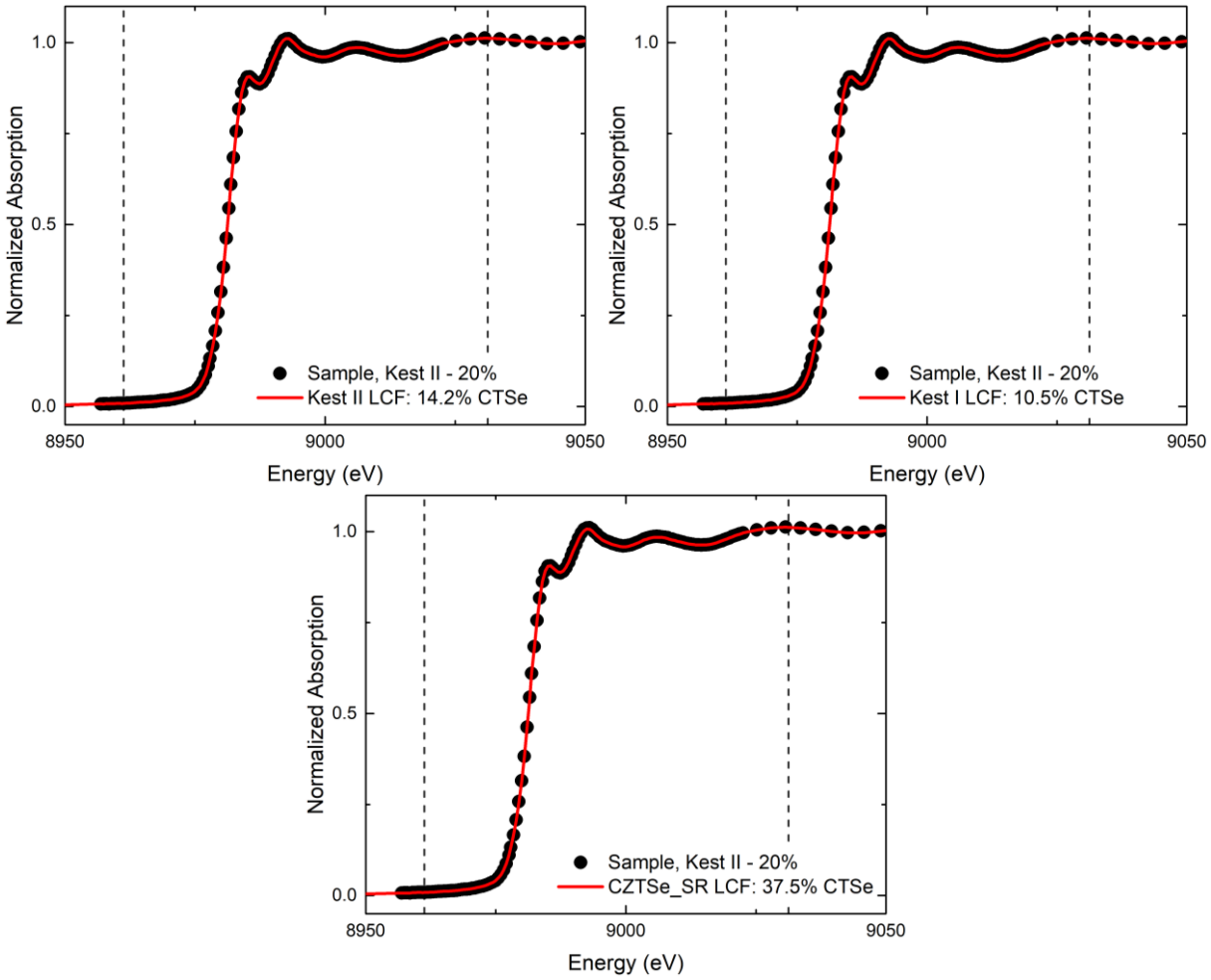

Figure 3.24 – Examples of measured data and spectra fitted by LCF analysis of the Kest II-CTSe mixtures measured at the Cu K-edge, using different CZTSe standards.

Starting with the Kest I-ZnSe mixtures measured at the Se K-edge and with the same comparison between spectra of the kesterite standards (Figure 3.25), it can be observed that differences are much more subdued when measuring at the this edge. The stoichiometric reference's spectrum does not show the same identifiable regions of separation from the other standards, instead showing a very small shift along the energy range following the absorption maximum. The Kest I and Kest II spectra still appear to mostly coincide at all energies, with differences on the same order as those observed in the Cu K-edge. Such spectra make it difficult to draw any preliminary conclusions other than that any differences in results from the use of the CZTSe_SR standard will most likely be on a smaller scale than what was seen above.

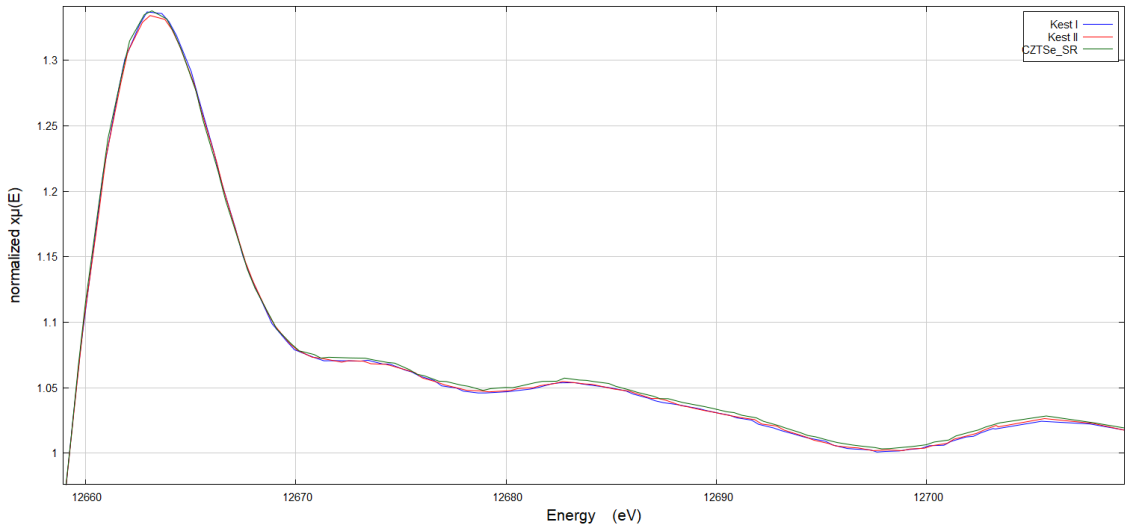

Figure 3.25 – Comparison between the XANES regions of the Kest I, Kest II and CZTSe_SR normalized spectra measured at the Se K-edge.

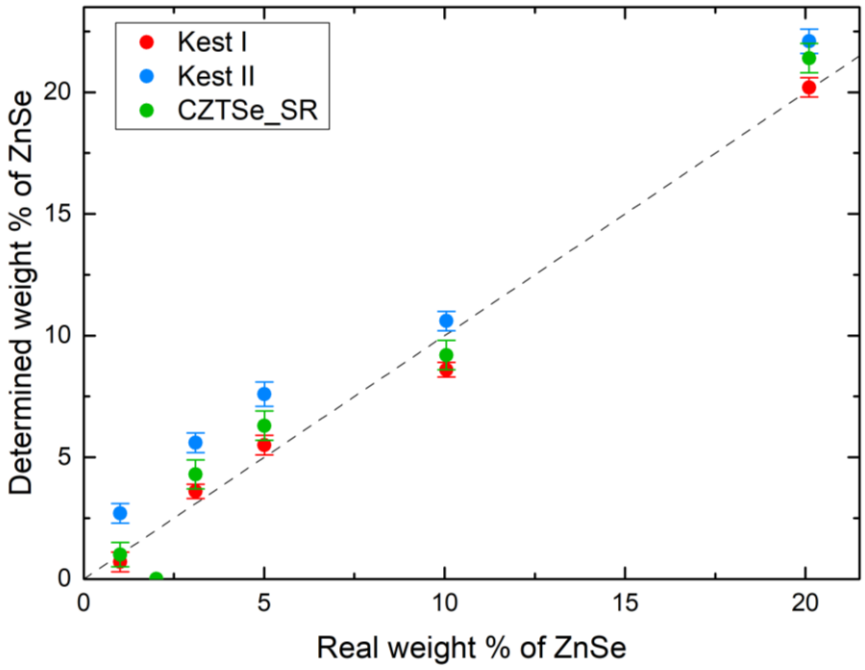

Figure 3.26 – Weight percentages of ZnSe determined by LCF of the spectra measured at the Se K-edge, for each kesterite standard used.

The weight percentages of ZnSe obtained from LCF analysis of the mixture spectra are presented in Figure 3.26. In this case, the results from the use of all three standards are very close together, with actual percentages being shifted from the results with Kest I by no more than 2%, although the same trend is still observable among the sets of results. Unlike what was observed previously, the weight percentages obtained with the use of CZTSe_SR are now generally the second lowest, while Kest II has the highest values.

Despite observing a smaller influence due to the choice of standard in this set of samples, an interesting addition to the study was done by using Cu_2SnSe_3 as another kesterite standard. The similarity between the spectra of the CTSe and Kest II standards measured at the selenium edge has been pointed out already, and because existing differences are comparable to those seen in the stoichiometric reference measured at the Cu K-edge, there was a valid reason to expect this to be a test with interesting results.

The weight percentages of ZnSe obtained with the CTSe standard are shown together with the previous results in Figure 3.27 and are the highest by far, being completely outside an acceptable error bar. On the other hand, it appears that the tendency that was kept in the first sets of results is still maintained for this standard.

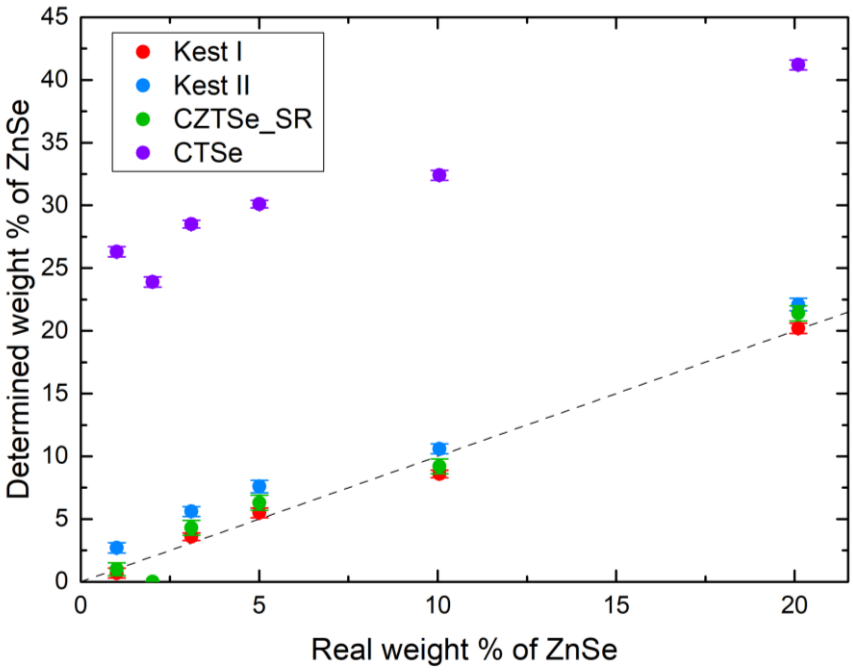

Figure 3.27 – Results from Figure 3.26 with the addition of the ZnSe weight percentages obtained with the use of CTSe as the kesterite standard.

Performing the analysis on the quality of the fits leads to the conclusion that all fitted spectra match the measured data well enough for one to assume that any of the tested standards could be used to study the presence of ZnSe. As an example, figures showing the complete set of fits for the 10% ZnSe sample can be seen below.

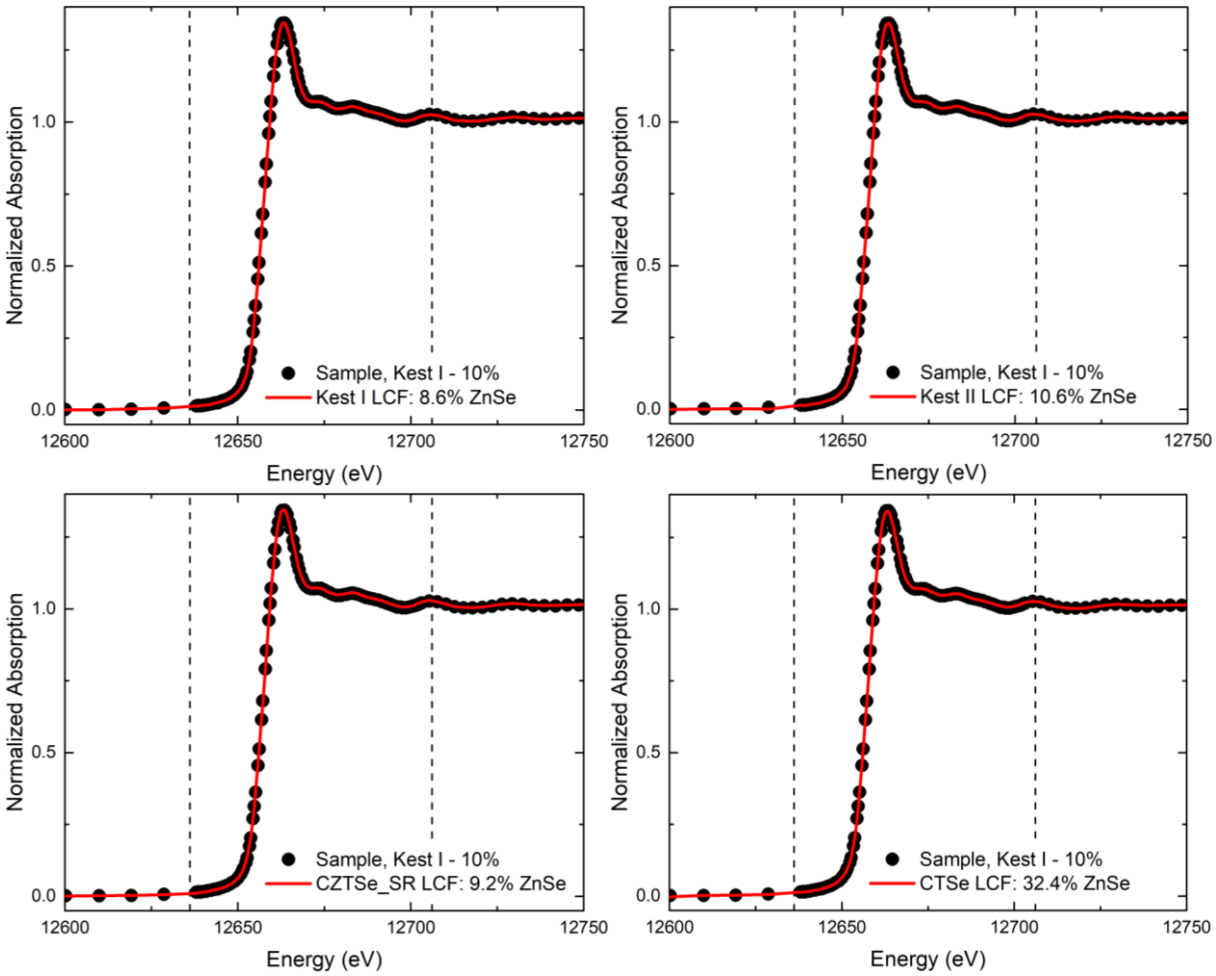

Figure 3.28 – Examples of measured data and spectra fitted by LCF analysis of the Kest I-ZnSe mixtures measured at the Se K-edge, using different CZTSe standards.

Earlier in this study, it was shown that XANES is capable of quantifying the ZnSe secondary phase with a high degree of accuracy at all concentrations, when using the correct kesterite standard. Those results make this the most informative case to consider, from the point of view of this method's application in real-world circumstances. This investigation reveals that using a kesterite standard measured from samples with different stoichiometries still results in well-fitted spectra and weight percentages of ZnSe evidencing only a small influence, which further solidifies the previous conclusions. However, observations when using CTSe as a kesterite standard suggest that this might not always be case. Fit quality using this standard is also acceptable but ZnSe percentages obtained are dramatically increased, by over 20%. If CTSe is thought of as the most extreme case of off-stoichiometric CZTSe, then it might be possible that using standards with stoichiometries further away the correct one would lead to results outside an acceptable error bar.

In the case of the Kest II-CTSe mixtures measured also at Se K-edge, observations from comparing the spectra of the kesterite standards (Figure 3.29) are similar to the previous ones. Spectra are still not very distinct from each other even with the different normalization applied, though the separation of the Kest I spectrum from the rest is now the most evident.

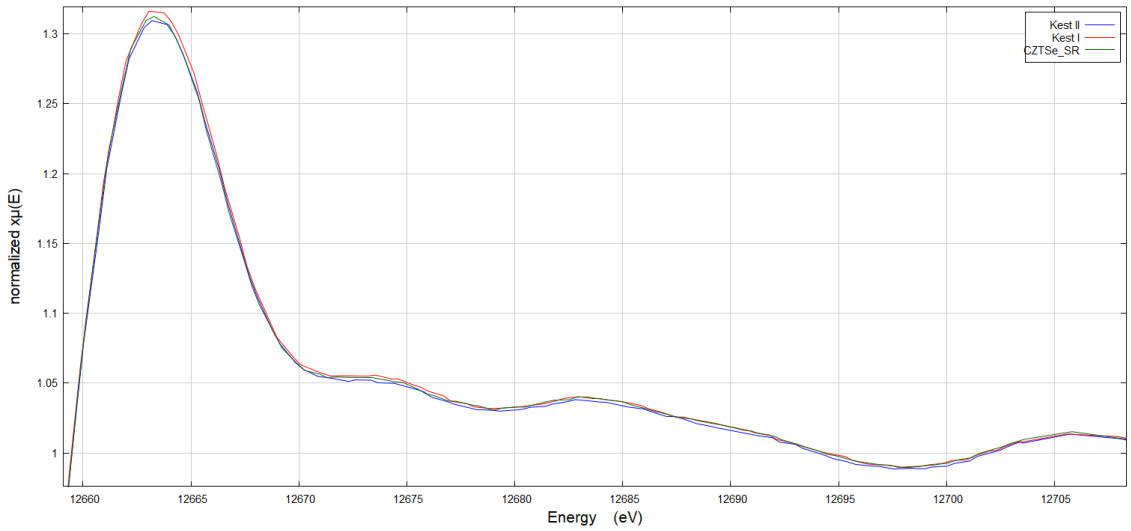

Figure 3.29 – Comparison between the XANES regions of the Kest II, Kest I and CZTSe_SR normalized spectra measured at the Se K-edge.

The weight percentages of CTSe obtained from the analysis with each standard, presented in Figure 3.30, mostly follow the results seen so far. The percentages from the use of the two incorrect standards again increase somewhat proportionally in relation to the original values obtained with Kest II, with a constant trend among them still identifiable.

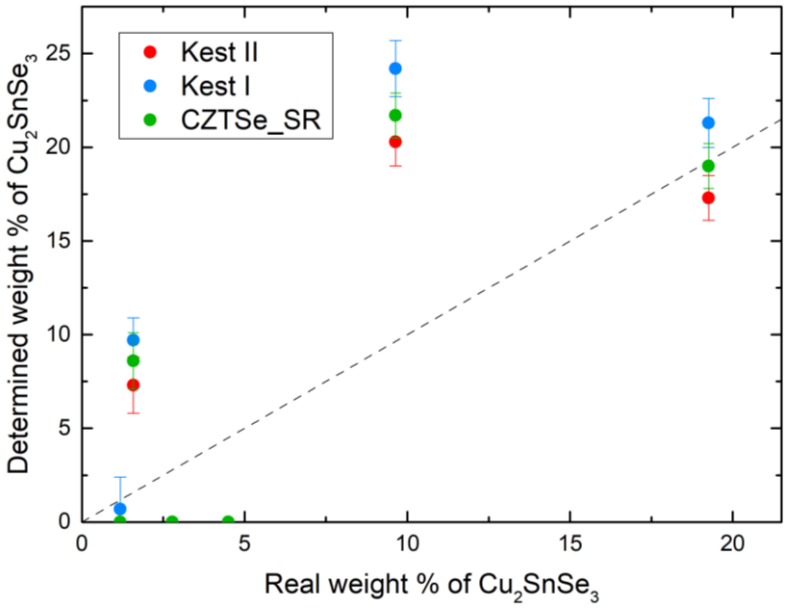

Figure 3.30 – Weight percentages of CTSe determined by LCF of the spectra measured at the Se K-edge, for each kesterite standard used.

Ordering of the sets of results is similar to the one seen in the ZnSe mixtures, with the positions of Kest II and Kest I reversed. However, the separation between points is significantly higher, which could be linked to the lack of precision and accuracy in quantification of the CTSe phase, determined in Chapter 3.3. Although the percentage at 20% becomes closer to the real value with the use of CZTSe_SR, this is only due to the inaccuracy of the original measurement, which would not happen in every case. These observations still point towards conclusions equivalent to the ones for measurements at the Cu K-edge, as the influence of a kesterite standard with incorrect stoichiometry is noticeable. Yet the degree of this influence is smaller, which indicates that the difference in stoichiometry would have to be larger to cause effects on the same scale.

Fit quality with these samples is acceptable enough to also consider the two tested standards as right choices to study the presence of CTSe. Figures showing the complete set of fits for the 20% CTSe sample as an example can be seen below.

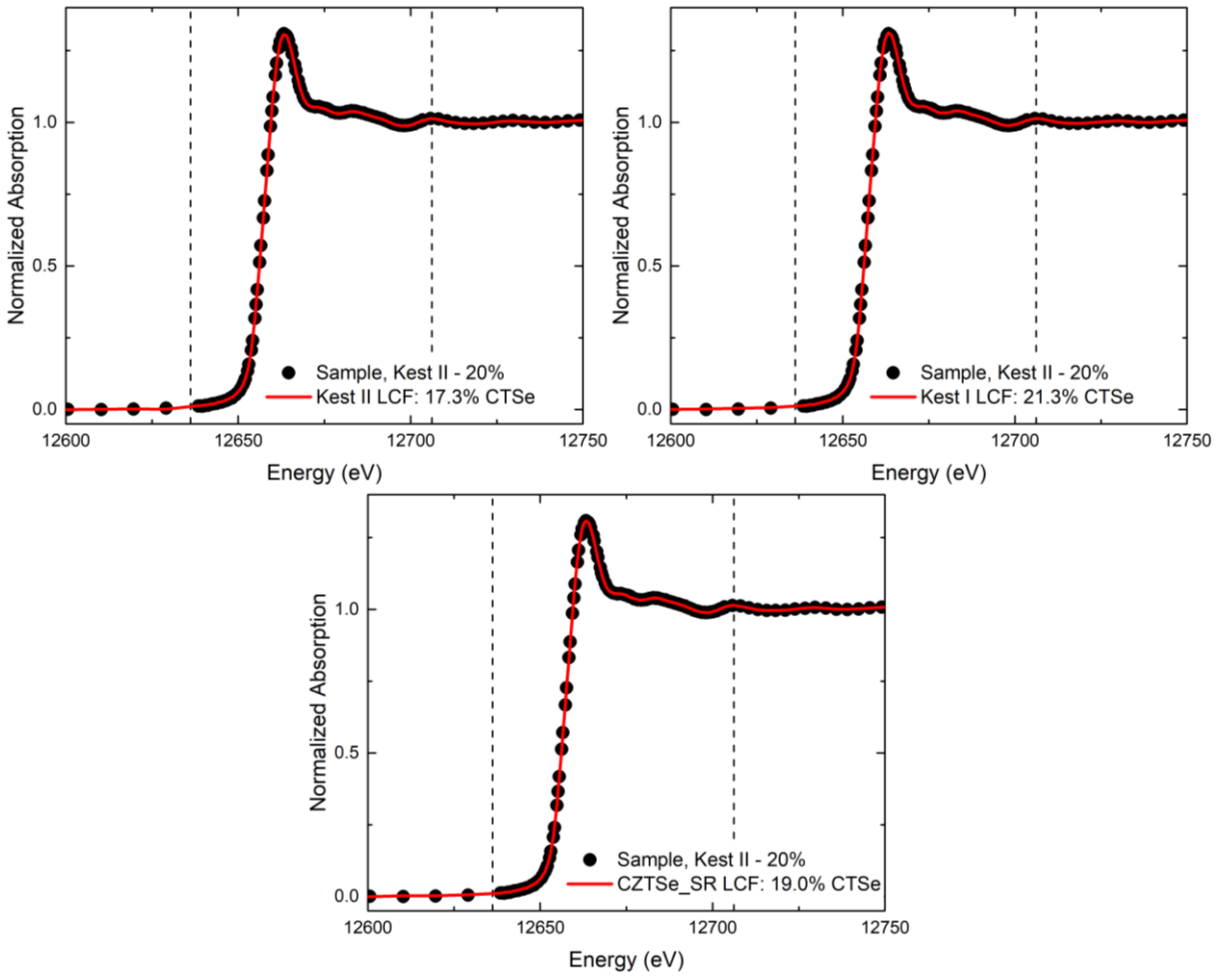

Figure 3.31 – Examples of measured data and spectra fitted by LCF analysis of the Kest II-CTSe mixtures measured at the Se K-edge, using different CZTSe standards

4. XANES analysis of off-stoichiometric CZTSe samples

The previous study on the application of XANES analysis to the detection of secondary phases in $Cu_2ZnSnSe_4$ was performed on samples with artificially created, and therefore known, phase contents. To take the research into its next logical step, normal sample conditions need to be tested – results of such a study would reveal how well the conclusions reached so far are translated into real-world scenarios. To that end, samples used in this section are comprised of off-stoichiometric $Cu_2ZnSnSe_4$, whose compositions and phase contents have been determined by WDX analysis, and that provide good examples of the usual kesterite samples obtained from synthesis of this material. LCF analysis is performed by introducing the standards of all secondary phases determined to be in contents of the samples. Such knowledge may not always be available when using this method in normal conditions, but using it here can decrease the influence of factors detrimental to the analysis, such as missing standards or false detections.

Many of the samples synthesized by L. E. Valle Rios [16] were measured by transmission mode XANES, at both the Cu and Se K-edges, during the first beamtime. Since detection of ZnSe at the Se K-edge has proven to be the only one with a capacity for quantification at all concentrations, samples that had been determined to have ZnSe in their phase contents by WDX analysis were chosen among the entire set of data. Furthermore, since only CuSe and Cu_2Se standards had been additionally measured, samples were restricted to only containing those phases. In total, four samples fitting these criteria were available. On these, the detection of ZnSe phase was again tested in order to determine whether the detection capacity observed in the mixtures is observed in these real-world samples. Among the measured samples, there were also four single-phase $Cu_2ZnSnSe_4$. Data from these samples was used to repeat the investigation on the influence of standard's stoichiometry on the results of the LCF analysis. Unfortunately, due to an incompatibility between distinct beamtime measurements, there was no possibility to use Kest I and Kest II as standards among this data set – and, conversely, to use these single-phase samples on the previous study. However, the stoichiometric reference was measured in both beamtimes. In this work, single-phase samples were codenamed according to the number attributed in Table 4.1, as CZTSe_01, CZTSe_02, CZTSe_07, and CZTSe_21.

No.	Sample	Cu/(Zn+Sn)	Error	Zn/Sn	Error	Secondary Phases
1	CZTSe_01	0.978	0.017	1.077	0.015	Single phase
2	CZTSe_02	0.911	0.016	1.127	0.016	Single phase
5	C0025-2	1.027	0.018	0.995	0.014	CuSe; Cu_2Se; ZnSe
7	CZTSe_07	0.967	0.017	1.045	0.015	Single phase
10	C0025-4	1.014	0.018	1.017	0.014	CuSe; Cu_2Se; ZnSe
12	B0050-4	0.998	0.017	1.042	0.015	CuSe; ZnSe
20	A0075-6	0.890	0.015	1.134	0.016	ZnSe
21	CZTSe_21	0.945	0.016	1.149	0.016	Single phase

Table 4.1 – Overview of the off-stoichiometric CZTSe samples synthesised by L. E. Valle Rios used in this chapter: Cation ratios and phase content information obtained from WDX analysis [16].

4.1. Detection of ZnSe secondary phase

The procedure applied here is the same described in the first sections of the previous chapter. The first step was then the preliminary normalization of the reference spectra, in order to determine the magnitude of energy shift necessary. The normalized standard's energy at half-height was located at 12647.233 eV. Therefore, the data required an energy shift of 10.767 eV that took into account the influence of the monochromator angle, according to the procedure described in Chapter 2.3, to place the energy at half-height at the theoretical Se K-edge energy value of 12658 eV [21].

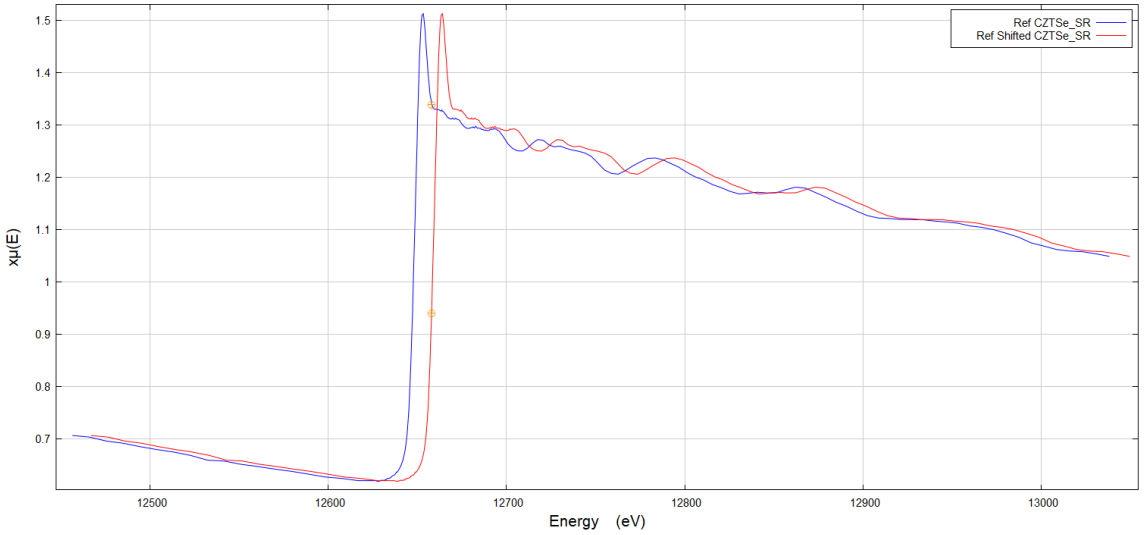

Figure 4.1 – Comparison between the raw and shifted data of the off-stoichiometric samples, using the CZTSe_SR reference spectrum as an example.

Dealing with measurements at the selenium edge once again, the normalization applied to the reference spectra was identical to the one used in the case of the mixtures also measured at this edge, after making sure that it produced well normalized spectra. The normalization consisted of quadratic polynomial in a post-edge range from 145 to 366 eV and a pre-edge range from -150 to -35 eV. As for the normalization of the sample spectra, the choice was also based on previous experiences with this edge. A normalization that intersected most of the fine structure fluctuations was always found to result in well fitted spectra and accurate weight percentages when analysing both the ZnSe and the CTSe mixtures, testing of that same normalization choice was found to work for these samples as well. Parameters of this normalization were a second degree polynomial in a range from 120 to 315 eV and a pre-edge range from -150 to -45 eV.

The LCF analysis was performed using the standards of secondary phases found in the samples by WDX and using the stoichiometric reference as the kesterite standard – considering this to be most "neutral" option of standard – in a fitting range from -20 to 50 eV relative to the edge position. Spectra fitted to the measured data of these samples show a high degree of fit quality in most cases. Fits of samples C0025-2 and C0025-4 present the best quality, matching the data very well, while the fitted spectrum of sample A0075-6 shows a slight mismatch to the measured data in the region just after the edge. It has to be considered that since the phase contents of the samples under analysis were not produced artificially, there are more factors to take into account. These include a higher probability that the information about their phase contents is incomplete, considering the statistical factors on which the accuracy of WDX measurements relies. Therefore, a lower fit quality can actually be an indication that the weight of some secondary phase standard is missing from the LCF analysis of the spectra. The weight percentages of the ZnSe phase obtained from the analysis are presented in the table below.

Sample	XANES ZnSe %	Error %	Determined ZnSe %	Error %
A0075-6	15.0	1.6	14.0	1.3
B0050-4	8.3	0.7	7.7	0.6
C0025-2	3.1	1.2	2.8	1.0
C0025-4	1.0	0.8	0.9	0.7

Table 4.2 – Results from LCF analysis of the off-stoichiometric samples' spectra regarding the ZnSe phase, using CZTSe_SR as the kesterite standard.

As can be observed, detection of the ZnSe phase occurred in all the analysed samples to some degree. Because there is no information regarding the actual ZnSe phase content of these samples, it is impossible to evaluate the accuracy of the weight percentages determined. Though if the extensive investigation performed on the mixtures is considered, the combined effects of introducing other secondary phase standards and the use of a kesterite standard of incorrect stoichiometry could influence the quantification capacity to some extent. However, the intended result was still achieved, since detection of the ZnSe phase was successful for the entire group of samples.

4.2. Additional secondary phase standards

Although there was a constricted number of secondary phase standards available, the fact that not all of them were present in the phase contents of two samples – A0075-6 and B0050-4 – made it possible to also test in this chapter the response of the linear combination analysis to the inclusion of additional secondary phase standards.

The analysis of both samples was conducted by adding the remaining secondary phase standards to the original set, again using CZTSe_SR as the kesterite standard. In the case of sample A0075-6, which contains only the ZnSe phase, this resulted in three new combinations. Sample B0050-4 only lacks Cu_2Se, so one new set of standards was used. The determined weight percentages for all standards weighed in each combination are presented in the table below, starting with the original combination.

Sample	Secondary Phase	XANES %	Error %	Determined %	Error %
A0075-6	ZnSe	15.0	1.6	14.0	1.3
	ZnSe	15.6	1.5	14.6	1.3
	CuSe	7.3	2.7	9.5	2.3
	ZnSe	8.0	2.1	7.1	1.8
	Cu_2Se	11.7	4.0	14.9	4.4
	ZnSe	10.9	2.3	9.9	2.0
	CuSe	4.9	4.2	4.4	3.6
	Cu_2Se	7.5	2.8	9.8	3.3
B0050-4	ZnSe	8.3	0.7	7.7	0.6
	CuSe	5.7	1.4	5.2	1.2
	ZnSe	2.1	0.9	1.9	0.8
	CuSe	2.6	2.3	2.3	2.0
	Cu_2Se	9.6	1.0	12.3	1.2

Table 4.3 – Results from LCF analysis of the off-stoichiometric samples' spectra for each set of standards, using CZTSe_SR as the kesterite standard.

The LCF analysis of these combinations show that not only do the additional secondary phases always have an attributed weight in the fitted spectra but that in some cases their weight percentage exceeds those of the original secondary phases. Moreover, fit quality generally presents an improvement. As explained before, it is not statistically impossible that secondary phases existing in the samples were not measured during the WDX analysis, resulting in incomplete information regarding their phase contents. Considering this possibility, it could be

that these results show the existence of these missing secondary phases, since their weight percentages are not insignificant in most cases.

But if these phases were present in higher concentrations than those measured by WDX, that would contradict the statistical explanation, because then they should have been more easily detectable than those actually measured. In the end, combining the results of this study on the two types of samples would point to the possibility that this method does not handle the incorporation of standards of secondary phases not present in the samples, likely leading to false detections and influencing the quantification of the remaining phases. But real conclusions are still impossible to reach; this is a study that requires more extensive and controlled data than what is presented here, so further investigation is necessary.

4.3. Stoichiometry of the $Cu_2ZnSnSe_4$ standard

The XANES analysis on the detection of the ZnSe phase is here repeated, replacing CZTSe_SR with each of the four off-stoichiometric CZTSe samples as the kesterite standard. Comparing the spectra of all the standards (Figure 4.2) presents a different situation than the one seen with Kest I and Kest II, there are some points where a separation between spectra is very evident, particularly at the energy of highest absorption. This could be expected given their more distinct stoichiometries and possibly indicates that the influence of using these kesterite standards will be on a greater scale than what was seen previously.

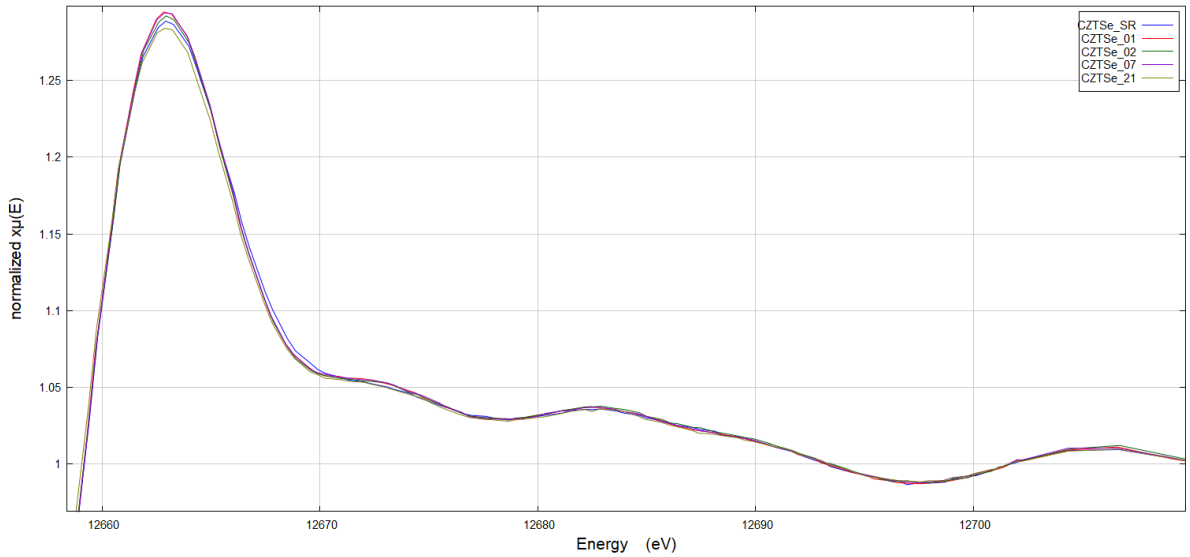

Figure 4.2 – Comparison between the XANES regions of the CZTSe_SR, CZTSe_01, CZTSe_02, CZTSe_07 and CZTSe_21 normalized spectra.

In evaluating the quality of the spectra fitted by LCF, it can be observed that fits of the same sample are, in general, not very distinct. The energy ranges where fitted and measured spectra are non-matching are consistent, regardless of the standard used, and are usually concentrated on the right side of the highest fluctuation. The most observable effect happens when using CZTSe_21, in which the contrast is more perceptible, but even these fits would still be considered acceptable. As an example, figures showing the complete set of fits for the sample B0050-4 can be seen below.

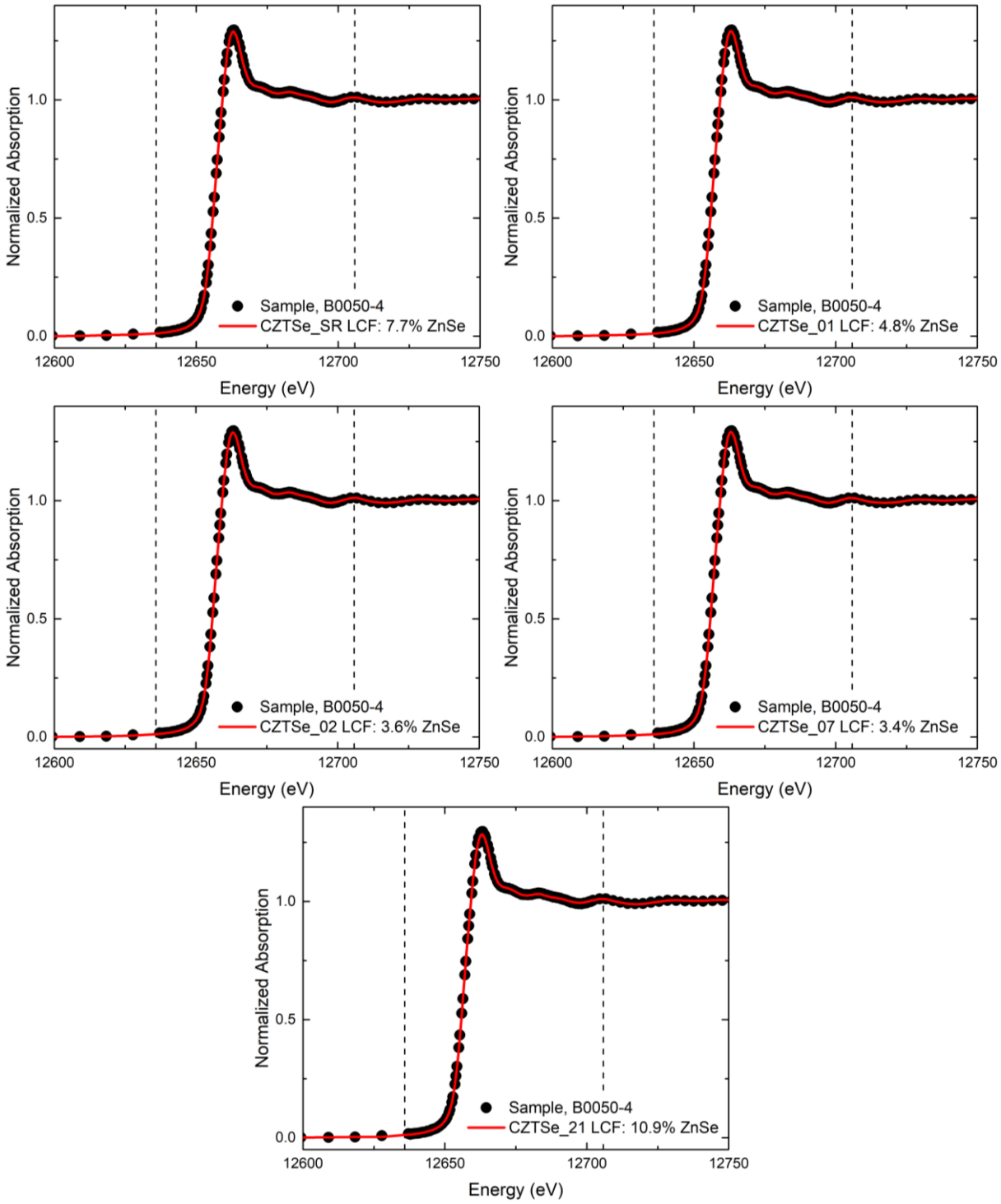

Figure 4.3 – Examples of measured data and spectra fitted by LCF analysis of the off-stoichiometric samples, using different CZTSe standards.

The determined ZnSe weight percentages obtained from LCF analysis are presented in Figure 4.4. Although the spacing between points is clearly not as constant, results still appear to present a slight trend between samples. Percentages of phase content are evidently disposed according to the standard used – points from using CZTSe_02 and CZTSe_07 are, for the most part, coincident; slightly above are those from the use of CZTSe_01, followed by the original

points with CZTSe_SR; and the highest values result from using CZTSe_21. Discrepancy between weight percentages also depends on the standard, with the lowest being at the level seen with the ZnSe mixtures, and the highest being much more separated.

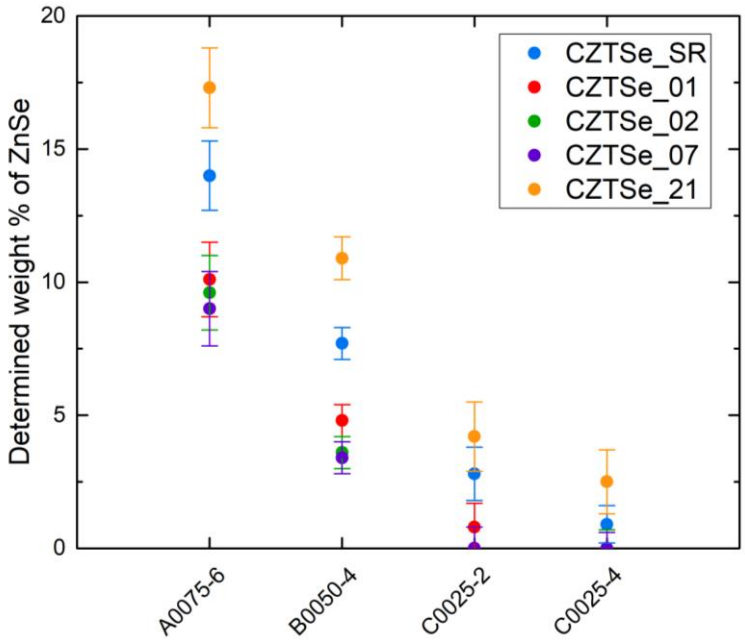

Figure 4.4 – ZnSe weight percentages determined by LCF of the off-stoichiometric samples' spectra, for each kesterite standard used.

The fact that using CZTSe_21 results in the highest ZnSe weight percentages might be connected to the quality of the corresponding fitted spectra. As mentioned above, the spectra obtained when using this standard have the most discernible discrepancy from the measured counterparts, which could mean that the corresponding ZnSe percentages are overestimated in relation to the real value. However, this assumes a direct link between fit quality with each kesterite standard and accuracy of results, which may not always be the only factor to consider when dealing with real-world samples. An interesting case occurs with the C-type samples, for which the use of certain standards eliminates the detection of ZnSe, indicating that the detection capacity may be damaged when phase concentrations are already small. The cation ratios Cu/(Zn+Sn) and Zn/Sn from the kesterite phases of the analysed samples were plotted in Figure 4.5 in an attempt at understanding how these could be related to influence of the kesterite standards. But in comparing the ratios of each sample to the ratios of the standards and how far apart they are, the ordering of the weight percentages seen in Figure 4.5 does not seem to be directly related. This suggests that the influence of the kesterite standard in XANES analysis is more complex than just a relation between stoichiometries.

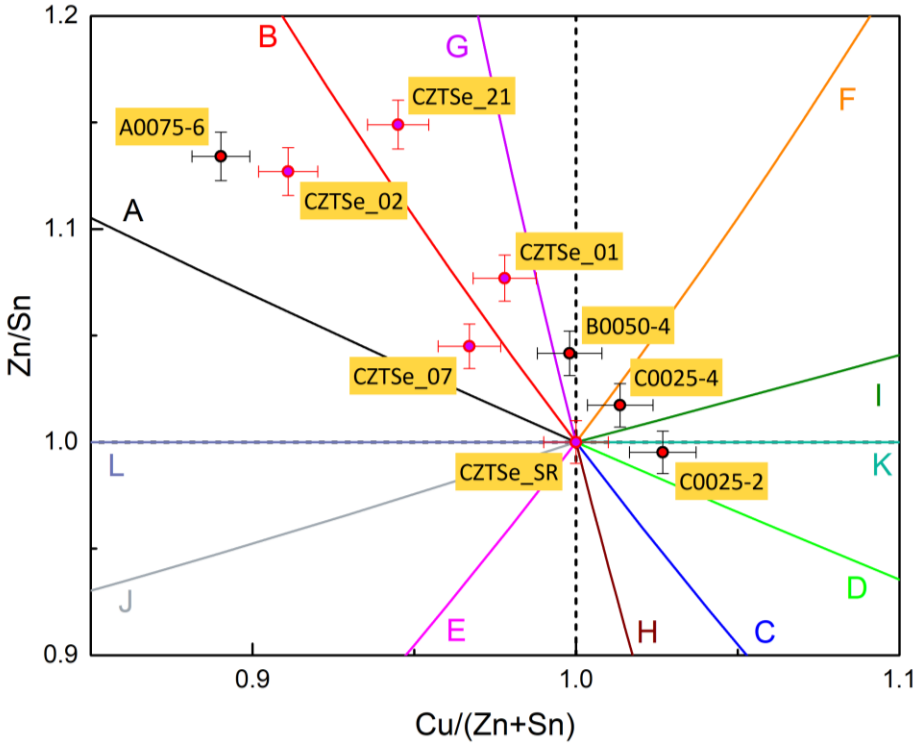

Figure 4.5 – Cation ratio plot showing the kesterite phases of the off-stoichiometric samples used.

Observations from this investigation are not on the same level as those reached from studying the ZnSe mixtures, seeing as the influence of the kesterite standards on the quantification capacity is much larger in some cases, a result that could be due to the use of standards with more diverse off-stoichiometric compositions. The conclusion than can be drawn from this study seems to be that application of the XANES method without proper knowledge of the kesterite compositions – and subsequent use of an incorrect kesterite standard – leads to inaccurate measures of ZnSe weight percentages, even if the fit quality appears acceptable. But phase contents determined by WDX analysis depend on a number of factors that can precipitate an incomplete view of a sample's phase content. This fact has to be considered here for the reason that precise conclusions are still reliant on a knowledge of the complete phase contents of the samples studied, and the use of the corresponding standards on the linear combination fitting. Even then, the method's capacity for quantification of the other phases may still influence the quantification of the ZnSe phase. This means that any concrete findings about this method cannot be solely grounded on study with so many unknowns. Nevertheless, it can be said that in real-world scenarios, where there is usually no indication of the real quantitative phase contents, it would be impossible to judge the collected results by their actual values. And when evaluating the fit quality provides no support on this judgement, there would seem to be no possibility of quantifying the phase contents solely with XANES analysis.

5. Re-annealing of highly off-stoichiometric CZTSe samples

In previous studies on the flexibility of the kesterite structure, this material was synthesized using cation ratios within the limits of 0.8 and 1.2 for both Cu/(Zn+Sn) and Zn/Sn ratios [26], with no existence threshold found. An investigation focused on finding the existence limits of CZTSe was elaborated for which eight samples of various off-stoichiometry types were synthesized with Cu/(Zn+Sn) and Zn/Sn cation ratio values which were thought to be well above what would allow the formation of any kesterite phases. Structural and chemical analysis showed that although there was a large amount of secondary phases present in the samples, several kesterite phases were still found in each of them, as shown in Figure 5.1. It was then concluded that the existence limits had not been reached yet. Nevertheless, the synthesised samples were extremely heterogeneous, so an attempt at minimizing the amount of secondary phases and perhaps reduce the number of kesterite phases to a single one by means of a second thermal annealing was thought to be worthwhile. This attempt is the focus of this chapter, where the effects of the re-annealing on the eight off-stoichiometric $Cu_2ZnSnSe_4$ samples will be determined. To do this, studies through XRD and WDX analysis were carried out, the findings of which will be presented and explained.

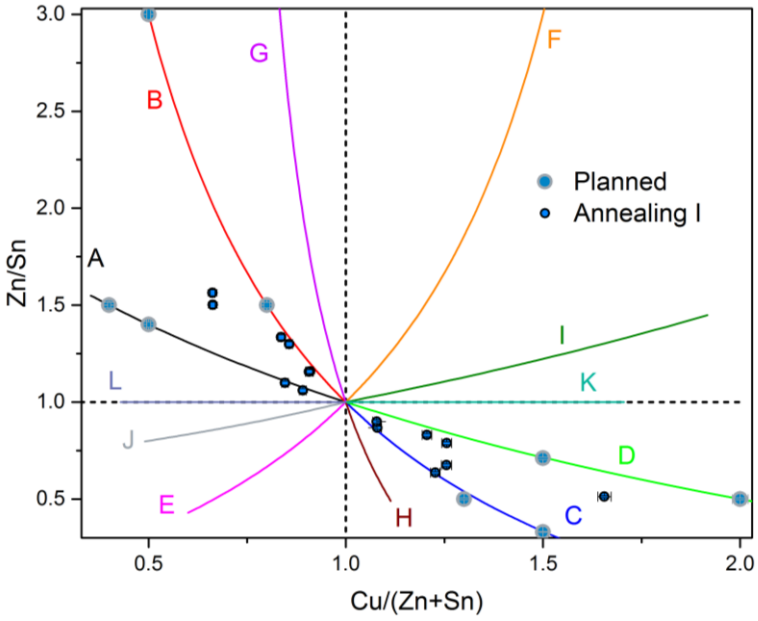

Figure 5.1 – Cation ratio plot containing planned ratios and ratios of the kesterite phase obtained by WDX measurements of the synthesised samples.

5.1. XRD analysis

As the first step in this investigation, diffraction patterns of every sample were obtained by performing high resolution XRD measurements with the PANalytical X'Pert PRO MRD diffractometer, as explained in Chapter 2.4. The purpose of collecting this data was the phase characterization of the samples, with the intention of comparing the results against those from before they were subjected to the re-annealing process. The measured patterns have good resolution, even at the level of the least intense peaks, making it harder to miss structural information due to experimental factors.

The simulated diffraction patterns used in the PowderCell analysis were the same as those used in the investigation of these samples after the first annealing. In these simulated patterns are included the most commonly encountered secondary phases in kesterite, such as ZnSe, Cu_2SnSe_3, CuSe, Cu_2Se, SnSe, and $SnSe_2$, as well as several other less common phases. The first standard added is always that of the CZTSe main phase, subsequently testing for the presence of all possible secondary phases, with the final objective of finding matches for all the peaks in the measured patterns.

From the analysis of the A-type samples' patterns, it was concluded that the two phase contents included both ZnSe and $SnSe_2$, in addition to the $Cu_2ZnSnSe_4$ main phase. The presence of $SnSe_2$ was primarily determined due to this being the only phase that could account for the lowest angle peak observed in the patterns, but also due to the peaks around the 43-50° region of 2θ. The relation between the intensities of this and other $SnSe_2$ peaks didn't correspond to the one seen in the measured data, in which some peaks were not even detected, but this could be explained by some remaining preferred orientation that couldn't be eliminated at the time of preparing the sample for measurements. Another observation regarding the $SnSe_2$ phase is that the diffraction peaks that correspond to it are much more intense in sample A-002, making its presence more noticeable and suggesting a higher content of this phase. Due to the overlap of the peaks from ZnSe with those from $Cu_2ZnSnSe_4$, the presence of this secondary phase was mostly determined from taking into consideration the peak shapes found in the higher 2θ region, which indicated the need for some secondary phase's influence, and the good agreement with the measured intensities when considering the effect of the two overlapping phases.

The diffraction patterns of the two samples can be seen in Figures 5.1 and 5.2, where the most intense peaks and those most helpful in identifying the phase contents have been color-coded according to the phases whose peaks match. For the purpose of comparison, the diffraction patterns obtained after the first annealing have been normalized to the maximum intensity measured in the corresponding re-annealed sample's pattern and both were plotted together.

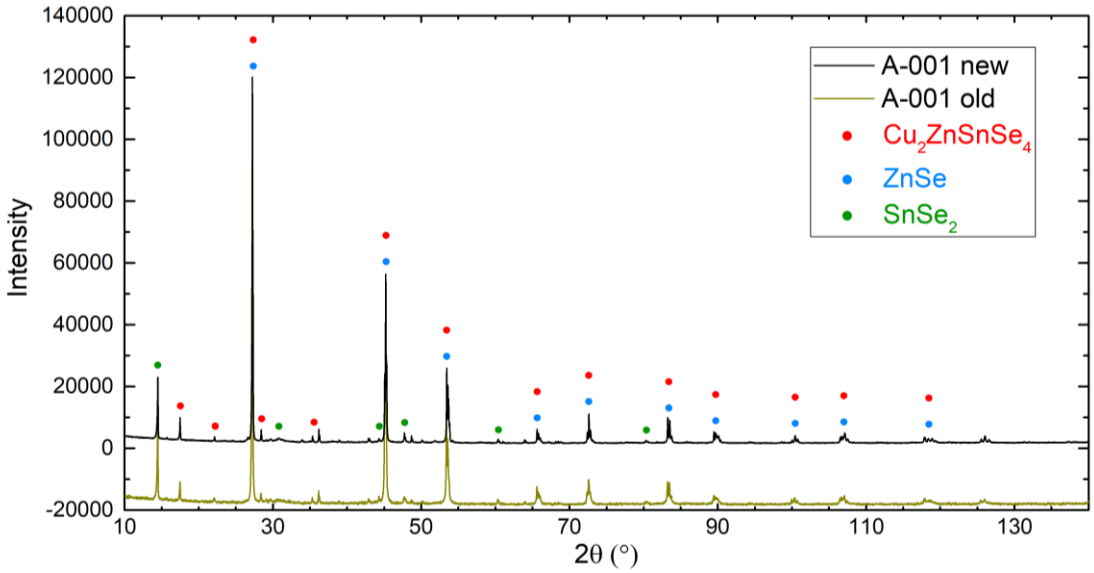

Figure 5.2 – Diffraction patterns from sample A-001, with color-coded diffraction peaks.

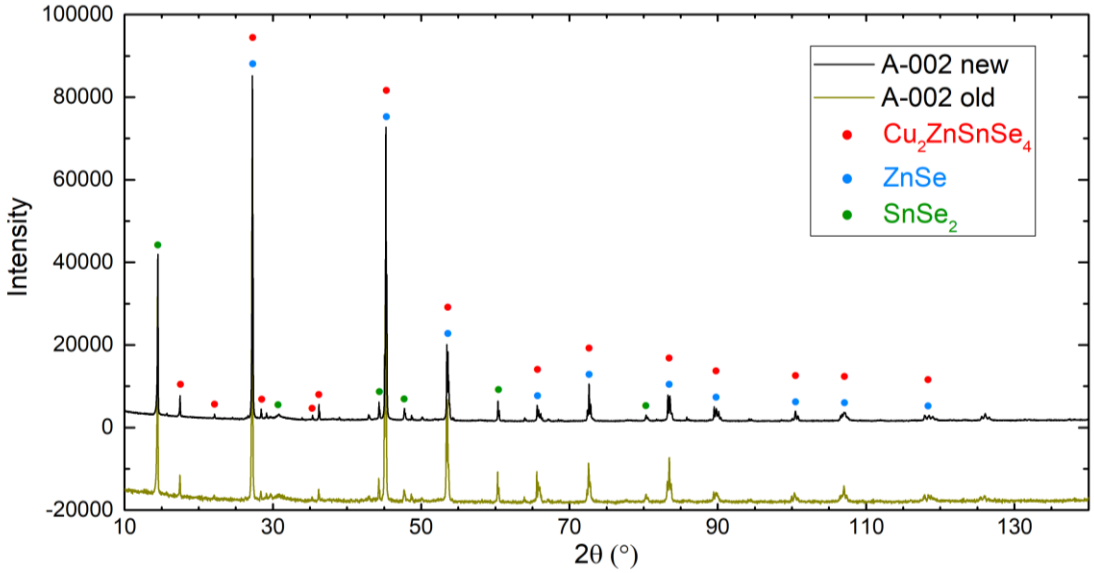

Figure 5.3 – Diffraction patterns from sample A-002, with color-coded diffraction peaks.

Looking at the patterns measured from the first annealing samples shows that they are virtually identical to the second annealing counterparts, suggesting that the phase contents remained unchanged after the process. In sample A-002, diffraction peaks corresponding to the $SnSe_2$ phase also show the same increased intensity that was mentioned above.

In analysing the B-type samples, the only secondary phase whose presence could be determined was that of ZnSe. Even though the overlap of the peaks from both phases was still identifiable at lower angles of diffraction, at higher ones its effects become much more pronounced, making it possible to identify the influence of ZnSe with certainty.

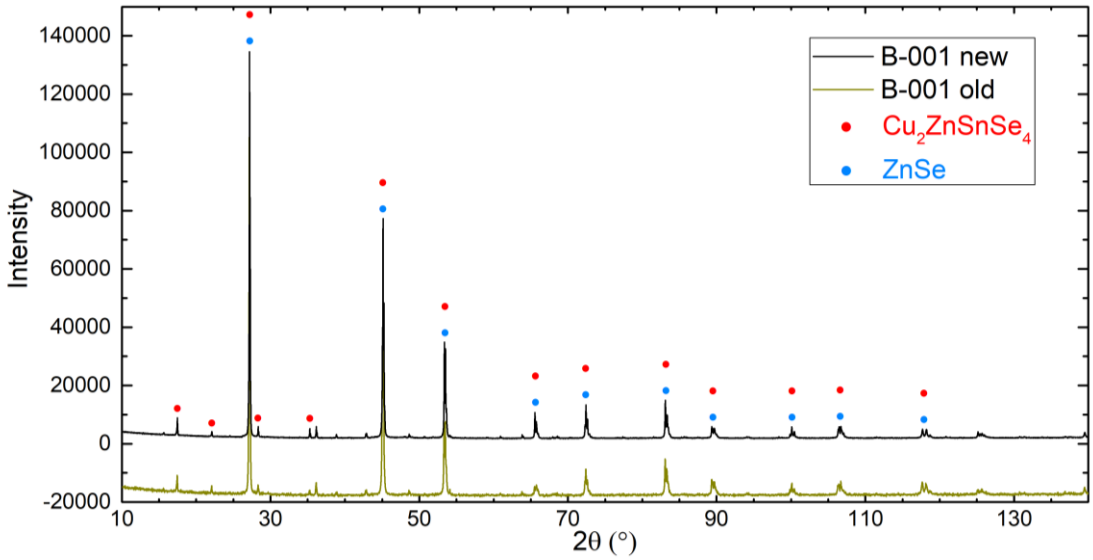

Figure 5.4 – Diffraction patterns from sample B-001, with color-coded diffraction peaks.

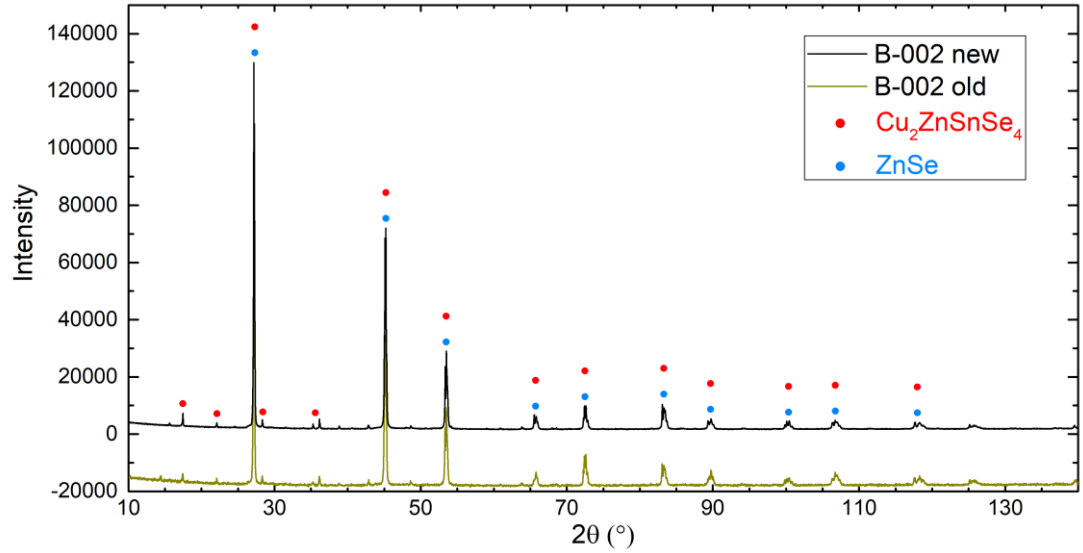

Figure 5.5 – Diffraction patterns from sample B-002, with color-coded diffraction peaks.

The previous investigation on the B-001 sample similarly concluded that only the ZnSe phase and the main phase were included in its contents, as observed from looking at the patterns from Figure 5.4. Regarding the first annealing of the B-002 sample, the presence of the $SnSe_2$ phase could be additionally identified by the low intensity peak located at $2\theta \approx 14.5°$, though no other peaks could be matched. In the present investigation, however, there were no traces of this peak, so ZnSe remained the only identified secondary phase. This indicates that the phase content of sample B-002 suffered slight alterations after being re-annealed.

The phase contents of the two C-type samples were again found to be identical to one another and determined to contain Cu_2SnSe_3, $SnSe_2$ and CZTSe. The influence of CTSe could be observed more clearly at higher diffraction angles, since this was the only phase that could explain the broadening of some of the measured peaks, and by considering the predicted effect of the overlap on the peaks' intensities. The presence of $SnSe_2$ was once again identified due to the diffraction peak at $2\theta \approx 14.5°$, whose existence in both samples could only be attributed to this phase.

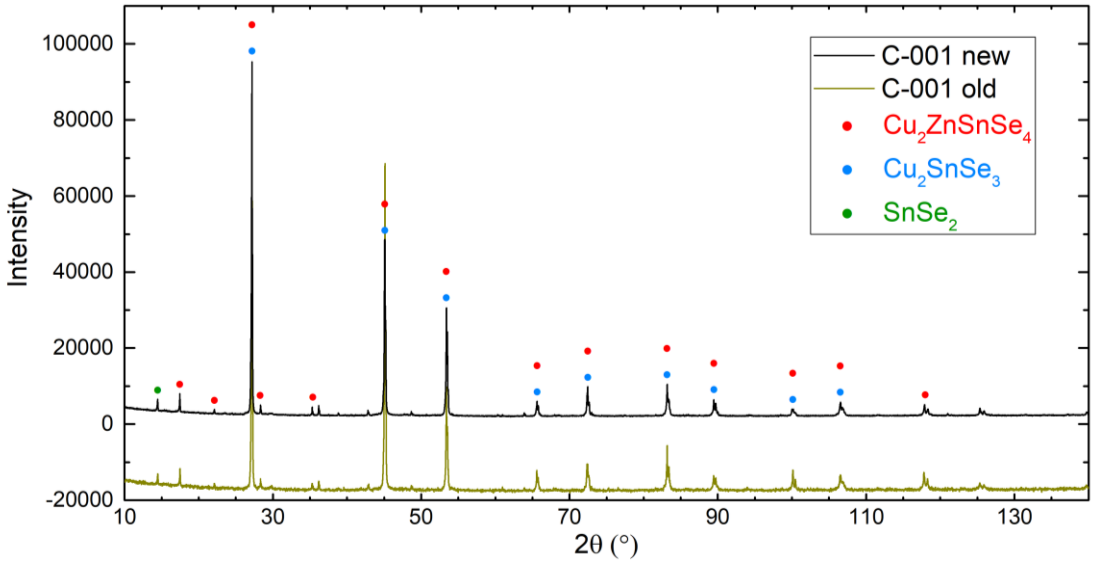

Figure 5.6 – Diffraction patterns from sample C-001, with color-coded diffraction peaks.

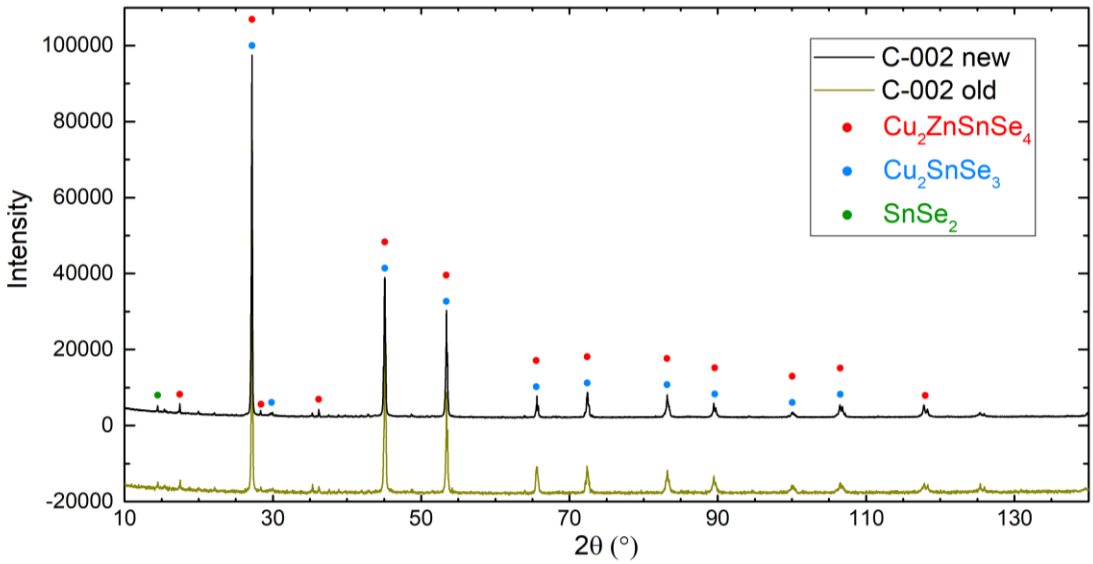

Figure 5.7 – Diffraction patterns from sample C-002, with color-coded diffraction peaks.

Analysis of these samples prior to the re-annealing concluded the same phase contents as those presented above, which can be understood by looking at the similarity between the first and second annealing patterns in Figures 5.6 and 5.7.

The investigation of the two D-type samples showed that there were several peaks close to the shoulders of the main diffraction peaks of the kesterite phase (Figure 5.8). The existence of the peaks wasn't explained from the previously found secondary phases, but was instead identified to come from the presence of the Cu_2Se phase. The shape of the highest intensity peaks in the pattern of sample D-002 suggested the presence of yet another secondary phase. This was determined to be the Cu_2SnSe_3 phase, whose presence explained the peak broadening and indications of additional peaks besides those from CZTSe.

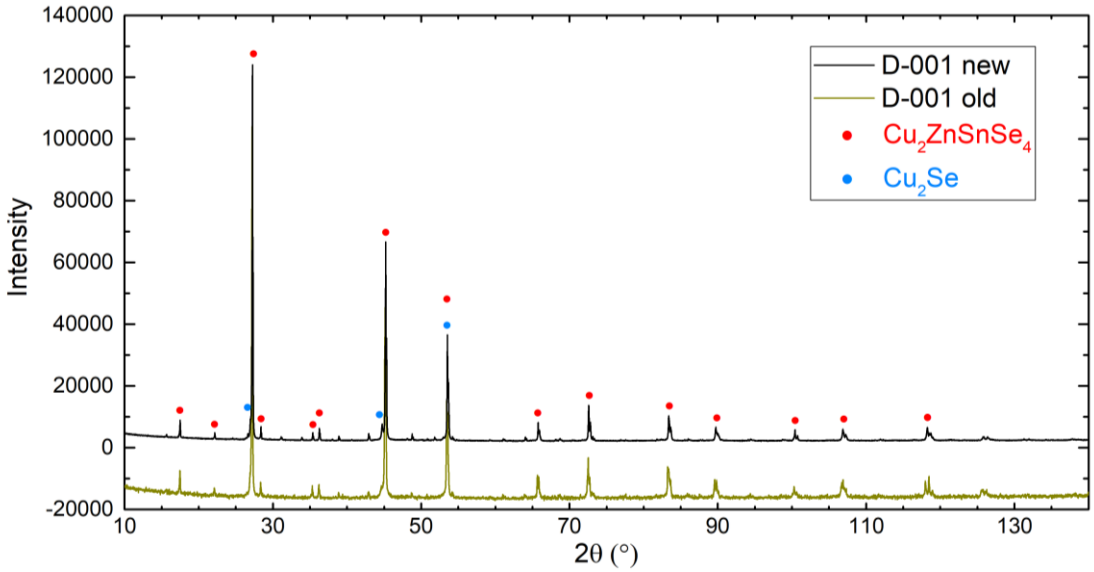

Figure 5.8 – Diffraction pattern from sample D-001, with color-coded diffraction peaks.

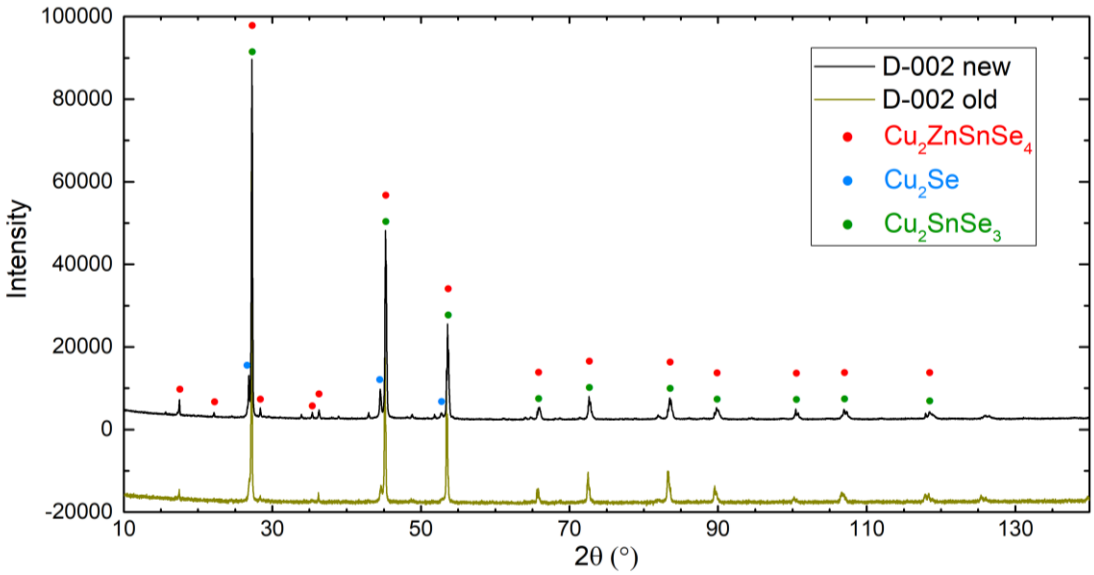

Figure 5.9 – Diffraction pattern from sample D-002, with color-coded diffraction peaks.

The observation of the patterns corresponding to the first annealing indicates that almost no changes were induced in the phase contents as a result of the re-annealing process, since all peaks can still be identified, albeit those matching the Cu_2Se secondary phase are now clearer in general.

At the end of this structural study and considering all the observations exposed, the general conclusion is that the second annealing doesn't seem to have introduced any major changes in the structural content of the samples, meaning that the phases contained in the samples have remained the same. Indeed, the patterns obtained show no notable differences from those measured after the samples were first annealed and the investigation carried out confirms this similarity. Since no refinement has been employed, nothing can be concluded in quantitative terms, only results from WDX analysis will reveal if the phases have suffered a change in composition or have been reduced to a smaller group of distinct compositions.

5.2. WDX analysis

Following from the phase characterization of the re-annealed samples, WDX measurements were performed in order to acquire knowledge on the chemical composition. Results from this analysis provide information on the composition of the CZTSe main phase, but also on the presence and composition of any secondary phases that might be found.

The data obtained at the end of the measurements was cleaned of points whose total mass percentages were below 95% and above 100%, already filtering out incoherent information from the measured data, points that were too deviated from the average of each grain then also had to be removed. Each measured point and grain average was considered to have an error of around 2% to account for the highly disordered element percentages determined, a consequence of the high heterogeneity of these samples. Doing a sample-by-sample sweep, points of any of the four elements found outside the error bar were eliminated and grains with a satisfying number of points remaining were considered acceptable. Certain cases occurred where a grain presented two different compositions, these were divided and considered as two different grains so that there would be no unnecessary loss of information. For every sample, the complete set of cleaned grains were divided according to which phase they belonged to, by being attentive to the element ratios, and the averaged atomic percentages of each grain were plotted according to the phase. The cation ratios Cu/(Zn+Sn) and Zn/Sn were then calculated for the kesterite phases found.

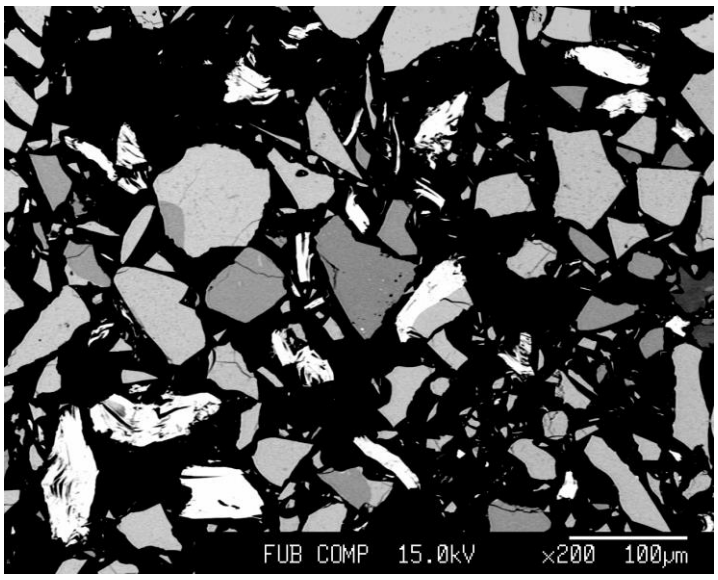

Figure 5.10 – BSE micrograph of sample A-002, $SnSe_2$ detected in white grains.

As presented in Table 5.1, analysis of the two A-type samples found secondary phases of ZnSe and $SnSe_2$, in agreement with the results from the structural characterization, though one point of pure Zn was also measured in sample A-002. This further confirms that the secondary phase contents of the A-type samples have remained mostly unchanged after being re-annealed.

Sample	Secondary phases	
	Annealing I	Annealing II
A-001	$SnSe_2$; ZnSe	$SnSe_2$; ZnSe
A-002	$SnSe_2$; ZnSe	$SnSe_2$; ZnSe; Zn

Table 5.1 – Secondary phases found in the A-type samples by WDX analysis, before and after the re-annealing.

Regarding the kesterite phases in sample A-001 (Figure 5.11), three distinct compositions were found which means that the second annealing was unable to reduce the number of kesterite phases from the two previously found. The compositions themselves appear to have become more concentrated towards the lowest Cu/(Zn+Sn) value of the previous phases and a Zn/Sn value more or less in between, generally shifting to become more Cu-poor and closer to the A-type line. Concentration of the phase compositions has also made it so that none of them surpass the cation ratio limits of the planned composition, like it happened prior to the re-annealing. Results for sample A-002 are equal to the ones of A-001 in that the number of kesterite phases increased from two to three, as seen in Figure 5.12. Observations about the change in compositions are also quite similar since the phases became more concentrated, tending towards the same value of Cu/(Zn+Sn) but growing slightly more Zn-rich.

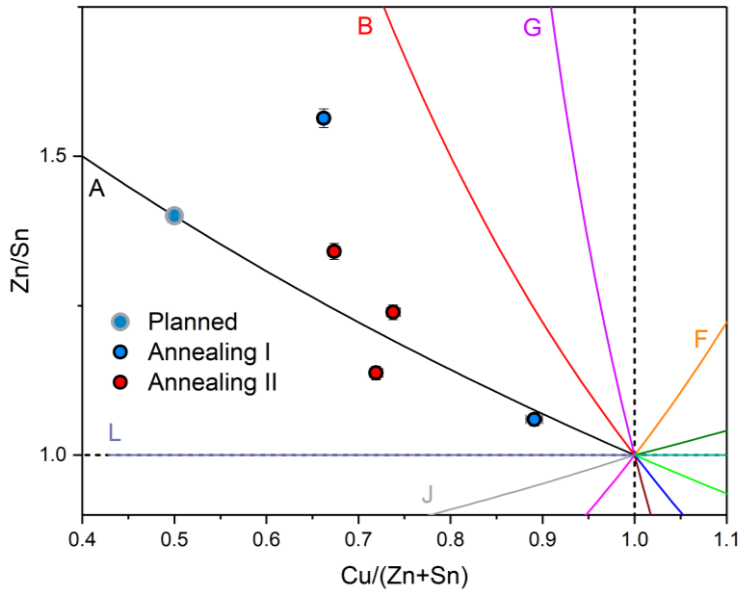

Figure 5.11 – Cation ratio plot of results from WDX measurements of sample A-001.

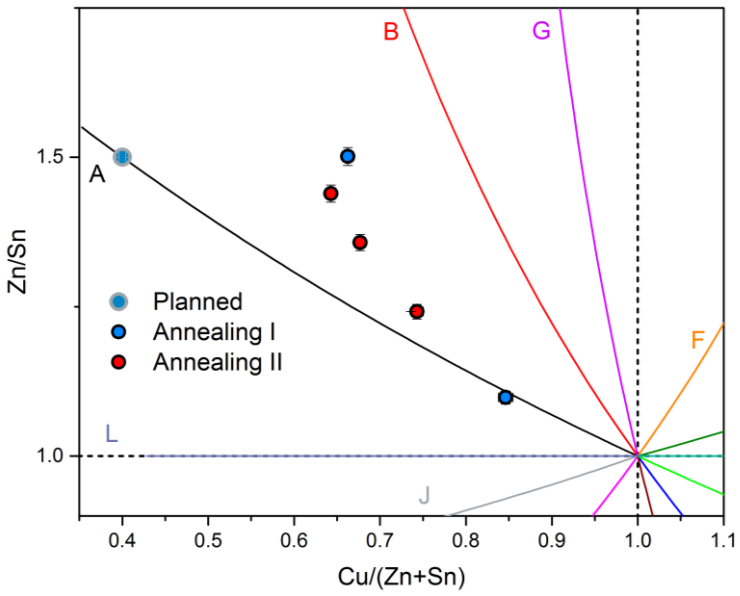

Figure 5.12 – Cation ratio plot of results from WDX measurements of sample A-002.

Results from the B-type samples identify the presence of the ZnSe secondary phase in both samples (Table 5.2), again matching the information acquired from the diffraction patterns and showing that the secondary phase contents have indeed stayed mostly the same.

Sample	Secondary phases	
	Annealing I	Annealing II
B-001	ZnSe	ZnSe
B-002	ZnSe	ZnSe

Table 5.2 – Secondary phases found in the B-type samples by WDX analysis, before and after the re-annealing.

As shown in Figures 5.13 and 5.14, the number of kesterite phases found in sample B-001 also increased to three compositions from the previous two, as is the case for sample B-002. Two of the phase's compositions in B-001 have seemingly only increased in the value of the Zn/Sn ratio, shifting closer to the B-type line from the two previous compositions found. However, the third phase's composition is found in a more Cu-poor region with a lower Cu/(Zn+Sn) ratio than that of the planned composition and a Zn/Sn ratio in between the two previous ones. Kesterite phase compositions in sample B-002 have shifted to a significantly lower Cu/(Zn+Sn) ratio region, though the Zn/Sn ratios have mostly stayed at the same level. Phases found are just as concentrated as the ones determined before the second annealing.

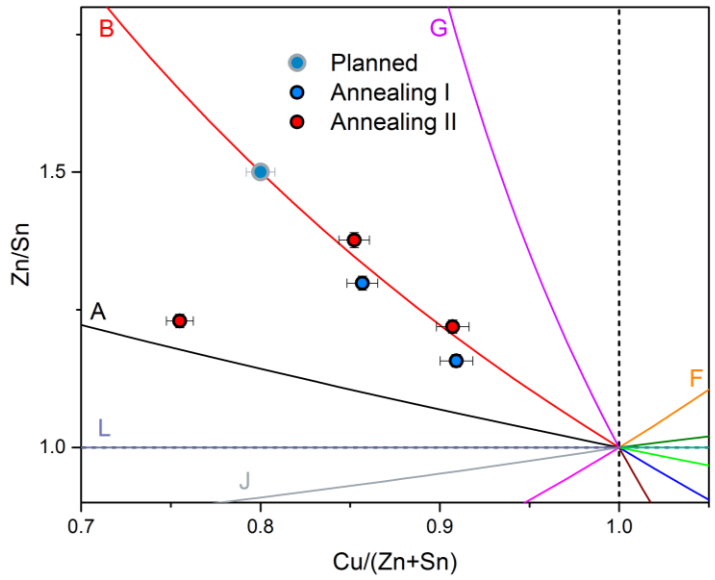

Figure 5.13 – Cation ratio plot of results from WDX measurements of sample B-001.

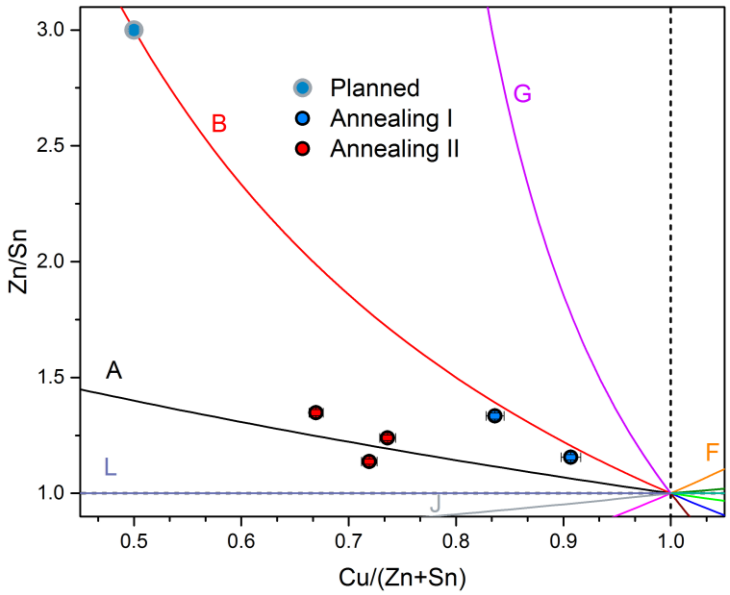

Figure 5.14 – Cation ratio plot of results from WDX measurements of sample B-002.

As seen in Table 5.3, investigation on the data of the C-type samples revealed that grains of Cu_2SnSe_3 and $SnSe_2$ secondary phases were successfully measured, confirming the findings of the study with X-ray diffraction. Still, the presence of Cu_2Se was also determined in sample C-002. Lack of success in identifying the presence of this phase in the sample's diffraction pattern could be explained by the complete overlap of its peaks by those of Cu_2SnSe_3, which would be hard to notice in a basic analysis with the PowderCell software. The WDX measurement of sample C-002 after the first annealing found no grains of $SnSe_2$, but assuming that grains belonging to this phase were simply not probed at the time, the earlier observation that the secondary phase content of this sample suffered no changes could still be correct.

Sample	Secondary phases	
	Annealing I	Annealing II
C-001	$SnSe_2$; Cu_2SnSe_3	$SnSe_2$; Cu_2SnSe_3
C-002	Cu_2SnSe_3; Cu_2Se	Cu_2SnSe_3; Cu_2Se; $SnSe_2$

Table 5.3 – Secondary phases found in the C-type samples by WDX analysis, before and after the re-annealing.

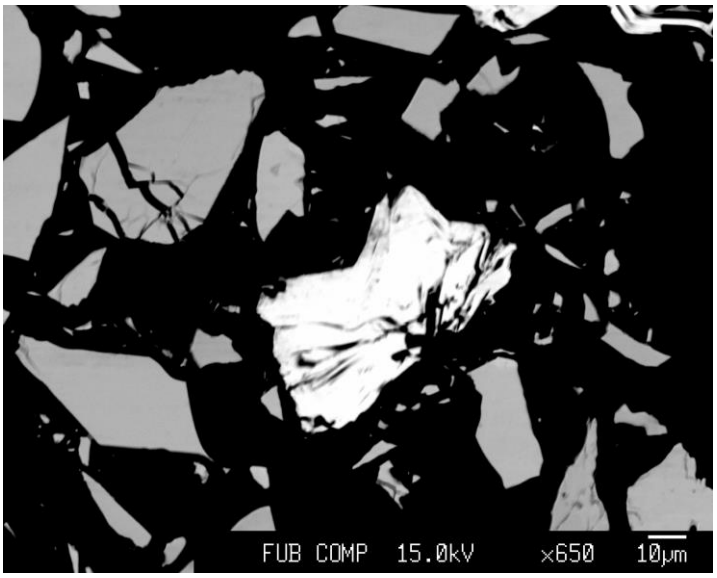

Figure 5.15 – BSE micrograph of sample C-002, displaying a white grain of $SnSe_2$.

Two distinct kesterite phases were measured in each C-type sample, meaning that the amount of phases found before the second annealing was maintained. Compositions of these phases in sample C-001 seem to have shifted from those of the first annealing by an increase of the Cu/(Zn+Sn) ratios and a decrease of the Zn/Sn ratios, with one of phases almost reaching the planned composition. The D-type fraction of the measured phases has also increased, as seen in Figure 5.16. Kesterite phase compositions of sample C-002 follow the opposite trend by concentrating in lower Cu/(Zn+Sn) ratios than those from the first annealing, which can be seen in Figure 5.17. Furthermore, D-type fractions of these phases have decreased since the compositions are closer to the C-type off-stoichiometry line.

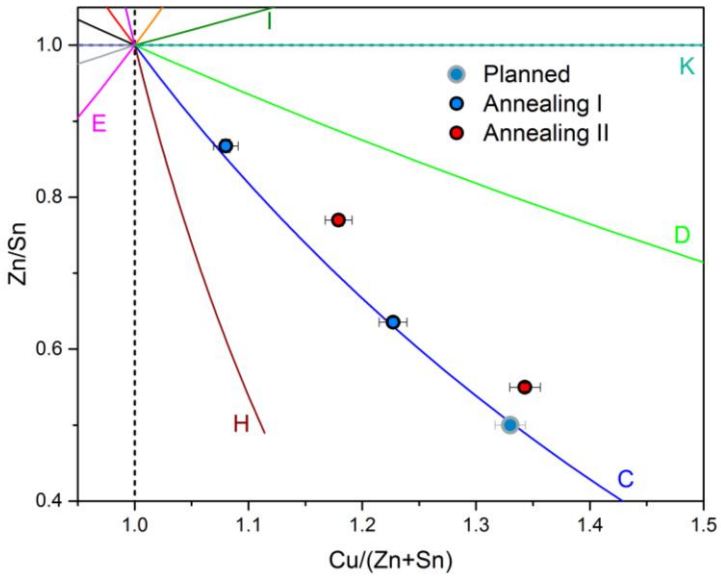

Figure 5.16 – Cation ratio plot of results from WDX measurements of sample C-001.

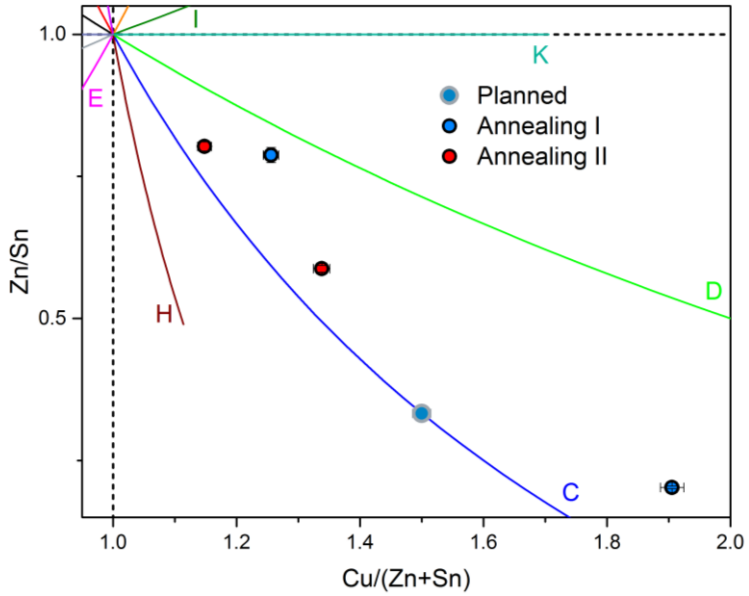

Figure 5.17 – Cation ratio plot of results from WDX measurements of sample C-002.

Secondary phases detected by WDX measurements of the D-type samples are in agreement with the contents determined by the structural study and results are presented in Table 5.4. In sample D-001, only Cu_2Se was found, as it happened when studying the sample before the re-annealing. In sample D-002, both Cu_2Se and Cu_2SnSe_3 were found, though analysis of the sample after being first annealed found $SnSe_2$ and Cu_2SnSe_3 instead. This means that the secondary phase content of this sample underwent some changes, though the presence of the same Cu_2Se peaks in the old diffraction pattern still suggests that this phase was also present in the sample prior to the second annealing.

Sample	Secondary phases	
	Annealing I	Annealing II
D-001	Cu_2Se	Cu_2Se
D-002	Cu_2SnSe_3; $SnSe_2$	Cu_2SnSe_3; Cu_2Se

Table 5.4 – Secondary phases found in the D-type samples by WDX analysis, before and after the re-annealing.

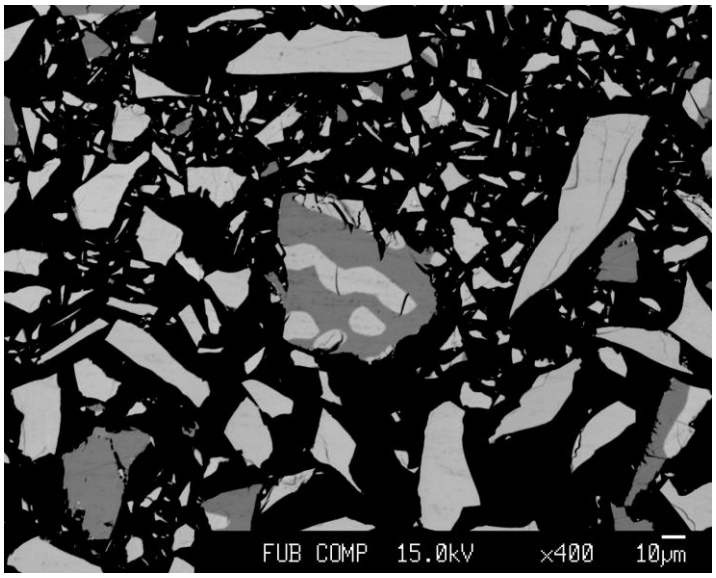

Figure 5.18 – BSE micrograph of sample D-002, displaying a dark grey-light grey grain where Cu_2SnSe_3 and Cu_2Se were detected.

Similarly to the C-type samples, the amount of distinct kesterite phases in the D-type samples have remained the same, with each sample containing two different compositions. Comparably to the changes seen in sample C-002, phase compositions in sample D-001 have also concentrated in lower Cu/(Zn+Sn) ratios and become closer to the D-type line (Figure 5.19), lowering the C-type fraction of these kesterite phases. Changes in the phase compositions of sample D-002 are almost identical to the ones observed in sample C-001. The same shift in relation to the ratios of the first annealing, causing compositions to become more Cu-rich and slightly more Zn-poor, is easily observed by comparing Figures 5.16 and 5.20. Again, the D-type fraction of the determined compositions increased as they have shifted towards the corresponding off-stoichiometry type line.

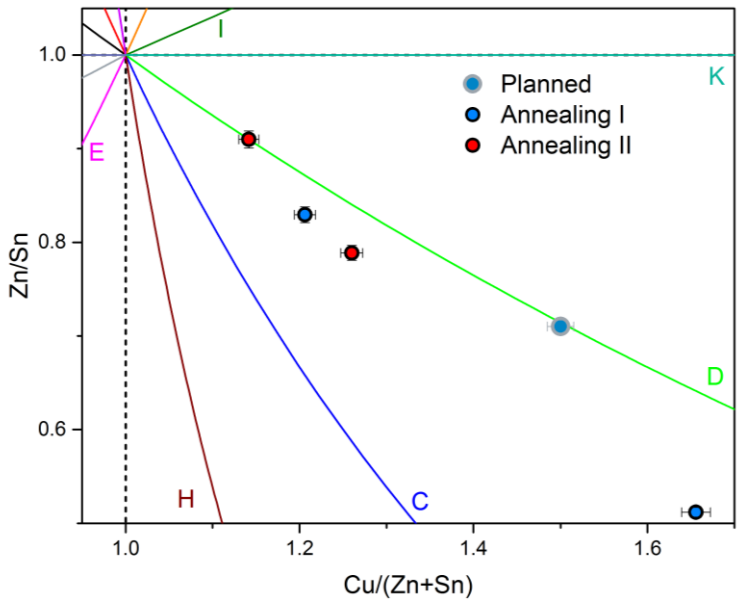

Figure 5.19 – Cation ratio plot of results from WDX measurements of sample D-001.

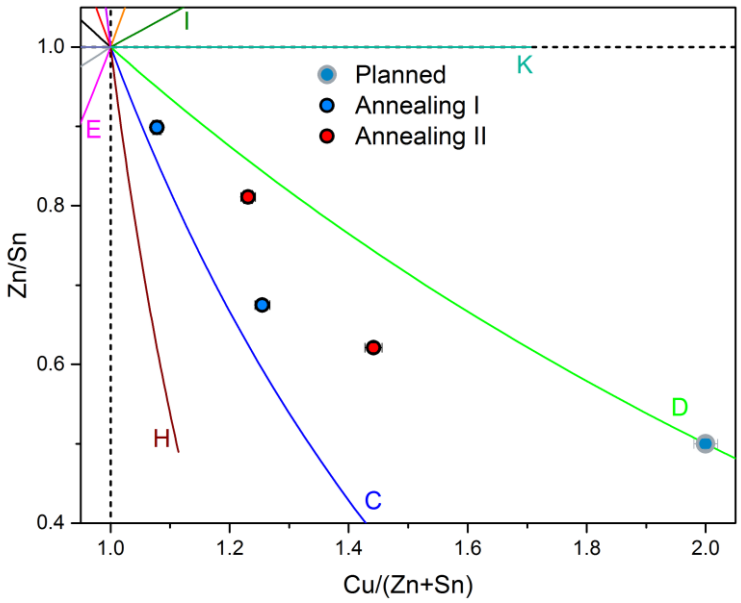

Figure 5.20 – Cation ratio plot of results from WDX measurements of sample D-002.

WDX analysis results confirm that the qualitative phase contents of the entire set of samples have stayed mostly identical after the second annealing took place, with the exception of some small changes in samples C-002 and D-002. Regarding the composition of the kesterite phases, the opposite of the intended outcome occurred and, instead of reducing the diversity of CZTSe compositions in each sample, the number actually increased or remained identical. The compositions themselves have shown a shift from the previous cation ratios, but these are not similar enough across samples to identify the exact effects of the re-annealing in general parameters, though some compositions appear to shift in the direction of off-stoichiometry lines.

Ultimately, the conclusion is still that it has proven impossible to reduce the amount of distinct CZTSe phases to a single one in any of the samples by influence of a second thermal annealing.

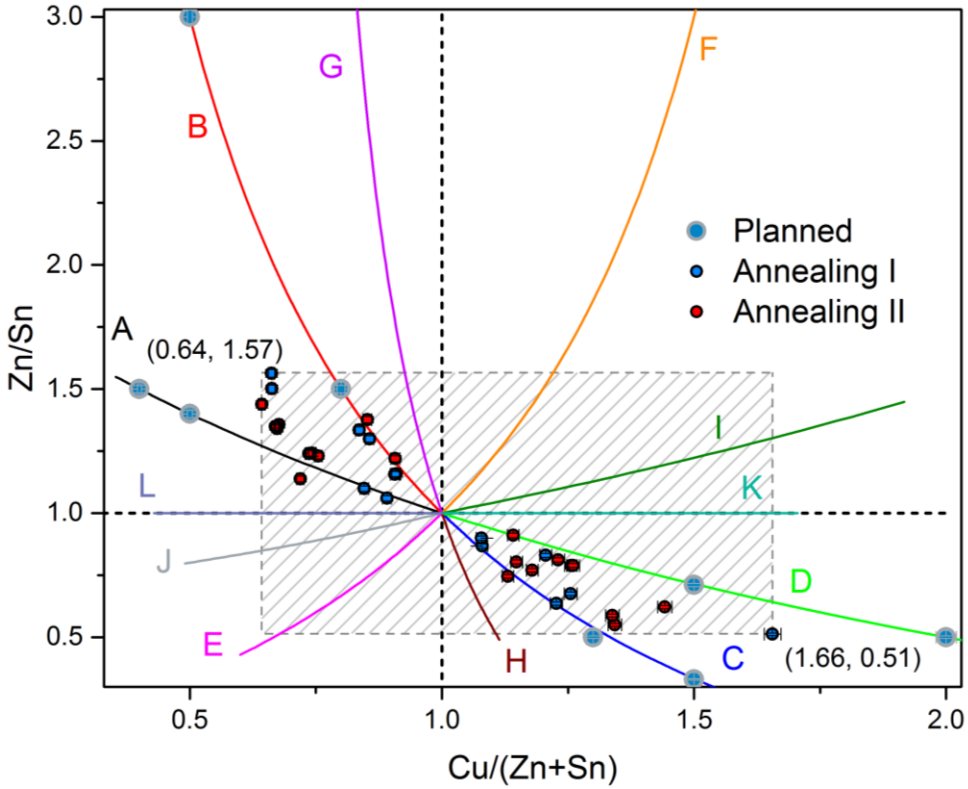

Figure 5.21 – Complete set of results from WDX measurements, showing all the kesterite compositions measured and possible existence limits of this phase.

Even though this process was unable to improve the homogeneity of the samples, results do appear to show potential limits to the existence of the kesterite phase, since none of the compositions measured have crossed outside the boundaries shown in Figure 5.21. However, further investigations need to be performed on this topic.

6. Discussion and Conclusions

As its main objective, this work set out to investigate the limitations of XANES analysis when applied to the detection of secondary phases in $Cu_2ZnSnSe_4$, an investigation which had never been performed until now. Both theory and literature supported the hypothesis that this method would be capable of not only detection but even quantification of multiple secondary phases, so there was a strong basis for this project.

To test the method, the two sets of kesterite-secondary phase mixture samples were analysed through linear combination analysis, from which detection limits could be established using the knowledge of the real secondary phase concentrations in each them. Regarding the Cu_2SnSe_3 mixtures, it was shown that for measurements at the Cu K-edge the detection limit could be found at 5% phase concentration, with phase contents below this mark being completely undetected in the analysis. Quantification was determined to be impossible due to the underestimation and implied lack of precision presented by the obtained percentages. Analysis of measurements of these mixtures at the Se K-edge did not offer improvements – apart from a localized detection at 2% concentration, reliable detection only seems possible starting at 10%. From the discrepancy between obtained and real weight percentages CTSe up to 10% it can only be surmised that quantification can be disregarded completely. Quantification at 20% is hard to evaluate due to the lack of a logical trend in the results, which also suggests a lack of precision in the determination of the weight percentages, even though a certain relative accuracy is observable at this concentration. In general, results from the ternary mixtures reveal a need for further investigation, as there is a potential for detection – especially at the Cu edge – but more precise measurements must be conducted to truly understand the extent of this capacity.

Observations were more straight-forward with the ZnSe mixtures measured at the Se K-edge. The obtained weight percentages of ZnSe phase were very close to the real concentrations for all sample investigated – with the exclusion of the 2% mixture, for which results showed signs of some statistical defect. Analysis of the real-world off-stoichiometric samples known to contain ZnSe supports the results, since the phase was detected in all samples. Considering these findings, it can be concluded that XANES is indeed a functioning method when applied to the detection and quantification of the ZnSe phase for samples measured at the Se K-edge.

In testing the addition of other secondary phase standards to the LCF analysis, an influence was sometimes observed in every set of sample data but the results obtained were not enough to understand it at a significant level. Detection capacity, however, appears to be unaffected by these changes in analytical conditions. The results of the same tests applied to the off-stoichiometric samples were basically equivalent, in the end. Every added secondary phase whose presence in the samples had not been determined by the WDX measurements was still detected by the LCF analysis, which was accompanied by an increase in fit quality. This would either suggest that those secondary phases are actually present or that false detections occurred, but there are many additional factors to consider when analysing real-world samples, so concrete conclusions cannot be drawn. Aside from these changes, detection of the ZnSe phase continued to occur for every sample, which follows the observations with the mixture samples.

Investigation on the influence of the kesterite standard's stoichiometry had some interesting results, showing that the method's efficiency can be connected to the standards that are used. Each separate standard use concluded in different secondary phase weight percentages, but mostly conserved the trend observed in the original results. In the case of the CTSe mixtures, the difference was large enough to conclude that different standards can have a notable influence in the percentages determined, though this influence was bigger for measurements at the copper edge. In the case of the ZnSe mixtures, the difference in secondary phase weight percentages was very subtle, still being contained within a small error bar and therefore preserving the very precise quantification capacity observed previously. The same study revealed somewhat opposite results when applied to the quantification of ZnSe on the off-stoichiometric samples, where percentages from the CZTSe_SR and CZTSe_21 standards were always distinctly separated from the rest. Again, it's hard to build conclusions based on these observations, given the high number of factors that come with the real-world samples. A safe approach to application of this method should be the use of a kesterite standard with at least similar stoichiometry to that of the sample analysed, as the ZnSe mixture samples have shown no issue with the standards that fulfil this condition. Otherwise, the use of incorrect standards may carry an overestimation, underestimation or even complete nullification of the presence of some secondary phases. But this also means that application of this method to the problem of secondary phase detection in CZTSe will not work by itself, since the stoichiometry of the sample and standards must be investigated prior to using XANES analysis.

The second objective of this work consisted in investigating the effects of a second thermal annealing on samples of high heterogeneity. Investigation of these effects was divided into structural and compositional studies by measuring the re-annealed samples with the XRD and WDX techniques, respectively. The structural study concluded that the secondary phases present in the samples had a high degree of similarity to those determined in the synthesised samples. This similarity could be easily seen for most samples by comparing the diffraction patterns corresponding to the two annealing steps. Chemical characterization of the samples confirmed that the secondary phases contained in the samples had remained mostly identical after the re-annealing. Distinct kesterite phase amounts per sample, however, either increased or also remained the same. Looking at the individual compositions in each sample revealed that these were always shifted from the previously measured kesterite phases in some way, with a tendency towards off-stoichiometry lines being observed in some samples. But despite the fact that the phase compositions of some samples had also become closer, the conclusion remained that the application of the second thermal annealing had no major benefits in increasing the homogeneity of the samples.

References

[1] Fraunhofer ISE, *"Photovoltaics Report", 2017.* https://www.ise.fraunhofer.de/content/dam/ise/de/documents/publications/studies/Photovoltaics-Report.pdf

[2] Persson, C., *Electronic and optical properties of Cu_2ZnSnS_4 and $Cu_2ZnSnSe_4$.* Journal of Applied Physics, 2010. **107**(5): p. 053710-1--053710-8-053710.

[3] Shockley, W. and H.J. Queisser, *Detailed Balance Limit of Efficiency of p-n Junction Solar Cells*. Journal of Applied Physics, 1961. **32**(3): p. 510-519.

[4] Wang, W., et al., *Device Characteristics of CZTSSe Thin-Film Solar Cells with 12.6% Efficiency*. Advanced Energy Materials, 2014. **4**(7).

[5] X. Liu et al., *The current status and future prospects of kesterite solar cells: a brief review*. Prog. Photovolt: Res. Appl, 2016, **24:** p. 879-898.

[6] Ahn, S., et al., *Determination of band gap energy (Eg) of Cu2ZnSnSe4 thin films: On the discrepancies of reported band gap values*. Applied Physics Letters, 2010. **97**(2): p. 021905.

[7] Lee, Y.S., et al., *Cu2ZnSnSe4 Thin-Film Solar Cells by Thermal Co-evaporation with 11.6% Efficiency and Improved Minority Carrier Diffusion Length*. Advanced Energy Materials, 2015. **5**(7)

[8] Berg, D.M. and P.J. Dale, *Kesterites, in Copper Zinc Tin Sulfide-Based Thin-Film Solar Cells*. 2014, John Wiley & Sons Ltd. p. 107-132.

[9] Gosavi, S.R., et al., *Physical, optical and electrical properties of copper selenide (CuSe) thin films deposited by solution growth technique at room temperature*. Journal of Alloys and Compounds, 2008. **448**(1–2): p. 344-348.

[10] Sousa, A.P.C.d., *Investigation of detection limits of ZnSe and Cu_2SnSe_3 secondary phases in $Cu_2ZnSnSe_4$,* in Departamento de Fisica. 2016, Universidade de Coimbra.

[11] Just. J., et al., *Secondary phases and their influence on the composition of the kesterite phase in CZTS and CZTSe thin films*. Phhys. Chem. Chem. Phys., 2016. **18,** 15988.

[12] Schnohr, C.S., Ridgway, M.C., *X-Ray Absorption Spectroscopy of Semiconductors*, Springer Series in Optical Sciences, Vol. 190, 2015, Springer-Verlag, Berlin, Heidelberg.

[13] Newville, M., *The Fundamentals of XAFS*, 2004. www.xafs.org/Tutorials

[14] Kelly, S.D., Hesterberg, D., Ravel, B., *Analysis of soils and minerals using X-ray absorption spectroscopy, in Methods of Soil Analysis—Part 5: Mineralogical Methods*, Soil Science Society of America Book Series No. 5, Madison (2008).

[15] FRITSCH Pulverisette 23 mini-mill, http://www.fritsch-international.com/sample-preparation/milling/ball-mills/details/product/pulverisette-23/ (Accessed 24 Sept. 2017).

[16] Valle Rios, L.E., *Structural trends in off-stoichiometric kesterite type compound $Cu_2ZnSnSe_4$ semiconductor*. 2016, Freie Universität Berlin.

[17] Colina-Ruiz, R. A. et al, *Local atomic structure and analysis of secondary phases in non-stoichiometric Cu_2ZnSnS_4 using X-ray absorption fine structure spectroscopy*. Journal of Alloys and Compounds, 2017. **714:** p. 381-389.

[18] "Übersichtsplan BESSY II", https://www.helmholtz-berlin.de/quellen/bessy/instruments-photons/index_de.html (Accessed 5 Aug. 2017).

[19] Helmholtz-Zentrum Berlin für Materialien und Energie, *KMC-2: an X-ray beamline with dedicated diffraction and XAS endstations at BESSY II*. Journal of large-scale research facilities, 2016, 2, A49. http://dx.doi.org/10.17815/jlsrf-2-65

[20] XANES station, https://www.helmholtz-berlin.de/pubbin/igama_output?modus=einzel&sprache=en&gid=1694&typoid (Accessed 5 Aug. 2017).

[21] B. Ravel, M. Newville, ATHENA, ARTEMIS, HEPHAESTUS: data analysis for X-ray absorption spectroscopy using IFEFFIT, J. Synchrotron Radiat., 2005, **12**, 537–541.

[22] Ravel, B., *ATHENA: XAS Data Processing*, 2017. http://bruceravel.github.io/demeter/documents/Athena/index.html

[23] Pecharsky, V.K. and P.Y. Zavalij, Fundamentals of powder diffraction and structural characterization of materials. Vol. 69. 2009: Springer.

[24] Kraus, W., Nolze, G., *POWDER CELL – a program for the representation and manipulation of crystal structures and calculation of the resulting X-ray powder patterns*, J. Appl. Cryst., 1996, **29**, 301-303.

[25] Clarke, A.R., Microscopy techniques for materials science. 2002, Woodhead Publishing.

[26] Valle Rios, L. E., et al., *Existence of off-stoichiometric single phase kesterite*. *Journal of Alloys and Compounds*, 2016. **657**: p. 408-413.

Appendices

Appendix A1. Results from analysis of the Cu_2SnSe_3 mixtures measured at the Cu K-edge

A1.1. Normalizations

Normalization 1							
Sample	Real CTSe %	XANES CTSe %	Error %	Determined CTSe %	Error %	R-factor	χ^2
Kest II - 20%	19.26(2)	17.6	1.4	14.2	1.0	0.0000029	0.00006
Kest II - 10%	9.64(1)	7.6	2.2	6.0	1.6	0.0000079	0.00018
Kest II - 5%	4.50(1)	7.2	3.3	5.7	2.5	0.0000174	0.00039
Kest II - 3%	2.78(1)	0.0	0.0	0.0	0.0	0.0000183	0.00041
Kest II - 2%	1.58(1)	0.0	0.0	0.0	0.0	0.0000218	0.00048
Kest II - 1%	1.18(1)	0.0	0.0	0.0	0.0	0.0000098	0.00021

Normalization 2							
Sample	Real CTSe %	XANES CTSe %	Error %	Determined CTSe %	Error %	R-factor	χ^2
Kest II - 20%	19.26(2)	34.2	1.6	28.7	1.1	0.0000070	0.00014
Kest II - 10%	9.64(1)	0.0	0.0	0.0	0.0	0.0000480	0.00096
Kest II - 5%	4.50(1)	0.0	0.0	0.0	0.0	0.0000084	0.00017
Kest II - 3%	2.78(1)	9.2	3.3	7.3	2.4	0.0000288	0.00059
Kest II - 2%	1.58(1)	0.0	0.0	0.0	0.0	0.0000990	0.00198
Kest II - 1%	1.18(1)	0.0	0.0	0.0	0.0	0.0000798	0.00160

Normalization 2							
Sample	Real CTSe %	XANES CTSe %	Error %	Determined CTSe %	Error %	R-factor	χ^2
Kest II - 20%	19.26(2)	15.2	1.7	12.2	1.2	0.0000032	0.00007
Kest II - 10%	9.64(1)	0.0	0.0	0.0	0.0	0.0000062	0.00013
Kest II - 5%	4.50(1)	0.0	0.0	0.0	0.0	0.0000133	0.00029
Kest II - 3%	2.78(1)	0.0	0.0	0.0	0.0	0.0000165	0.00035
Kest II - 2%	1.58(1)	0.0	0.0	0.0	0.0	0.0000234	0.00049
Kest II - 1%	1.18(1)	0.0	0.0	0.0	0.0	0.0000116	0.00024

A1.2. Addition of secondary phase standards

+ Cu_2Se							
Sample	Secondary Phase	XANES %	Error	Determined %	Error %	R-factor	χ^2
Kest II - 20%	Cu_2SnSe_3 Cu_2Se	17.2 0.7	1.3 1.9	13.9 0.2	0.9 0.7	0.0000028	0.00006
Kest II - 10%	Cu_2SnSe_3 Cu_2Se	7.0 1.0	2.2 3.1	5.5 0.3	1.7 1.0	0.0000076	0.00017
Kest II - 5%	Cu_2SnSe_3 Cu_2Se	6.3 1.4	3.3 4.7	5.0 0.5	2.5 1.6	0.0000168	0.00037
Kest II - 3%	Cu_2SnSe_3 Cu_2Se	0.0 0.0	0.0 0.0	0.0 0.0	0.0 0.0	0.0000183	0.00041
Kest II - 2%	Cu_2SnSe_3 Cu_2Se	0.0 0.0	0.0 0.0	0.0 0.0	0.0 0.0	0.0000218	0.00048
Kest II - 1%	Cu_2SnSe_3 Cu_2Se	0.0 0.0	0.0 0.0	0.0 0.0	0.0 0.0	0.0000098	0.00021

+ CuSe							
Sample	Secondary Phase	XANES %	Error	Determined %	Error %	R-factor	χ^2
Kest II - 20%	Cu_2SnSe_3 CuSe	20.3 0.0	2.2 0.4	16.5 0.0	1.5 0.2	0.0000030	0.00007
Kest II - 10%	Cu_2SnSe_3 CuSe	12.6 0.0	3.7 0.7	10.0 0.0	2.7 0.3	0.0000082	0.00018
Kest II - 5%	Cu_2SnSe_3 CuSe	12.2 0.0	5.5 1.0	9.7 0.0	4.0 0.5	0.0000178	0.00039
Kest II - 3%	Cu_2SnSe_3 CuSe	0.0 0.0	0.0 0.0	0.0 0.0	0.0 0.0	0.0000183	0.00041
Kest II - 2%	Cu_2SnSe_3 CuSe	0.0 0.0	0.0 0.0	0.0 0.0	0.0 0.0	0.0000218	0.00048
Kest II - 1%	Cu_2SnSe_3 CuSe	0.0 0.0	0.0 0.0	0.0 0.0	0.0 0.0	0.0000098	0.00021

A1.3. Stoichiometry of the CZTSe standard

Sample	CZTSe Standard	XANES CTSe %	Error %	Determined CTSe %	Error %	R-factor	χ^2
Kest II - 20%	Kest II	17.6	1.4	14.2	1.0	0.0000029	0.00006
	Kest I	13.3	1.1	10.5	0.8	0.0000018	0.00004
	CZTSe_SR	43.8	2.4	37.5	1.6	0.0000160	0.00035
Kest II - 10%	Kest II	7.6	2.2	6.0	1.6	0.0000079	0.00018
	Kest I	3.9	2.5	3.0	1.9	0.0000089	0.00020
	CZTSe_SR	31.5	1.7	26.1	1.1	0.0000080	0.00018
Kest II - 5%	Kest II	7.2	3.3	5.7	2.5	0.0000174	0.00039
	Kest I	3.2	3.5	2.5	2.6	0.0000179	0.00040
	CZTSe_SR	27.7	1.5	22.8	1.0	0.0000063	0.00014
Kest II - 3%	Kest II	0.0	0.0	0.0	0.0	0.0000183	0.00041
	Kest I	0.0	0.0	0.0	0.0	0.0000213	0.00047
	CZTSe_SR	14.5	1.5	11.5	1.1	0.0000062	0.00014
Kest II - 2%	Kest II	0.0	0.0	0.0	0.0	0.0000218	0.00048
	Kest I	0.0	0.0	0.0	0.0	0.0000302	0.00066
	CZTSe_SR	18.5	1.4	14.9	1.0	0.0000055	0.00012
Kest II - 1%	Kest II	0.0	0.0	0.0	0.0	0.0000098	0.00021
	Kest I	0.0	0.0	0.0	0.0	0.0000153	0.00034
	CZTSe_SR	22.9	1.9	18.6	1.3	0.0000101	0.00022

Appendix A2. Results from analysis of the ZnSe mixtures measured at the Se K-edge

A2.1. Normalizations

Normalization 1							
Sample	Real ZnSe %	XANES ZnSe %	Error %	Determined ZnSe %	Error %	R-factor	χ^2
Kest I - 20%	20.10(2)	21.0	0.5	19.7	0.4	0.0000208	0.00055
Kest I - 10%	10.05(1)	9.2	0.3	8.5	0.3	0.0000062	0.00016
Kest I - 5%	5.01(1)	6.1	0.4	5.7	0.4	0.0000137	0.00035
Kest I - 3%	3.10(1)	4.4	0.3	4.1	0.3	0.0000069	0.00018
Kest I - 2%	2.01(1)	0.0	0.0	0.0	0.0	0.0000226	0.00058
Kest I - 1%	1.01(1)	0.7	0.3	0.6	0.3	0.0000094	0.00024

Normalization 2							
Sample	Real ZnSe %	XANES ZnSe %	Error %	Determined ZnSe %	Error %	R-factor	χ^2
Kest I - 20%	20.10(2)	21.5	0.5	20.2	0.4	0.0000148	0.00040
Kest I - 10%	10.05(1)	9.3	0.3	8.6	0.3	0.0000060	0.00016
Kest I - 5%	5.01(1)	5.9	0.4	5.5	0.4	0.0000136	0.00036
Kest I - 3%	3.10(1)	3.9	0.3	3.6	0.3	0.0000070	0.00019
Kest I - 2%	2.01(1)	0.0	0.0	0.0	0.0	0.0000248	0.00066
Kest I - 1%	1.01(1)	0.8	0.4	0.7	0.4	0.0000095	0.00025

Normalization 3							
Sample	Real ZnSe %	XANES ZnSe %	Error %	Determined ZnSe %	Error %	R-factor	χ^2
Kest I - 20%	20.10(2)	22.0	0.4	20.6	0.3	0.0000123	0.00033
Kest I - 10%	10.05(1)	9.2	0.3	8.5	0.3	0.0000069	0.00018
Kest I - 5%	5.01(1)	5.8	0.5	5.4	0.4	0.0000155	0.00040
Kest I - 3%	3.10(1)	4.0	0.3	3.7	0.3	0.0000084	0.00022
Kest I - 2%	2.01(1)	0.0	0.0	0.0	0.0	0.0000182	0.00048
Kest I - 1%	1.01(1)	0.8	0.4	0.7	0.4	0.0000096	0.00025

A2.2. Addition of secondary phase standards

+ Cu_2Se							
Sample	Secondary Phase	XANES %	Error	Determined %	Error %	R-factor	χ^2
Kest I - 20%	ZnSe Cu_2Se	21.5 0.0	0.8 0.6	20.2 0.0	0.6 0.8	0.0000148	0.00040
Kest I - 10%	ZnSe Cu_2Se	9.3 0.0	0.5 0.4	8.6 0.0	0.4 0.5	0.0000060	0.00016
Kest I - 5%	ZnSe Cu_2Se	5.7 0.0	0.8 0.6	5.3 0.0	0.7 0.8	0.0000136	0.00036
Kest I - 3%	ZnSe Cu_2Se	3.6 0.0	0.5 0.4	3.3 0.0	0.4 0.5	0.0000070	0.00019
Kest I - 2%	ZnSe Cu_2Se	0.0 0.0	0.0 0.0	0.0 0.0	0.0 0.0	0.0000248	0.00066
Kest I - 1%	ZnSe Cu_2Se	0.8 0.0	0.6 0.5	0.7 0.0	0.5 0.7	0.0000095	0.00025

+ Cu_2SnSe_3							
Sample	Secondary Phase	XANES %	Error	Determined %	Error %	R-factor	χ^2
Kest I - 20%	ZnSe Cu_2SnSe_3	21.6 0.0	7.6 6.2	20.3 0.0	5.9 4.6	0.0000148	0.00040
Kest I - 10%	ZnSe Cu_2SnSe_3	9.3 0.0	4.7 2.8	8.6 0.0	4.0 2.9	0.0000060	0.00016
Kest I - 5%	ZnSe Cu_2SnSe_3	12.7 17.6	6.7 3.9	11.8 18.2	5.5 3.6	0.0000118	0.00031
Kest I - 3%	ZnSe Cu_2SnSe_3	9.0 13.3	4.7 2.8	8.3 13.7	4.0 2.6	0.0000059	0.00016
Kest I - 2%	ZnSe Cu_2SnSe_3	1.0 10.2	8.5 4.9	0.9 10.5	7.8 4.6	0.0000196	0.00052
Kest I - 1%	ZnSe Cu_2SnSe_3	4.6 10.1	5.7 3.3	4.2 10.4	5.0 3.1	0.000089	0.00024

+ SnSe							
Sample	Secondary Phase	XANES %	Error	Determined %	Error %	R-factor	χ^2
Kest I - 20%	ZnSe	21.2	0.7	19.9	0.5	0.0000149	0.00040
	SnSe	0.0	0.2	0.0	0.3		
Kest I - 10%	ZnSe	9.5	0.4	8.8	0.3	0.0000059	0.00016
	SnSe	0.2	0.1	0.3	0.1		
Kest I - 5%	ZnSe	6.6	0.6	6.1	0.5	0.0000128	0.00034
	SnSe	0.6	0.2	0.8	0.3		
Kest I - 3%	ZnSe	4.7	0.4	4.3	0.4	0.0000056	0.00015
	SnSe	0.8	0.1	1.0	0.1		
Kest I - 2%	ZnSe	0.0	0.0	0.0	0.0	0.0000248	0.00066
	SnSe	0.0	0.0	0.0	0.0		
Kest I - 1%	ZnSe	0.6	0.6	0.6	0.6	0.000095	0.00025
	SnSe	0.0	0.2	0.0	0.3		

A2.3. Stoichiometry of the CZTSe standard

Sample	CZTSe Standard	XANES CTSe %	Error %	Determined CTSe %	Error %	R-factor	χ^2
Kest I - 20%	Kest I	21.5	0.5	20.2	0.4	0.0000148	0.00040
	Kest II	23.6	0.6	22.1	0.5	0.0000245	0.00067
	CZTSe_SR	22.8	0.8	21.4	0.6	0.0000512	0.00139
	Cu_2SnSe_3	43.9	0.6	41.2	0.4	0.0000434	0.00118
Kest I - 10%	Kest I	9.3	0.3	8.6	0.3	0.0000060	0.00016
	Kest II	11.4	0.5	10.6	0.4	0.0000225	0.00060
	CZTSe_SR	9.9	0.7	9.2	0.6	0.0000408	0.00109
	Cu_2SnSe_3	34.8	0.5	32.4	0.4	0.0000346	0.00092
Kest I - 5%	Kest I	5.9	0.4	5.5	0.4	0.0000136	0.00036
	Kest II	8.2	0.6	7.6	0.5	0.0000248	0.00066
	CZTSe_SR	6.8	0.7	6.3	0.6	0.0000387	0.00103
	Cu_2SnSe_3	32.4	0.4	30.1	0.3	0.0000266	0.00071
Kest I - 3%	Kest I	3.9	0.3	3.6	0.3	0.0000070	0.00019
	Kest II	6.1	0.5	5.6	0.4	0.0000207	0.00055
	CZTSe_SR	4.6	0.7	4.3	0.6	0.0000406	0.00108
	Cu_2SnSe_3	30.8	0.4	28.5	0.3	0.0000248	0.00066
Kest I - 2%	Kest I	0.0	0.0	0.0	0.0	0.0000248	0.00066
	Kest II	0.0	0.0	0.0	0.0	0.0000314	0.00083
	CZTSe_SR	0.0	0.0	0.0	0.0	0.0000634	0.00168
	Cu_2SnSe_3	25.9	0.6	23.9	0.4	0.0000449	0.00119
Kest I - 1%	Kest I	0.8	0.4	0.7	0.4	0.0000095	0.00025
	Kest II	2.9	0.4	2.7	0.4	0.0000149	0.00040
	CZTSe_SR	1.1	0.6	1.0	0.5	0.0000314	0.00083
	Cu_2SnSe_3	28.5	0.5	26.3	0.4	0.0000323	0.00086

Appendix A3. Results from analysis of the Cu_2SnSe_3 mixtures measured at the Se K-edge

A3.1. Normalizations

Normalization 1							
Sample	Real CTSe %	XANES CTSe %	Error %	Determined CTSe %	Error %	R-factor	χ^2
Kest II - 20%	19.26(2)	16.9	1.4	17.3	1.2	0.0000203	0.00052
Kest II - 10%	9.64(1)	19.9	1.5	20.3	1.3	0.0000251	0.00063
Kest II - 5%	4.50(1)	0.0	0.0	0.0	0.0	0.0000602	0.00157
Kest II - 3%	2.78(1)	0.0	0.0	0.0	0.0	0.0000557	0.00144
Kest II - 2%	1.58(1)	7.1	1.6	7.3	1.5	0.0000256	0.00066
Kest II - 1%	1.18(1)	0.0	0.0	0.0	0.0	0.0000272	0.00070

Normalization 2							
Sample	Real CTSe %	XANES CTSe %	Error %	Determined CTSe %	Error %	R-factor	χ^2
Kest II - 20%	19.26(2)	15.2	1.1	15.5	1.0	0.0000133	0.00035
Kest II - 10%	9.64(1)	20.6	1.7	21.0	1.4	0.0000293	0.00076
Kest II - 5%	4.50(1)	0.0	0.0	0.0	0.0	0.0000438	0.00118
Kest II - 3%	2.78(1)	0.0	0.0	0.0	0.0	0.0000347	0.00092
Kest II - 2%	1.58(1)	5.7	1.4	5.8	1.4	0.0000193	0.00051
Kest II - 1%	1.18(1)	0.0	0.0	0.0	0.0	0.0000341	0.00090

Normalization 3							
Sample	Real CTSe %	XANES CTSe %	Error %	Determined CTSe %	Error %	R-factor	χ^2
Kest II - 20%	19.26(2)	15.2	1.7	15.5	1.5	0.0000293	0.00076
Kest II - 10%	9.64(1)	19.7	1.9	20.1	1.6	0.0000362	0.00093
Kest II - 5%	4.50(1)	0.0	0.0	0.0	0.0	0.0000709	0.00188
Kest II - 3%	2.78(1)	0.0	0.0	0.0	0.0	0.0000642	0.00169
Kest II - 2%	1.58(1)	5.4	2.0	5.5	1.9	0.0000405	0.00106
Kest II - 1%	1.18(1)	0.0	0.0	0.0	0.0	0.0000379	0.00099

A3.2. Addition of secondary phase standards

+ ZnSe							
Sample	Secondary Phase	XANES %	Error	Determined %	Error %	R-factor	χ^2
Kest II - 20%	Cu_2SnSe_3 ZnSe	15.9 0.0	10.2 2.1	16.2 0.0	8.8 1.9	0.0000204	0.00052
Kest II - 10%	Cu_2SnSe_3 ZnSe	34.6 5.5	8.9 2.3	35.3 5.0	6.6 2.1	0.0000240	0.00061
Kest II - 5%	Cu_2SnSe_3 ZnSe	0.0 2.4	9.8 16.9	0.0 2.2	10.0 15.3	0.0000568	0.00148
Kest II - 3%	Cu_2SnSe_3 ZnSe	0.0 0.0	0.0 0.0	0.0 0.0	0.0 0.0	0.0000557	0.00144
Kest II - 2%	Cu_2SnSe_3 ZnSe	0.0 0.0	0.0 0.0	0.0 0.0	0.0 0.0	0.0000296	0.00076
Kest II - 1%	Cu_2SnSe_3 ZnSe	13.8 6.2	6.6 11.6	14.2 5.7	6.2 10.1	0.0000253	0.00065

+ Cu_2Se							
Sample	Secondary Phase	XANES %	Error	Determined %	Error %	R-factor	χ^2
Kest II - 20%	Cu_2SnSe_3 Cu_2Se	24.6 4.0	1.9 3.1	24.8 5.2	1.8 3.8	0.0000164	0.00042
Kest II - 10%	Cu_2SnSe_3 Cu_2Se	19.8 0.0	3.9 0.9	20.2 0.0	3.2 1.2	0.0000251	0.00063
Kest II - 5%	Cu_2SnSe_3 Cu_2Se	0.0 3.2	3.4 5.8	0.0 4.2	3.5 7.2	0.0000548	0.00143
Kest II - 3%	Cu_2SnSe_3 Cu_2Se	0.3 4.6	3.1 5.3	0.3 6.0	3.1 6.5	0.0000454	0.00117
Kest II - 2%	Cu_2SnSe_3 Cu_2Se	12.5 2.9	2.2 3.9	12.7 3.8	2.1 4.9	0.0000236	0.00061
Kest II - 1%	Cu_2SnSe_3 Cu_2Se	0.0 0.0	0.0 0.0	0.0 0.0	0.0 0.0	0.0000272	0.00070

+ SnSe							
Sample	Secondary Phase	XANES %	Error %	Determined %	Error %	R-factor	χ^2
Kest II - 20%	Cu_2SnSe_3	18.3	1.6	18.7	1.4	0.0000204	0.00052
	SnSe	0.0	0.3	0.0	0.4		
Kest II - 10%	Cu_2SnSe_3	17.1	1.7	17.4	1.5	0.0000237	0.00060
	SnSe	0.8	0.3	1.0	0.4		
Kest II - 5%	Cu_2SnSe_3	0.0	0.0	0.0	0.0	0.0000602	0.00157
	SnSe	0.0	0.0	0.0	0.0		
Kest II - 3%	Cu_2SnSe_3	0.0	0.0	0.0	0.0	0.0000557	0.00144
	SnSe	0.0	0.0	0.0	0.0		
Kest II - 2%	Cu_2SnSe_3	7.8	1.8	8.0	1.7	0.0000256	0.00066
	SnSe	0.0	0.3	0.0	0.4		
Kest II - 1%	Cu_2SnSe_3	0.0	0.0	0.0	0.0	0.0000272	0.00070
	SnSe	0.0	0.0	0.0	0.0		

A3.3. Stoichiometry of the CZTSe standard

Sample	CZTSe Standard	XANES CTSe %	Error %	Determined CTSe %	Error %	R-factor	χ^2
Kest II - 20%	Kest II	16.9	1.4	17.3	1.2	0.0000203	0.00052
	Kest I	20.8	1.6	21.3	1.3	0.0000295	0.00075
	CZTSe_SR	18.6	1.4	19.0	1.2	0.0000224	0.00057
Kest II - 10%	Kest II	19.9	1.5	20.3	1.3	0.0000251	0.00063
	Kest I	23.7	1.9	24.2	1.5	0.0000424	0.00107
	CZTSe_SR	21.3	1.5	21.7	1.2	0.0000238	0.00060
Kest II - 5%	Kest II	0.0	0.0	0.0	0.0	0.0000602	0.00157
	Kest I	0.0	0.0	0.0	0.0	0.0000283	0.00074
	CZTSe_SR	0.0	0.0	0.0	0.0	0.0000507	0.00132
Kest II - 3%	Kest II	0.0	0.0	0.0	0.0	0.0000557	0.00144
	Kest I	0.0	0.0	0.0	0.0	0.0000203	0.00053
	CZTSe_SR	0.0	0.0	0.0	0.0	0.0000475	0.00123
Kest II - 2%	Kest II	7.1	1.6	7.3	1.5	0.0000256	0.00066
	Kest I	9.5	1.3	9.7	1.2	0.0000196	0.00050
	CZTSe_SR	8.4	1.6	8.6	1.5	0.0000268	0.00069
Kest II - 1%	Kest II	0.0	0.0	0.0	0.0	0.0000272	0.00070
	Kest I	0.7	1.7	0.7	1.7	0.0000327	0.00084
	CZTSe_SR	0.0	0.0	0.0	0.0	0.0000209	0.00054

Appendix A4. Results from analysis of off-stoichiometric $Cu_2ZnSnSe_4$ samples measured at the Se K-edge

A4.1. Addition of secondary phase standards

Sample	Secondary Phase	XANES %	Error %	Determined %	Error %	R-factor	χ^2
A0075-6	ZnSe	15.0	1.6	14.0	1.3	0.0002633	0.00685
	ZnSe	15.6	1.5	14.6	1.3	0.0002233	0.00580
	CuSe	7.3	2.7	9.5	2.3		
	ZnSe	8.0	2.1	7.1	1.8	0.0002254	0.00586
	Cu_2Se	11.7	4.0	14.9	4.4		
	ZnSe	10.9	2.3	9.9	2.0	0.0002119	0.00551
	CuSe	4.9	4.2	4.4	3.6		
	Cu_2Se	7.5	2.8	9.8	3.3		
B0050-4	ZnSe	8.3	0.7	7.7	0.6	0.0000462	0.00120
	CuSe	5.7	1.4	5.2	1.2		
	ZnSe	2.1	0.9	1.9	0.8	0.0000275	0.00072
	CuSe	2.6	2.3	2.3	2.0		
	Cu_2Se	9.6	1.0	12.3	1.2		

A4.2. Stoichiometry of the CZTSe standard

Sample	CZTSe Standard	XANES ZnSe %	Error %	Determined ZnSe %	Error %	R-factor	χ^2
A0075-6	CZTSe_SR	15.0	1.6	14.0	1.3	0.0002633	0.00685
	CZTSe_01	10.9	1.7	10.1	1.4	0.0002619	0.00681
	CZTSe_02	10.3	1.6	9.6	1.4	0.0002303	0.00599
	CZTSe_07	9.7	1.6	9.0	1.4	0.0002330	0.00606
	CZTSe_21	18.5	1.9	17.3	1.5	0.0003759	0.00977
B0050-4	CZTSe_SR	8.3	0.7	7.7	0.6	0.0000462	0.00120
	CZTSe_01	5.1	0.7	4.8	0.6	0.0000392	0.00102
	CZTSe_02	3.8	0.7	3.6	0.6	0.0000416	0.00108
	CZTSe_07	3.7	0.7	3.4	0.6	0.0000376	0.00097
	CZTSe_21	11.6	0.9	10.9	0.8	0.0000884	0.00229
C0025-2	CZTSe_SR	3.1	1.2	2.8	1.0	0.0000582	0.00152
	CZTSe_01	0.9	1.0	0.8	0.9	0.0000406	0.00106
	CZTSe_02	0.0	0.9	0.0	0.8	0.0000286	0.00075
	CZTSe_07	0.0	0.9	0.0	0.8	0.0000326	0.00085
	CZTSe_21	4.7	1.5	4.2	1.3	0.0000846	0.00221
C0025-4	CZTSe_SR	1.0	0.8	0.9	0.7	0.0000257	0.00067
	CZTSe_01	0.0	0.7	0.0	0.6	0.0000184	0.00048
	CZTSe_02	0.0	0.8	0.0	0.7	0.0000222	0.00058
	CZTSe_07	0.0	0.7	0.0	0.6	0.0000163	0.00042
	CZTSe_21	2.8	1.3	2.6	1.2	0.0000630	0.00164

Appendix A5. Results from WDX measurements

A-001						
Main Phase	Formula	Cu/(Zn+Sn)	Zn/Sn	Type I	Type II	Secondary phases
1	$Cu_{1.52}Zn_{1.42}Sn_{0.91}Se_4$	0.66209	1.56366	B - 73.155%	A - 26.845%	$SnSe_2$; ZnSe
2	$Cu_{1.85}Zn_{1.06}Sn_{1.01}Se_4$	0.89092	1.05956	L - 21.075%	A - 78.925%	
Re-annealing						
1	$Cu_{1.62}Zn_{1.22}Sn_{0.73}Se_4$	0.737764	1.238969	B - 27.152%	A - 72.848%	$SnSe_2$; ZnSe
2	$Cu_{1.51}Zn_{1.30}Sn_{0.62}Se_4$	0.673665	1.340629	B - 37.880%	A - 62.120%	
3	$Cu_{1.57}Zn_{1.16}Sn_{1.03}Se_4$	0.719141	1.137421	L - 33.478%	A - 66.522%	

A-002						
Main Phase	Formula	Cu/(Zn+Sn)	Zn/Sn	Type I	Type II	Secondary phases
1	$Cu_{1.51}Zn_{1.39}Sn_{0.93}Se_4$	0.6626	1.50124	B - 65.817%	A - 34.183%	$SnSe_2$; ZnSe
2	$Cu_{1.78}Zn_{1.10}Sn_{1.00}Se_4$	0.84614	1.0981	L - 9.266%	A - 90.734%	
Re-annealing						
1	$Cu_{1.52}Zn_{1.31}Sn_{0.96}Se_4$	0.676906	1.357228	B - 43.401%	A - 56.599%	$SnSe_2$; ZnSe; Zn
2	$Cu_{1.47}Zn_{1.37}Sn_{0.95}Se_4$	0.642724	1.439142	B - 50.778%	A - 49.222%	
3	$Cu_{1.57}Zn_{1.22}Sn_{0.98}Se_4$	0.743056	1.241635	B - 30.817%	A - 69.183%	

B-001						
Main Phase	Formula	Cu/(Zn+Sn)	Zn/Sn	Type I	Type II	Secondary phases
1	$Cu_{1.84}Zn_{1.21}Sn_{0.93}Se_4$	0.85681	1.29833	B - 94.843%	A - 5.157%	ZnSe
2	$Cu_{1.89}Zn_{1.12}Sn_{0.97}Se_4$	0.90925	1.15725	B - 87.752%	A - 12.248%	
Re-annealing						
1	$Cu_{1.91}Zn_{1.15}Sn_{0.95}Se_4$	0.907214	1.219401	B - 90.789%	G - 9.211%	ZnSe
2	$Cu_{1.85}Zn_{1.25}Sn_{0.91}Se_4$	0.852256	1.376576	B - 89.862%	G - 10.138%	
3	$Cu_{1.65}Zn_{1.21}Sn_{0.98}Se_4$	0.755051	1.229827	B - 31.173%	A - 68.827%	

B-002						
Main Phase	Formula	Cu/(Zn+Sn)	Zn/Sn	Type I	Type II	Secondary phases
1	$Cu_{1.89}Zn_{1.12}Sn_{0.97}Se_4$	0.90691	1.15598	B - 85.665%	A - 14.335%	ZnSe
2	$Cu_{1.81}Zn_{1.24}Sn_{0.93}Se_4$	0.83631	1.33385	B - 92.784%	A - 7.216%	
Re-annealing						
1	$Cu_{1.62}Zn_{1.22}Sn_{0.98}Se_4$	0.736239	1.239340	B - 26.608%	A - 73.392%	ZnSe
2	$Cu_{1.51}Zn_{1.31}Sn_{0.97}Se_4$	0.669645	1.348376	B - 38.655%	A - 61.345%	
3	$Cu_{1.57}Zn_{1.16}Sn_{1.02}Se_4$	0.719141	1.137421	L - 33.478%	A - 66.522%	

C-001						
Main Phase	Formula	Cu/(Zn+Sn)	Zn/Sn	Type I	Type II	Secondary phases
1	$Cu_{2.20}Zn_{0.70}Sn_{1.1}Se_4$	1.2271	0.63524	C - 99.095%	D - 0.905%	$SnSe_2$;
2	$Cu_{2.08}Zn_{0.90}Sn_{1.03}Se_4$	1.08008	0.8675	C - 93.566%	D - 6.434%	Cu_2SnSe_3
Re-annealing						
1	$Cu_{2.19}Zn_{0.81}Sn_{1.05}Se_4$	1.179236	0.769806	C - 81.099%	D - 18.901%	$SnSe_2$;
2	$Cu_{2.31}Zn_{0.61}Sn_{1.12}Se_4$	1.342976	0.549747	C - 90.975%	D - 9.025%	Cu_2SnSe_3

C-002						
Main Phase	Formula	Cu/(Zn+Sn)	Zn/Sn	Type I	Type II	Secondary phases
1	$Cu_{2.70}Zn_{0.24}Sn_{1.20}Se_4$	1.90546	0.2027	C - 81.707%	D - 18.293%	Cu_2SnSe_3;
2	$Cu_{2.29}Zn_{0.80}Sn_{1.02}Se_4$	1.25581	0.78775	C - 42.268%	D - 57.732%	Cu_2Se
Re-annealing						
1	$Cu_{2.16}Zn_{0.84}Sn_{1.04}Se_4$	1.148140	0.802888	C - 82.251%	D - 17.749%	Cu_2SnSe_3;
2	$Cu_{2.32}Zn_{0.64}Sn_{1.10}Se_4$	1.338031	0.587554	C - 84.944%	D - 15.056%	Cu_2Se; $SnSe_2$

D-001						
Main Phase	Formula	Cu/(Zn+Sn)	Zn/Sn	Type I	Type II	Secondary phases
1	$Cu_{2.64}Zn_{0.55}Sn_{1.07}Se_4$	1.65573	0.51182	C - 48.466%	D - 51.534%	Cu_2Se
2	$Cu_{2.24}Zn_{0.84}Sn_{1.02}Se_4$	1.20611	0.82941	C - 39.484%	D - 60.516%	
Re-annealing						
1	$Cu_{2.30}Zn_{0.81}Sn_{1.02}Se_4$	1.260084	0.788739	C - 39.894%	D - 60.106%	Cu_2Se
2	$Cu_{2.18}Zn_{0.91}Sn_{1.00}Se_4$	1.141582	0.909895	C - 0%	D - 1%	

D-002						
Main Phase	Formula	Cu/(Zn+Sn)	Zn/Sn	Type I	Type II	Secondary phases
1	$Cu_{2.25}Zn_{0.72}Sn_{1.07}Se_4$	1.25533	0.67463	C - 84.293%	D - 15.707%	Cu_2SnSe_3;
2	$Cu_{2.09}Zn_{0.92}Sn_{1.02}Se_4$	1.07838	0.8987	C - 76.546%	D - 23.454 %	$SnSe_2$
Re-annealing						
1	$Cu_{2.45}Zn_{0.66}Sn_{1.06}Se_4$	1.441887	0.620959	C - 55.514%	D - 44.486%	Cu_2SnSe_3;
2	$Cu_{2.27}Zn_{0.83}Sn_{1.02}Se_4$	1.230840	0.811119	C - 39.327%	D - 60.673%	Cu_2Se